UNIVERSITY OF AGDER

Design of an Alkaline Electrolysis Stack

Yakdehige Sanath Kumara De Silva

Supervisor

Professor Peter Hugh Middleton

This masters thesis is carried out as a part of the education at the University of Agder and is therefore approved as a part of this education. However, this does not imply that the University answers for the methods that are used or the conclusions that are drawn.

University of Agder, 2017

Faculty of Engineering and Science

Department of Engineering Sciences

Abstract

Renewable energy promises a green energy future for the world. Hence, the electrolysis process has been identified as the most important method to produce hydrogen using renewable energy source. Moreover, during the last few years, people have enhanced the interest to expand and use the alkaline water electrolysis technology in different fields. Thus, the design of high performance compact electrolysis stack according to the selected specification is very important.

The main purpose of this research work is to design and fabricate a compact high performance electrolysis stack and to observe the electrolysis performance. Under this study, twelve different experiments have been implemented to observe the electrolysis performance. At the beginning, two different single cell alkaline electrolysers were fabricated and their performances monitored to select best cell for the stack. Thereafter, the several experiments were devised to improve the performance of the selected cell. Thus, the best performing cell was selected for the final stack. At last both monopolar and bipolar configuration of alkaline electrolysis stack are designed and implemented to compare the electrolysis performance of both configurations.

Throughout the design process, the SolidWorks was adopted as the design software platform. The modeling part of alkaline electrolyser was done using the MATLAB/SIMULINK environment. Under the modeling process the electrochemical equations are used to develop MATLAB/SIMULINK model. Consequently, the theoretical results are obtained by using developed mathematical model. Later, the performance of designed alkaline electrolysis stack is analyzed and compared with the theoretical results.

Acknowledgments

With great pleasure, I would like to take an opportunity to acknowledge the efforts of the people whose guidance, and corporation were vital to make this successful. First and foremost, I would like to express my profound gratitude to my supervisor, Professor Peter Hugh Middleton for his contribution and valuable thoughts and guidance in both subjective and documentary part when carrying out the work and supporting me in numerous ways. It was a great pleasure to work with him for the entire study period.

Secondly, I would like to thank Professor Joao Leal, Study Program Coordinator for renewable energy in university of Agder. He provided valuable information and advises throughout this work. You were always there, cheering me and refreshing with new energy and inspiration.

I must thank Norwegian State Educational Loan Fund for providing me the necessary financial support to complete my master's degree. Also, I acknowledge the Faculty of Engineering and science, University of Agder for providing me this valuable study opportunity and pleasant study environment for the studies. Furthermore, I would like to thank all the Academic staff members of the University of Agder for giving their invaluable knowledge. At last, my special thanks go to my wife who helped me in numerous situations to make this research study success.

Yakdehige Sanath Kumara De Silva,

Faculty of Engineering and Science,

University of Agder,

Grimstad, Norway

May, 2017.

Contents

List of Tables

List of Figures

Abbreviations

H_2	-	Hydrogen
O_2	-	Oxygen
SO_x	-	Sulfur oxides
NO_x	-	Nitrogen oxide
CO_2	-	Carbon dioxide
CO	-	Carbon Monoxide
PV	-	Photovoltaic
PEM	-	Proton Exchange Membrane
SOE	-	Solid Oxide Electrolysis
f_{H2}	-	Hydrogen production rate
H_2O	-	Water Molecules
KOH	-	Potassium Hydroxide
$NaOH$	-	Sodium Hydroxide
OH^-	-	Hydroxide Anions
$V2G$	-	Vehicle-to-Grid
AEST	-	Alkaline Electrolyser Simulation Tool
$Ni - MoRF$	-	Nickel-Molybdenum-Resorcinol-Formaldehyde
$Ni - C - Pt$	-	Nickel-Carbon-Platinum
HER	-	Hydrogen Evaluation Reaction
ECE	-	Electrochemical Equivalent
EMF	-	Electromotive Force
EIS	-	Electrochemical Impedance Spectroscopy
$RMSE$	-	Root Mean Square Error

Chapter 1

Introduction

This chapter offers the background information about the alkaline electrolysis process. The role and importance of this technology are explained under background and motivation. The literature review of the project is discussed by considering several research works. Thereafter, the problem description is demonstrated using goal and objective of the project. At last the methodology and report outline are discussed in detail.

1.1 Background and Motivation

Today the electrolysis process has been recognized as the most important method to generate hydrogen (H_2) for many power applications owing to their performance. Moreover, the hydrogen is identified as a upcoming fuel for a viable energy supply. The renewable energy source such as wind and solar thermal energy can be adopted to obtain hydrogen from electrolysis process. An increase in future demand for hydrogen is depending on the increasing demand for energy in both transportation and stationary applications. Nevertheless, the global energy demand has been increasing rapidly. Consequently, the traditional energy sources such as coal, gas and liquefied petrol are being reduced at an alarming rate. This problem could be solved by using renewable energy sources as a backup energy supply. These days the generation of hydrogen from the electrolysis process has become one of most useful renewable energy technology in the world.

At the very beginning, the fossil fuel sources were used to produce hydrogen. The great amounts of greenhouse gasses such as SO_x, NO_x, CO_2 and CO were emitted through that industrial and transportation processes, into the atmosphere with consequent damage to the environmental ecosystem. Hence, the water electrolysis technologies, photocatalysis processes and thermochemical cycles are currently deployed to produce hydrogen, which is completely free from greenhouse gasses. Among them, the water electrolysis technologies are widely used for hydrogen production. Since, water electrolysis process are most efficient and effective solutions to environmental problems especially global warming by gas emission. Thus, during the last few years, people have enhanced the interest to expand and use of water electrolysis technology in different fields.

Moreover, the wind energy and solar-PV can be used to generate hydrogen from water electrolysis. Then the whole process becomes a pollution free process. Furthermore, the alkaline electrolyser can be integrated into a renewable grid connected systems

[1], [2], renewable stand-alone power systems [1], [3] and renewable distributed energy generation systems based on micro-grids [1], [4]. Hence, the generation of hydrogen from electrolysis process has become important and useful renewable energy technology. Nevertheless, hydrogen is believed as safe for commonly used fuels [5], [6].

The alkaline electrolysis, PEM electrolysis (Proton Exchange Membrane) and Solid Oxide Electrolysis (SOE) are the main technologies for the electrolysis device. Even though the alkaline water electrolysis process is widely used to generate hydrogen. The schematic diagram of these three technologies is shown in Figure 1.1.

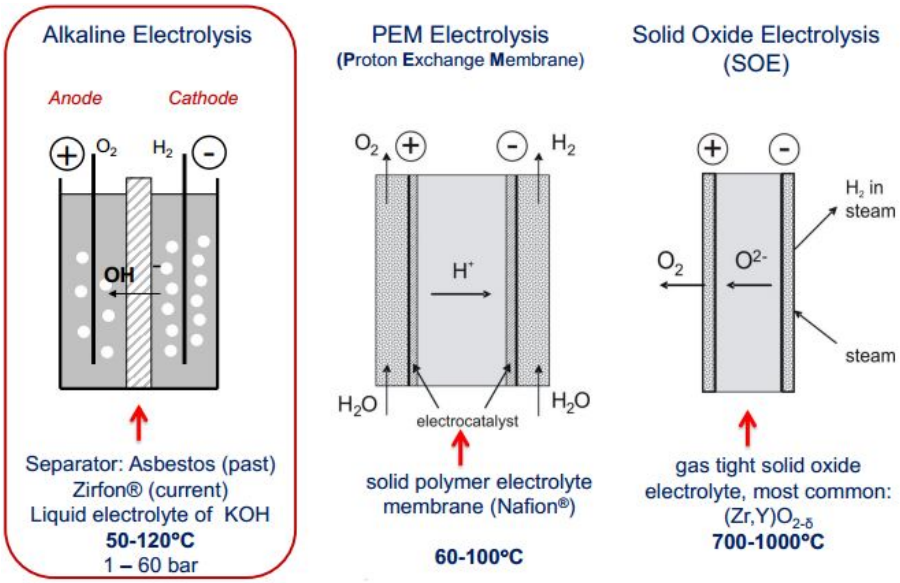

Figure 1.1: Main technologies for the water electrolysis [7]

In PEM electrolysis, gold, platinum and iridium are used as a base material which are very expensive. Hence, the manufacturing cost of the PEM electrolyser is extremely higher than other electrolysis device. Furthermore, the electrolysis efficiency of the PEM electrolyser is quite low when compared with the other electrolysis processes. Hence, the alkaline electrolyser is the mature technology for the electrolysis since it is capable of overcoming all these problems. The manufacturing cost of the alkaline electrolysis modules is also quite low. The ohmic loss of the alkaline electrolysis cell is mainly induced by electrical resistance of the electrolytes, which can be reduced by shortening the distance between the anode and cathode. Hence, the objective of this project is to design a compact alkaline electrolysis stack to generate hydrogen energy.

The first alkaline electrolyser was developed by William Nicholson, Ritter and Anthony Carlisle in 1800 [8],[9]. They were the first who decomposed water into hydrogen and oxygen by electrolysis. The term "Electrolysis" was acquainted by Faraday in 1834. First bipolar electrolyser was introduced by oerlikon and zrich in 1900 and the first commercial electrolyser operating under 30 bar pressers was developed by Lurgi in 1951 [9]. The size range of commercial alkaline electrolysis system is available from 1.8 to 5300 kW. Hydrogen production rate (f_{H2}) for commercial systems is $0.25 - 760 Nm^3/h$ [10], [9]. The operating temperature range is typically between

5 °C and 100 °C depending on the model. In some case, operating temperature can reach up to 400 °C [11]. As concerns the pressure, some models are operating at atmospheric pressure, but it can reach up to 448 bar. Nevertheless, the maximum electrolysis pressure is typically close to 25 - 30 bar [11]. In general, the apparent hydrogen generation efficiency of common industrial electrolysers is around 70%. The main drawback of such a system is high power dissipation value [12]. Moreover, the cobalt and tungsten based ionic activators (situ activating compounds) could be added directly into the electrolyte during the electrolytic process to increase the hydrogen generation rate from alkaline electrolysis process [7].

In alkaline electrolyser, the electrical energy can be treated as driving force of chemical reactions. The water molecules (H_2O) can be decomposed into hydrogen (H_2) and oxygen (O_2) gas through an electrochemical reaction by passing a direct current through the electrodes. The electrolyte is usually a 20 –40 wt% aqueous solution of potassium hydroxide (KOH) which enhance the ionic conductivity of the electrolyte. The sodium hydroxide (NaOH) also can be used as an electrolyte because of its higher conductivity. Figure 1.2 is illustrated the operating principle of alkaline electrolyser.

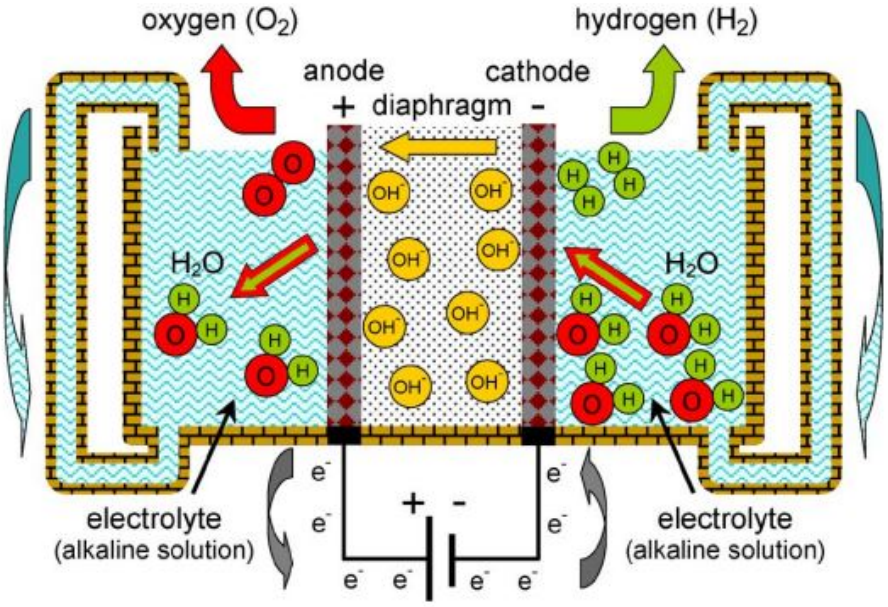

Figure 1.2: Operating principle of the alkaline electrolyser

The electrochemical reactions which are taken place in alkaline electrolyser, near the anode and cathode can be illustrated as follows [13],

$$(Cathode) \qquad 2H_2O + 2e^- \rightarrow 2OH^- + H_2 \uparrow \tag{1.1}$$

$$(Anode) \qquad 2OH^- \rightarrow H_2O + 2e^- + \frac{1}{2}O_2 \uparrow \tag{1.2}$$

$$(Total) \qquad 2H_2O \rightarrow H_2 + \frac{1}{2}O_2 \uparrow + H_2O \tag{1.3}$$

Throughout this reaction, two molecules of water are decomposed and hydrogen is formed at the cathode where water is reduced according to Eq. 1.1. Thereafter, the hydroxide anions (OH^-) migrate across the diaphragm to the anode. Thus, in the anode, oxygen is composed and the one molecule of water is regenerated according to the Eq. 1.2. At last, in the total reaction, one molecule of water is moved to the anode while decomposing one molecule of water into hydrogen and oxygen. Hence, the working principle behind the alkaline electrolyser is technologically very simple and the formed hydrogen can be reached a purity level between 95.5% - 99.9998%, and does not need any further rectification [14]. Furthermore, the water fed to an alkaline electrolyser has to be pure with an electrical conductivity below $5\mu S/cm$ [15].

1.2 Literature Review

Nowadays, several research studies have been presented for alkaline electrolyser. As mentioned early, alkaline electrolyser can be integrated with a renewable source such as wind and photovoltaic system. In Ref. [16], stand-alone operation of an alkaline water electrolyser fed by wind and photovoltaic systems is studied. In that analysis study, it was investigated that the electrolyser is performed properly, with regard to balance of plant and its principal electrochemical characteristics. Moreover, the mean energy efficiency of the electrolyser was found for each wind and PV system. The research study in [17], the authors observed that large scale alkaline electrolysers can be used to improve the frequency stability of the wind power system and it can be reduced fluctuations in system frequency. The solar powered alkaline electrolyser is investigated in Ref. [18] and the small signal model of the alkaline electrolyzer is obtained under this research study. In research work [19], the impact of the electric grid of by hydrogen production from alkaline electrolysers is discussed in detail. The alkaline electrolyser is integrated into stand along microhydro plant in [20] for controlling purposes.

In general, most static and dynamic models of alkaline electrolysers are developed by using MATLAB/ Simulink as a modeling software. The dynamic model of an alkaline type electrolyser has been developed in [21] for both electrochemical and thermal behavior of the electrolyser, which can be integrated with different kinds of renewable energy systems. In Ref. [22], a dynamic model of an alkaline electrolyser based on artificial neural networks is discussed. In that modeling study, operating temperature, current absorbed by the electrolyser and also the past value of cell voltage is employed as input for the model. The research works in [23] is presented two models, an alkaline electrolyser and V2G system which are used for demand response analysis in future distribution networks. In Ref. [24], the multi-physics model used for the design and diagnosis of the alkaline electrolyzers is developed to evaluate the electrolyser operating voltage. The alkaline electrolyser simulation tool (AEST) is presented in [25] based on a physics model of electrolyser performance. In that research work, the operating temperature, pressure, electrolyte concentration and current have been defined as the inputs of the electrolyser model. Moreover, the electrolysis cell performance and hydrogen production can be predicted.

Divers research studies have been done for alkaline electrolysers to increase performance by introducing different materials for electrode, electrolytes and separating

diaphragm. In the research work in [26], development of new materials for alkaline electrolyser is discussed. In that study, the author suggests that, the Ni-Mo RF electrodes and Ni-C-Pt electrodes can be used instead of nickel or nickel plated steel. The electrocatalytic properties of some FeR (R = rare earth metal) crystalline alloys are studied in [27] for the hydrogen evolution reaction (HER) in 1 M NaOH solution at $298K$. In that study it was found that, the $Fe_{90}Ce_{10}$ and $Fe_{90}MM_{10}$ (MM = mischmetal) electrodes have high catalytic efficiencies for the HER as compared with the G14 alloy. The electrocatalytic properties of new electrocatalysts for hydrogen evolution in alkaline water electrolysis are discussed in [28]. In that study, the author observed that the HER can be increased with the increase in molybdenum content and is dominated by electrode surface composition. In [29], the Zirfon^R material is used as a separator for alkaline water electrolyser instead of asbestos diaphragm. In that research work, it was investigated that, the Zirfon^R separator is highly stable in concentrated KOH solutions at elevated temperatures.

1.3 Problem Description

In this project, the design consideration of both monopolar and bipolar configurations of alka- line electrolysis stacks are discussed in detail. In the first phase of this project, two different singe cell alkaline electrolysers are designed and constructed to enable the observation of the cell performance, such as product gas flow rate, purity level of product gas, electrolysis power and efficiency of the cell. Thus, different materials are used for the separating diaphragm to increase the cell performance by decreasing over voltage losses inside the cell. Moreover, several experiments are conducted to minimize ohmic overvoltage by changing the separation (gap) between the anode and cathode. Thereafter, the best single cell alkaline electrolysis cell is selected for the design of the electrolysis stack by considering the performance of the designed single cell.

Usually, the flow rates of product gas are quite low in both single cell alkaline electrolysers. However, in the stack, we need to allow for the collection of the evolved gas in collection chambers. In this context, Solidworks was used to design inside gas collection chamber as part of the stack concept. In this study, the MATHLAB SIMULINK model is used to validate the practical results. This works will provide important information about design, modeling and testing of practical alkaline electrolysis stacks.

1.3.1 Goals

The main goal of this research is to design and fabricate a high performance, compact alkaline electrolyser stack to observe the electrolysis performance and to collect a considerable amount of product gas for general usage.

1.3.2 Objectives

The major objectives of this research project can be listed as follows,

- To Design of a single cell compact alkaline electrolyser using Solidworks software in order to minimize ohmic loss inside the cell.
- To Implement the designed electrolyser.
- To optimize the designed electrolyser using different materials for the separating diaphragm and changing the distance between the anode and cathode.
- To develop and implement monopolar and bipolar configuration of alkaline electrolysis stack.
- To develop and implement mathematical model for electrolyser using MATLAB/SIMULINK software.
- To analyze and compare the practical results with mathematical model.
- To compare the performance between monopolar and bipolar configuration of alkaline electrolysis stack.

1.4 Methodology

In this project, two important sections are discussed in details to observe the performance of the alkaline electrolysis stack as shown in Figure 1.3.

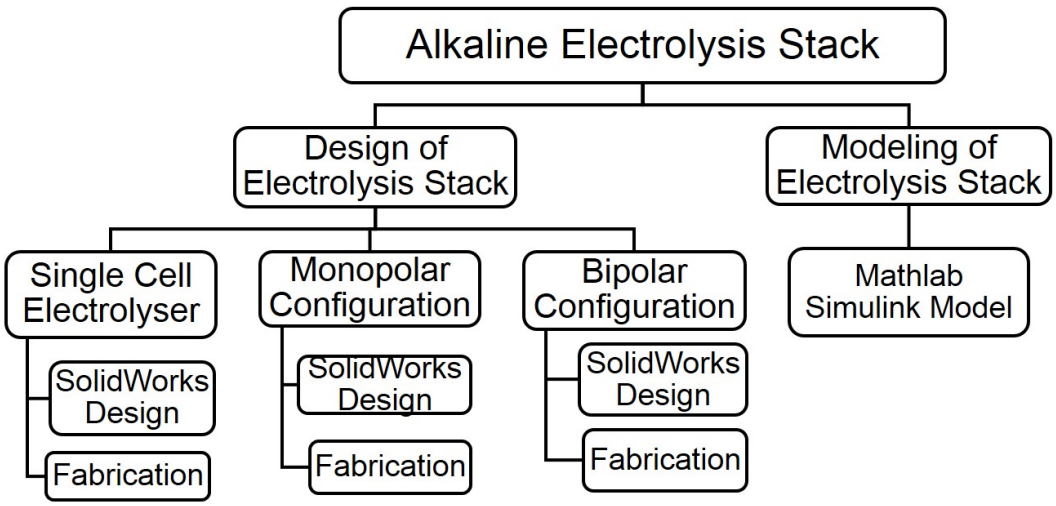

Figure 1.3: Overview of the Project

In order to design the alkaline electrolysis stack, the parameters related to the alkaline electrolyser should be considered. In this study monopolar and bipolar configurations

are developed to compare the performance of both configurations. At the beginning, two different single cell alkaline elecrolysers are fabricated and the observed cell performance used to select best cell design for the stack. Thereafter, several experiments are conducted to increase the performance of the selected cell. Thus, the best performing cell is selected for the final stack.

The design of the electrolysis stack can be divided into two main parts such as designing and fabrication, according to the Figure 1.3. Under the design part mainly, the three base plates (cell frame) are designed using SolidWorks 2014 software. When designing, the base plates the dimensions are selected in order to maintain proper spacing between the inside layers of alkaline electrolyser. Hence, to reduce the gas flow resistant inside the cell and to increase efficiency of the stack, the spacing between layers are quite important.

During fabrication the anode, cathode and separating diaphragm are placed between two base plates (or cell frame) respectively. In this model nickel coated stainless steel is used as a current collector plate. In order to maximize the sealing and prevent the leakage of alkaline electrolyser the silicone rubber is used as gasket material.

In this work, the MATHLAB SIMULINK model is used to validate the practical results. Modeling of the alkaline electrolyser in MATHLAB SIMULINK environment is basically based on electrochemical equations to observe the behavior of the alkaline electrolyser theoretically. The mathematical models of alkaline electrolyser is developed by considering MATLAB/SIMULINK. Characteristics for the model is captured for specific inputs and analyzed.

1.5 Report Outline

This project report consists of six chapters. The first chapter provides an introduction about the research project, including background and motivation. Problem statement, research objectives and goals are also defined in this chapter. Moreover, several research studies related to alkaline electrolysis stack are focused on the literature review.

The next chapters of this report are organized to present detailed information about the design, fabrication and modeling of the alkaline electrolser. **Chapter 2** presents the detailed information about design and fabrication of a single cell alkaline electrolyser with selected dimensions. Furthermore, the design of the stack is given in **Chapter 3**.

In **Chapter 4**, the mathematical model of alkaline electrolyser is developed and the polarization curve is obtained to compare with experimental results. **Chapter 5** presents the experiments and results of the project. Finally, the conclusions of the research study are given in **Chapter 6**.

Chapter 2

Design of a Single Cell Alkaline Electrolyser

In order to design the single cell alkaline electrolyser, the parameters related to the alkaline electrolyser should be considered. The relevant parameters and dimensions are described under this chapter. Throughout the design, SolidWorks is used as design software. This chapter offers the design concept of a single cell alkaline electrolyser and fabrication of the alkaline electrolysis cell. Under the design part, two different designs are explained in detail. Furthermore, the functions of all the parts of an alkaline electrolysis cell are discussed under the fabrication part.

2.1 SolidWorks Design of a Single Cell Alkaline Electrolyser

In this research project, two different designs of alkaline electrolyser are explained in detail. The purity level of product gasses is of great concern throughout the design. The hydrogen and oxygen are collected directly after the electrochemical reaction in the first design. Thus, in the second design, intermediate storage tanks are designed top of the electrolysis cell to collect hydrogen and oxygen after the electrochemical reaction. This helps to increase purity levels of product gasses. Throughout the project, SolidWorks 2014 is used as design software. Under the design part, specific dimensions are considered to increase the performance of the single cell.

2.1.1 First Design of Alkaline Electrolyser

The first design of an alkaline electrolyser basically consisted of the following parts, two base plates, electrolyte, anode, cathode and separating diaphragm. SolidWorks was used to design only the base plates, the remaining parts were made from materials in the laboratory. The dimensions of other parts were determined according to the dimension of base plates. The base plate consists of two different size square shape plates. These plates are designed by using the Extruded Boss/Base and Extruded cut tool in SolidWorks features library.

The dimensions of the first base plate is selected as 100 mm x 100 mm width and height respectively. The depth of extruded boss is 5 mm. The dimensions of the second blase plate is selected as 70 mm x 70 mm and the depth of extruded boss is 10 mm. The dimension of extruded cut in the case of the second base plate is selected as 50 mm x 50 mm and the depth of extruded cut is 10 mm. Hence, the maximum volume of electrolyte space became 10000 mm^3 (50 mm x 50 mm x 10 mm). This volume is used to decide the required electrolyte volume for the electrolysis cell. The base plate housings were designed to be fastened together using tie rods made from M8 size screwed rod (actually standard size M8 bolts were used). Thus, 8 mm diameter clamping holes were designed to fasten the base plates housings together. In this design, a special locking mechanism was used to prevent leakage of electrolyte. Figure 2.1 shows the locking mechanism of the single cell alkaline electrolyser.

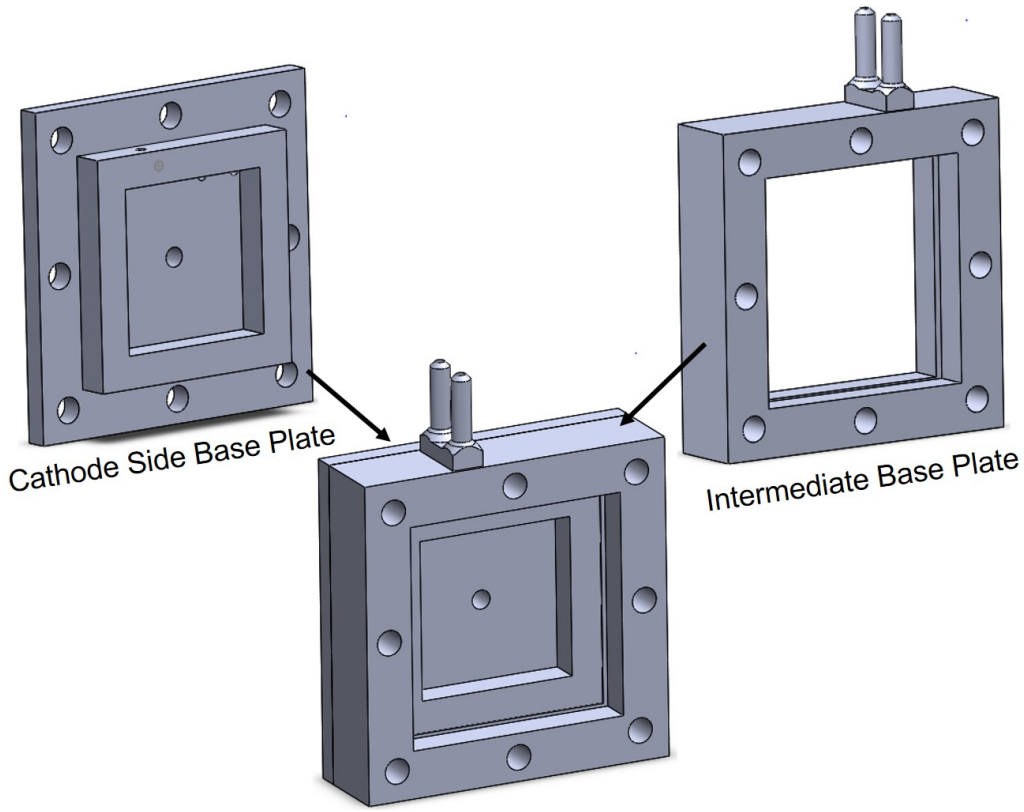

Figure 2.1: Locking mechanism of the alkaline electrolysis cell

The Extruded Boss/Base tool is used to design $H_2(g)$ and $O_2(g)$ outlet tubes and electrolyte inlet tube which has an outer diameter of 6 mm and an inner diameter of 3 mm. The chamfer tool in the features library is used to design the end of those outlet tubes. Specially, in the first design, the outlet tubes of the product gas are designed to be slightly longer to increase the purity level of the hydrogen and oxygen. The length of outlet tubes should be long enough to condense the water vapor ($H_2O(g)$) before entering to the product gas container.

The SolidWorks model of this project consists of three parts, namely, anode side base plate, cathode side base plate and intermediate base plate. Both anode side

and cathode side base plate are identical and the intermediate base plate is quite different. The product gas outlet tubes are designed on top of the intermediate base plate. The dimension of intermediate base plate is selected as 100 mm x 100 mm, same as the other base plate outer dimension. The dimension of extruded boss is 22 mm. The dimension of extruded cut is selected as 70 mm x 70 mm and the depth of the extruded cut is 22 mm. Finally, the standard drawing of designed single cell alkaline electrolyser is illustrated in Figure 2.2. The detailed dimensions of the alkaline electrolyser are illustrated in Appendix A.

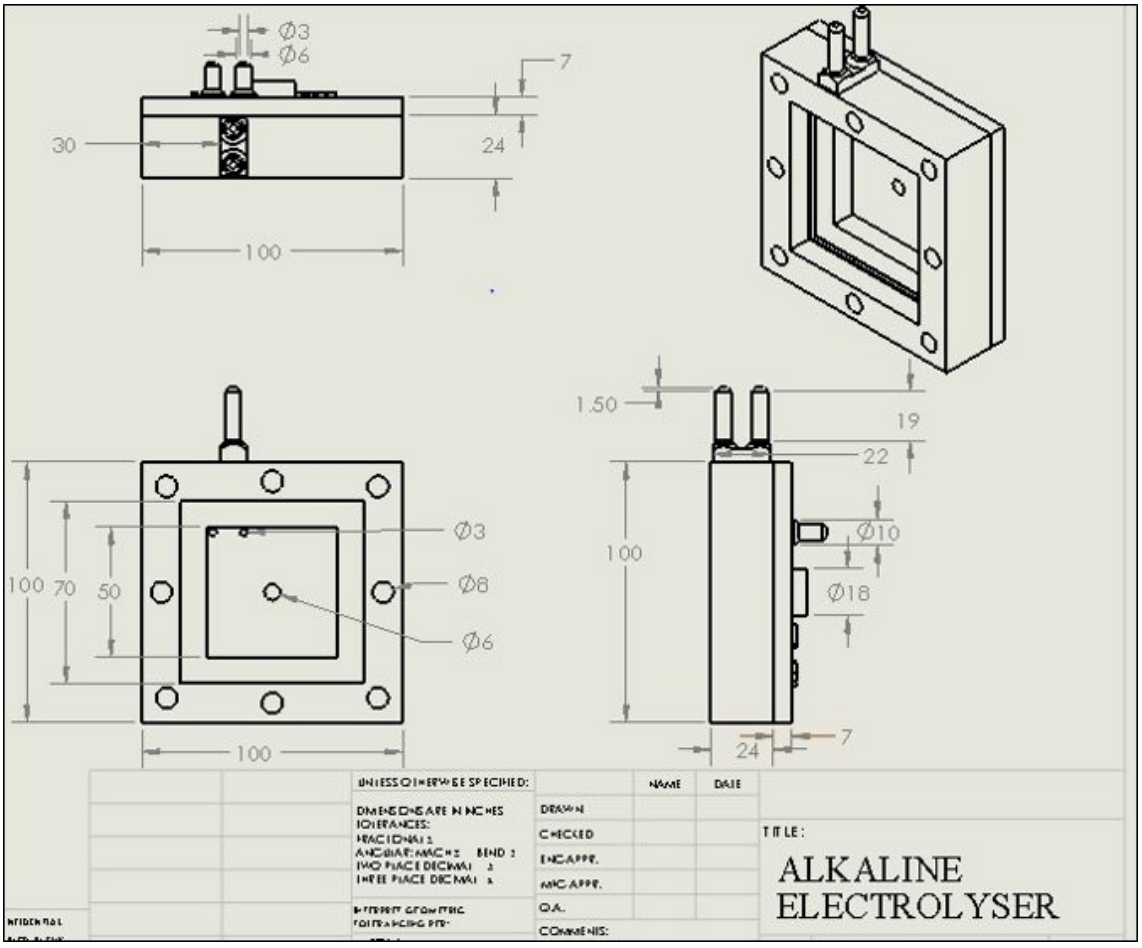

Figure 2.2: Standard drawing of the first design

2.1.2 Second Design of Alkaline Electrolyser

This design is almost same as the previous design. Hence, the same dimensions are used for this design also. The intermediate storage mechanism is used in this design to increase the purity level of hydrogen ($H_2(g)$) and oxygen ($O_2(g)$). This storage tank is able to condense the water vapor ($H_2O(g)$) before entering to the product gas containers. That is the major difference between those two designs. The same intermediate base plate in the first design is modified to get the second design of alkaline electrolyser. The intermediate storage mechanism is designed top of the intermediate base plate as illustrated in Figure 2.3.

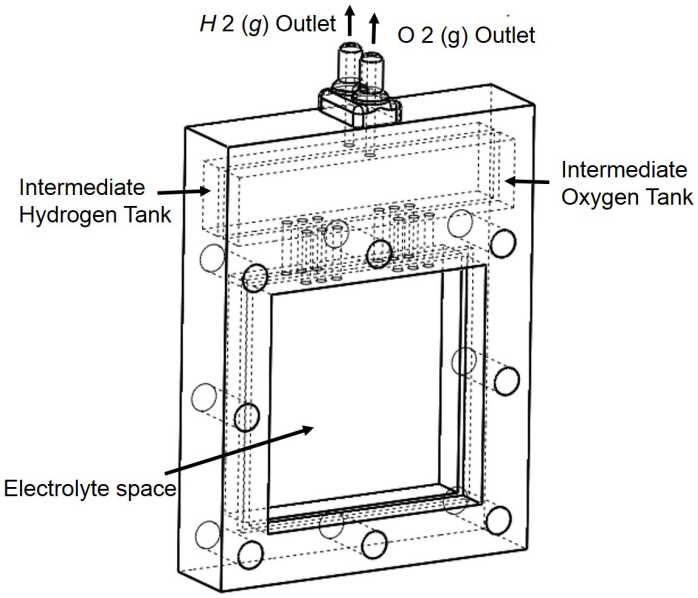

Figure 2.3: Modified intermediate base plate

In this design both intermediate hydrogen and oxygen tanks are identical. The dimension of each tank is taken as 90 mm x 7.5 mm x 25 mm length, width and height respectively. Hence, the maximum capacity of each storage tank should be 16875 mm^3. At length, the standard drawing of designed alkaline electrolyser is illustrated in Figure 2.4. The detailed dimensions of this alkaline electrolyser are illustrated in Appendix B.

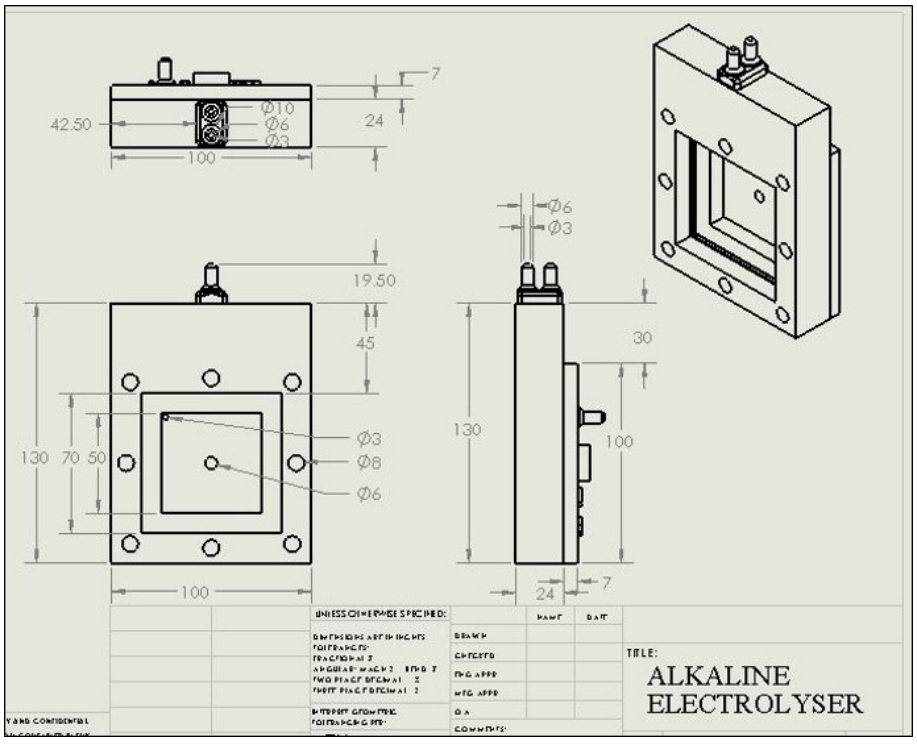

Figure 2.4: Standard drawing of the second design

2.2 Fabrication of Alkaline Electrolyser

In order to take the result from single cell alkaline Electrolyser, the assembly of the parts is quite important. As the first step, 3D print of designed alkaline electrolysis cell is taken by using the 3D printing machine which is available in the lab. The whole alkaline electrolysis cell consists of three base plate, anode, cathode, separating diaphragm, gasket and electrolyte. All the components of a single cell alkaline electrolyser are illustrated in Figure 2.5.

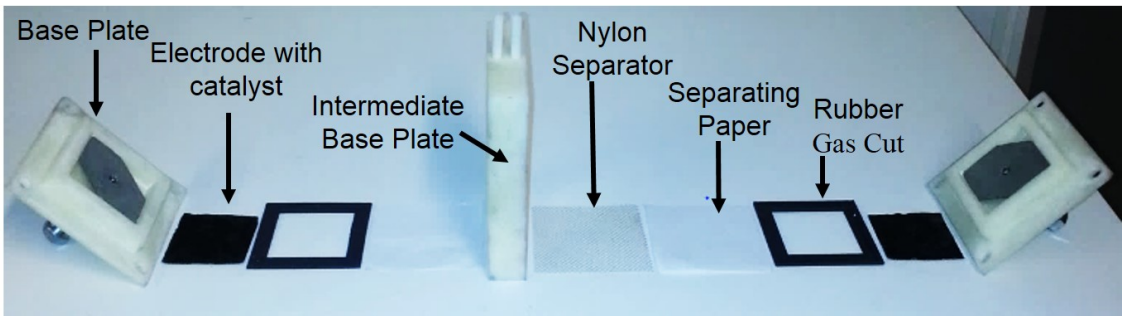

Figure 2.5: Basic parts of the alkaline electrolyser

2.2.1 Base Plates

The base plates are the outer frame of alkaline electrolyser. It works as a housing for the design. In this design, three base plates are used for the special locking mechanism as shown in figure 2.6.

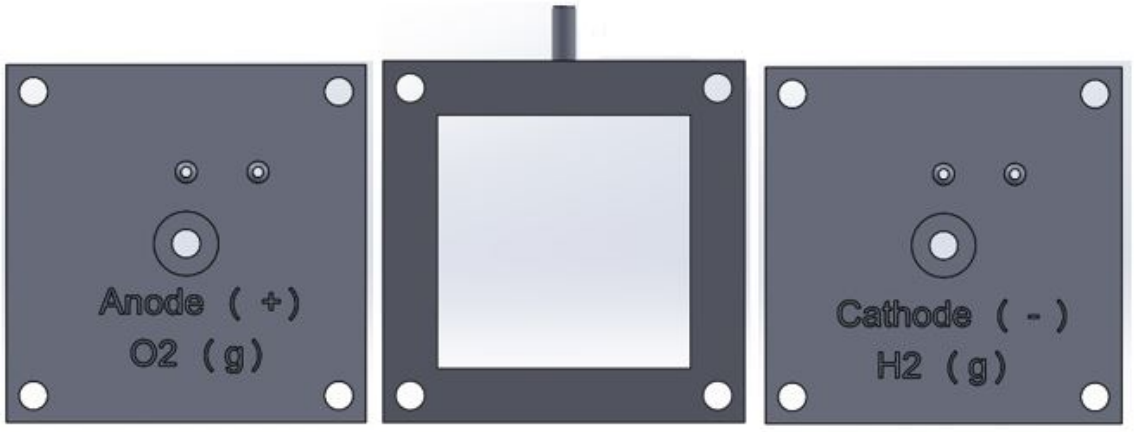

Figure 2.6: Base palates of the alkaline electrolyser

2.2.2 Electrodes

In general, both anode and cathode are called electrodes which separate oxygen and hydrogen respectively. Usually the anode is positive in a device which consume power,

and the cathode is negative in a device which provides a power, the opposite of a fuel cell. In this design the electrical power is consumed by the electrolysis cell. Hence, the anode is positive and negative charges move towards the anode. A cathode is negative in a device which consume power, and the cathode is positive in a device which provides a power. In this design the electrical power is consumed by the electrolyser. Thus, the cathode is negative and positive charges move towards the cathode. Moreover, the reduction electrochemical reaction occurs near the cathode as mentioned in Chapter 1. Considering the HER, the metal material for the cathode can be divided into three classes [30], [31];

- Metals with high overpotentials: Cd, Ti, Hg, Pb, Zn, Sn etc.
- Metals with middle overpotential: Fe, Co, Ni, Cu, Au, Ag, W etc.
- Metals with low overpotentials: Pt, Pd etc.

According to the oxygen evolution reaction, the metal material for the anode should be nickel (Ni), nickel plated steel or its alloy [30]. In general, same material can be used as cathode also. Under this design, the same material is used for anode and cathode which is illustrated in Figure2.7.

Figure 2.7: Porous Nickel Electrode

2.2.3 Separating Diaphragm

The separating diaphragm is used to separate the anode and cathode from each other. At the beginning the separating diaphragms (separator membrane) have been made of asbestos, but now asbestos is not used due to safety regulation of health. Nowadays,

they are mainly based on polybenzimides, polyphenylene sulphides, sulphonated polymers and composite materials [10]. Composite material based on ceramic materials or microporous materials such as polyethersulfone(PES) a reinforced, microporous polymer membrane, glass reinforced polyphenylene sulfide(PPS) compounds, nickel oxide layer on a mesh with titanium oxide, potassium titanate fine pored and predominantly ceramic [30]. The diaphragm must be kept the product gasses apart to maintain efficiency and safety. Moreover, the diaphragm has to be permeable to the water molecules and hydroxide ions.

2.2.4 Electrocatalyst

In order to increase the efficiency of electrolysis process, the electrocatalyst is added into the electrolyte solution. Thus, it is very important material for enhancing hydrogen production. Electrocatalyst is reduced the activation energy for the electrochemical reaction. In this design, electrocatalyst is used to increase the efficiency of the electrolysis process. The electrocatalyst is made by ourselves in the laboratory. The "Nafion perfluorinated resin solution" shown in figure 2.8 (a) and "Platinum on activated charcoal" shown in figure 2.8 (b) are used to make the electrocatalyst. The chemicals which used to make electrocatalyst are illustrated in Figure 2.8

(a) (b) (c)

Figure 2.8: Chemicals for the electrocatalyst

2.2.5 Electrolyte

The electrolyte is an aqueous solution which contained either potassium hydroxide (KOH) or sodium hydroxide ($NaOH$) with a typical concentration of 20 - 40 wt%. The hydrogen production and efficiency of electrolyser can be increased by adding

sodium chloride ($NaCl$) catalyst compound into the electrolyte solution [30]. It helps to enhance the process output. Furthermore, the lifetime of the electrode can be increased by adding ionic liquid into the electrolyte solution [30].

2.2.6 Sealing Gasket

In this design rubber is used as a gasket material. The sealing gasket is provided mechanical sealing between inside pats of alkaline electrolyser. Usually, it has the following function except sealing.

- Minimize the leakage of gases to the outer atmosphere.
- Minimize the leakage of electrolyte to the outer atmosphere.
- Avoid the mixing of product gases near the catalyst area.

The rubber gasket for this design is made by ourselves in the laboratory. For that, two types of chemical in the same amount (50% from each bottle) are mixed together. Thereafter, the mixture is poured into the designed mold and kept approximately two hours to dry that mixture. The figure 2.9 is illustrated the rubber gasket and designed mold for the gasket.

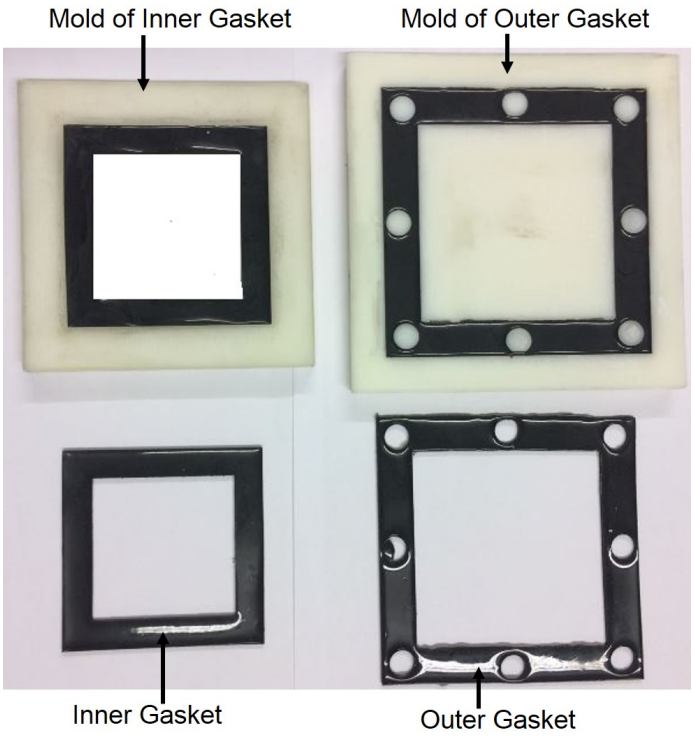

Figure 2.9: Rubber gasket and designed mold

At last both designed single cell alkaline electrolysers are assembled by placing all the component part in proper order. The final designs of both alkaline electrolysers are

illustrated in Figure 2.10 and 2.11 respectively.

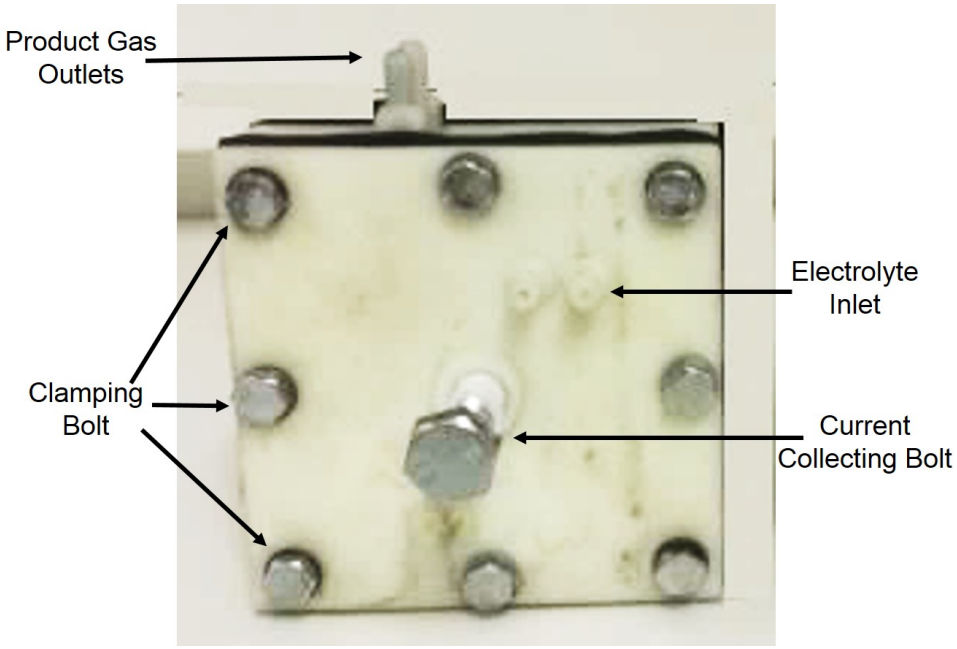

Figure 2.10: Assembled first alkaline electrolyser

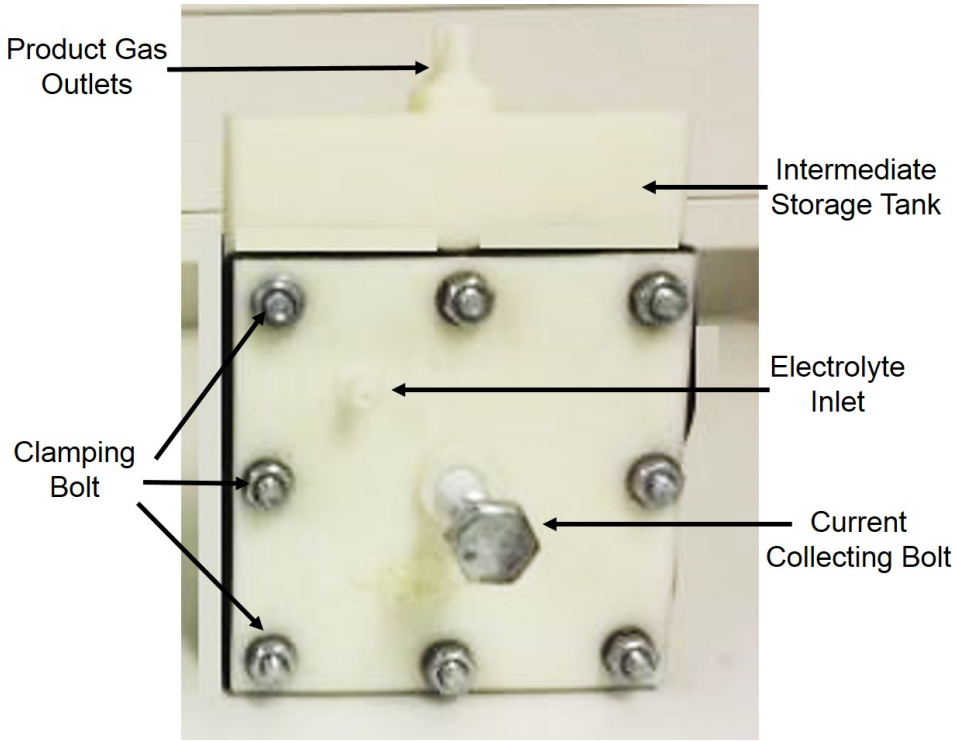

Figure 2.11: Assembled second alkaline electrolyser

Chapter 3

Design of Alkaline Electrolysis Stack

The single cell alkaline electrolyser is generated low amount of hydrogen gas per a minute, according to the calculation of Chapter 5. Hence, it is important to design alkaline electrolysis stack in order to produce high amount of hydrogen gas. Thus, this chapter focuses on the designing of both monopolar and bipolar configuration of alkaline electrolysis stack.

3.1 Configurations of Alkaline Electrolysis Stack

Usually, there are two alkaline electrolysis cell configurations namely, monopolar and bipolar. Figure 3.1 and Figure 3.2 are illustrated monopolar and bipolar cell configurations respectively. Where U_M and I_M are the voltage and current of the electrolysis module.

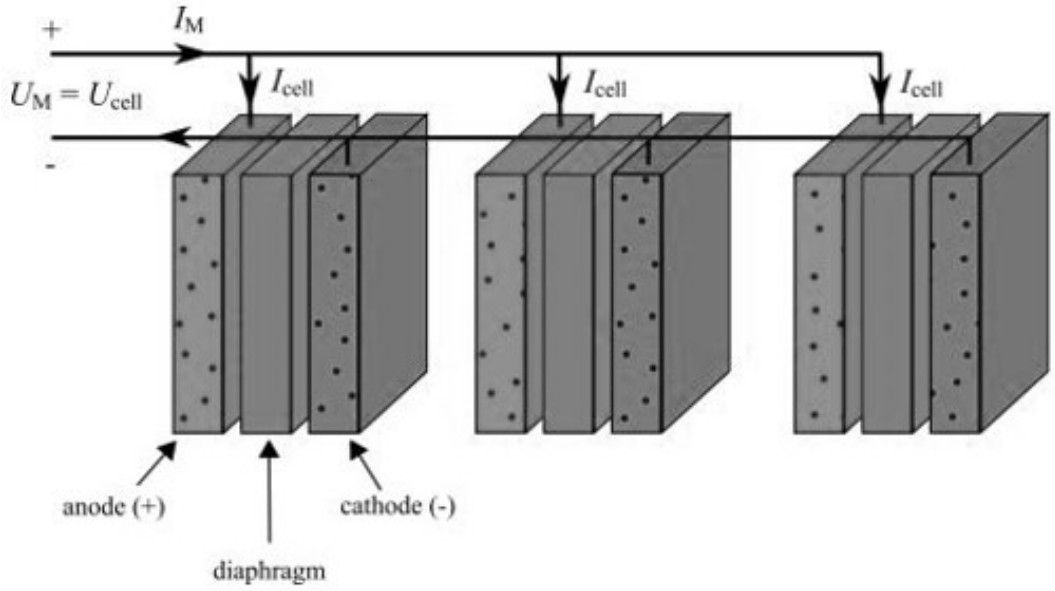

Figure 3.1: Monopolar cell configuration

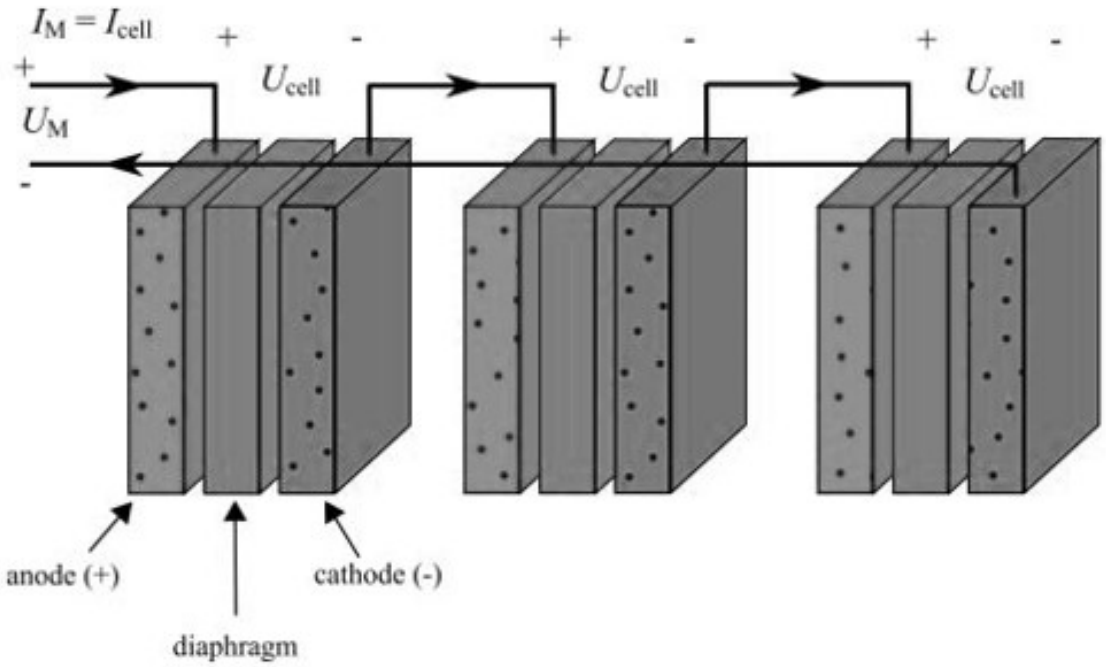

Figure 3.2: Bipolar cell configuration

3.2 Monopolar Alkaline Electrolysis Stack

In monopolar configuration, each electrolysis cells are connected in parallel to form a large module of electrolysis stack as shown in Figure 3.1. Hence, the voltage between individual pairs of electrodes is directly equal to the total cell voltage and the sum of cell current is equal to the total cell current. Furthermore, in this configuration same electrochemical reaction is occurred on both sides of each electrode. The reaction may be either the hydrogen evolution reaction or the oxygen evolution reaction, depend on the polarity of relevant electrodes.

3.2.1 Solidwork Design of Monopolar Alkaline Electrolysis Stack

The second design of single cell alkaline electrolyser is selected for this monopolar electrolysis stack. Since, it has better performance than the first design according to the calculation of Chapter 5. The stack consists of three single cells. However, the electrolysis efficiency of both designs was not enough for this kind of stack. Hence, some modification has been done for the second design through several experiments before using it as a part of the monopolar stack. In order to increase the electrolysis efficiency, the porous stainless steel current collector plates are used instead of the normal current collector plate as shown in Figure 3.3.

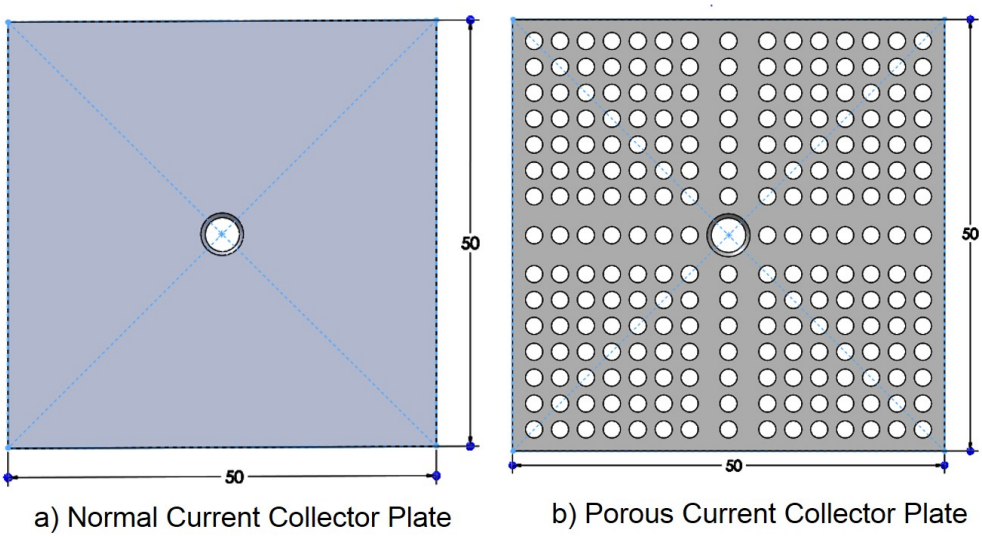

Figure 3.3: Improvement of the current collector plate

Figure 3.4 is illustrated standard drawing of monopolar alkaline electrolysis stack with relevant dimension. The dimensions of each single cell are exactly same as the dimensions of the second design of single cell alkaline electrolyser.

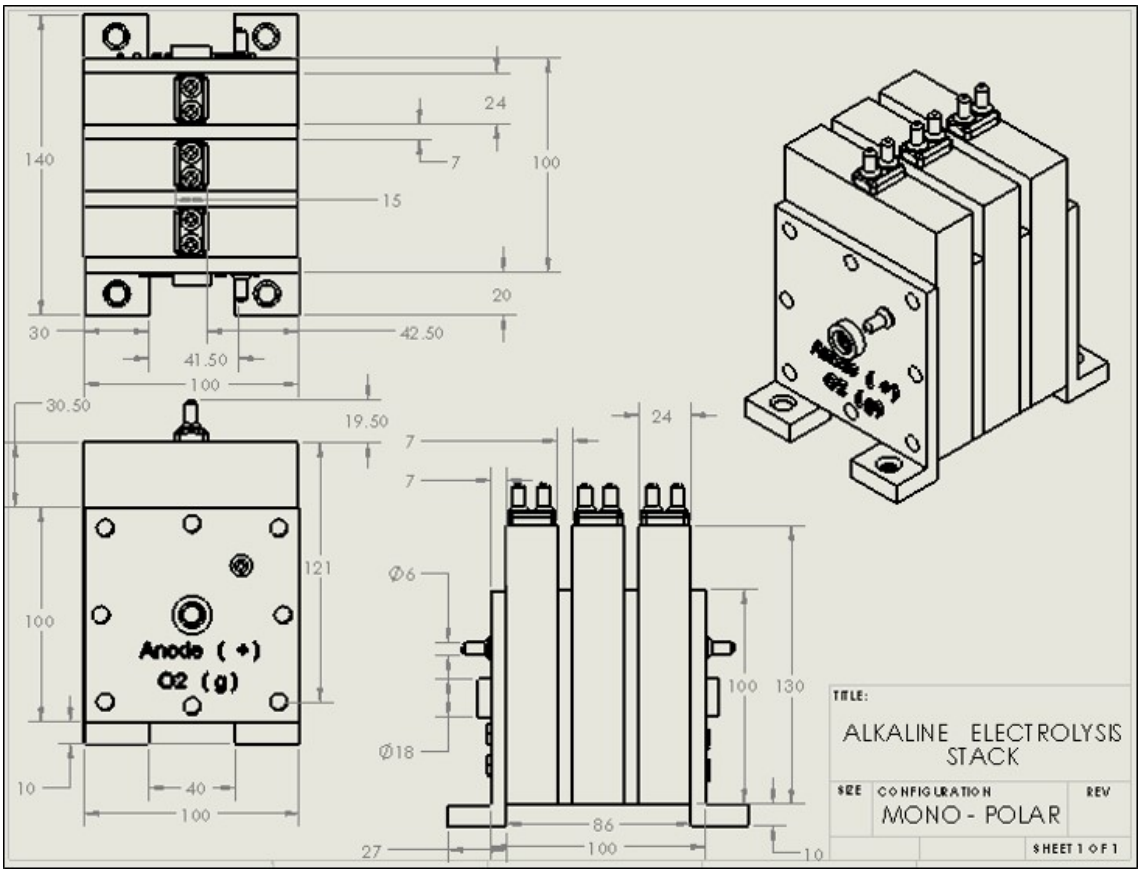

Figure 3.4: Standard drawing of the monopolar electrolysis stack

3.2.2 Fabrication of Monopolar Alkaline Electrolysis Stack

The fabrication part of monopolar alkaline electrolysis stack is very important to analyze and observe the stack performance. The bipolar plates and connecting rods are used to connect the cell together. The basic SolidWorks parts of monopolar alkaline electrolysis stack are shown in Figure 3.5.

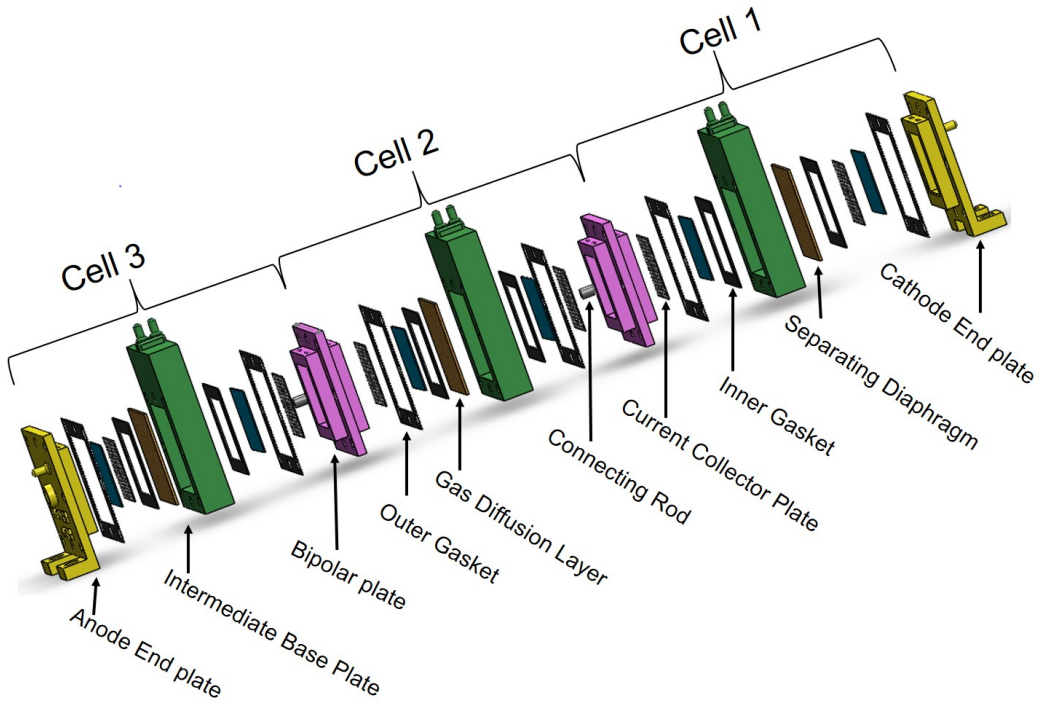

Figure 3.5: Basic SolidWorks parts of the monopolar alkaline electrolysis stack

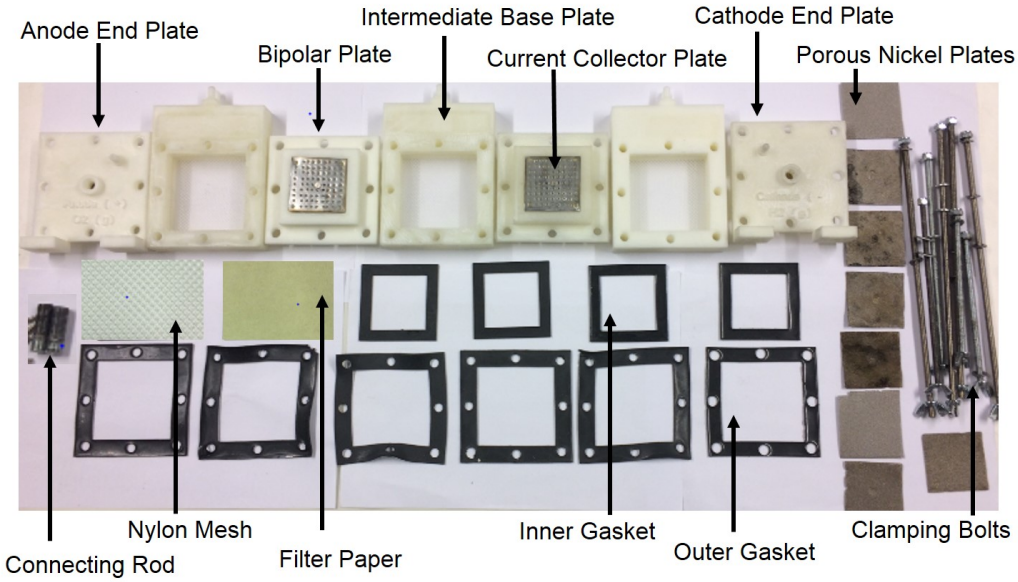

Figure 3.6: Basic practical parts of the monopolar alkaline electrolysis stack

Figure 3.6 is illustrated all the practical parts of this electrolysis stack. The gas impermeable plastic resin is used as a material for bipolar plates, intermediate base plates, anode and cathode end plates. The stainless steel is used as current collector plates. Consequently, it helps to prevent corrosion effect of the plates inside the KOH solution. Furthermore, the rubber is used as sealing gasket and porous nickel plate is used as a gas diffusion layer. The final stage of monopolar alkaline electrolysis stack is illustrated in Figure 3.7.

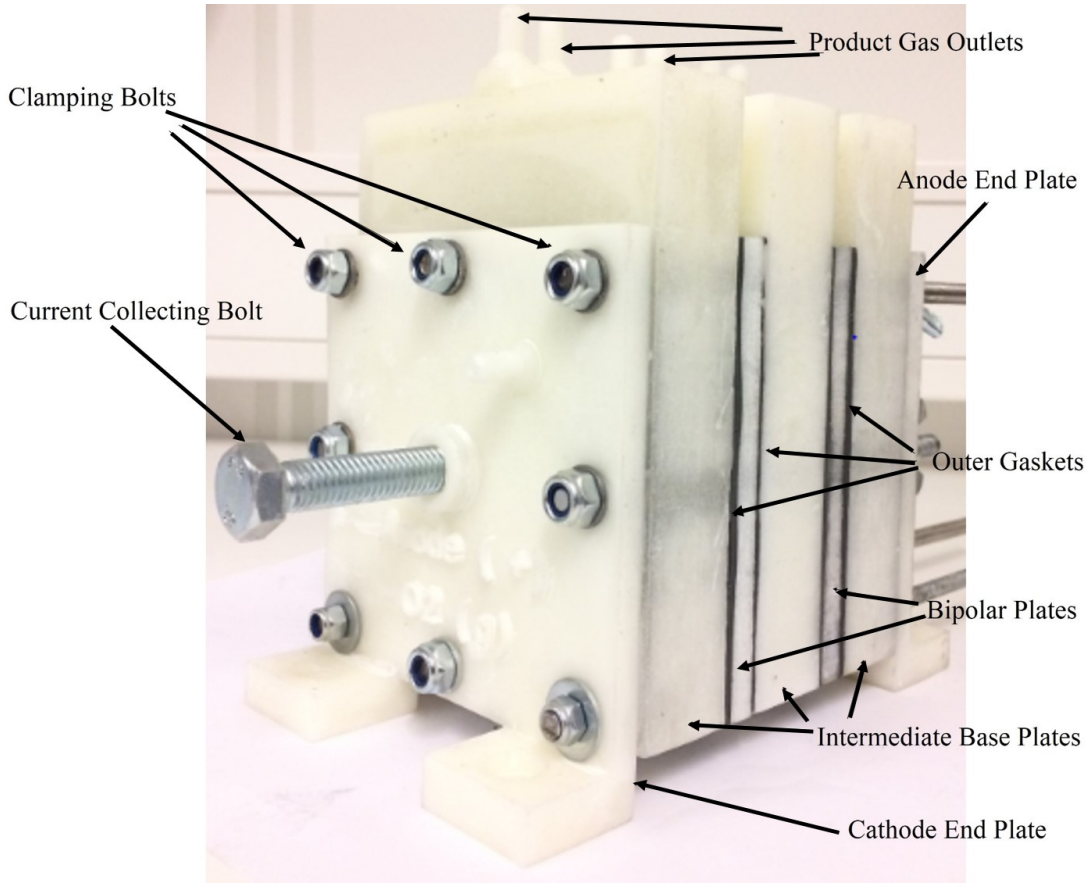

Figure 3.7: Final stage of the monopolar alkaline electrolysis stack

3.3 Bipolar Alkaline Electrolysis Stack

In bipolar configuration, each electrolysis cells are connected in series to form a large module of electrolysis stack as shown in Figure 3.2. Hence, the sum of all the voltages between individual pairs of electrodes is equal to the total cell voltage and the cell current is directly equal to the current which is passed through each individual cell. Furthermore, in this configuration two different electrochemical reactions, the hydrogen evolution reaction and the oxygen evolution reaction are occurred on both sides of each electrode. Thus, one side of electrode act as a cathode and other as anode at the same time.

The bipolar configuration has low ohmic loss when compared with monopolar configuration. Since bipolar configuration has a small gap between electrode than monopolar

configuration. The gap between electrodes is the distance that the ions have to travel in the electrolyte [32]. Thus, the smaller gap between electrode is given less resistance for ionic transportation by reducing ohmic loss inside the electrolysis stack. However, if the gap is too small, it would introduce electric sparks, posing an explosion hazard [33]. Hence, it is important to maintain optimal gap between electrodes to get better performance.

3.3.1 Solidwork Design of Bipolar Alkaline Electrolysis Stack

The design and fabrication process of bipolar alkaline electrolysis stack is more complicated than monpolar electrolysis stack. In this electrolysis stack also, second design of single cell alkaline electrolyser is selected to increase the stack performance. Moreover, few improvements have done to the current collector plate to enhance the electrolysis efficiency and product gas flow rate. The stack consists of three single cells as monopolar stack.

In bipolar configuration, the electrolyte should remain in between anode and cathode. Thus, the bipolar plate area must be free from the electrolyte. Hence, 1 mm thick rubber gasket is used to avoid leakages inside the stack. Furthermore, only one side of the anode and cathode should be touched with electrolyte. As discussed in monopolar stack, the stainless steel is used as a current collector plate to avoid corrosion effect of the plates inside the KOH solution. The maximum thickness of current collector plate is selected as 7 mm and industrial milling machine is adopted in the machining process of current collector plates. In order to increase contact area and intermediate electrolyte volume, longitudinal slots with 5 mm width and 2 mm depth are designed throughout the current collector plates as shown in Figure 3.8.

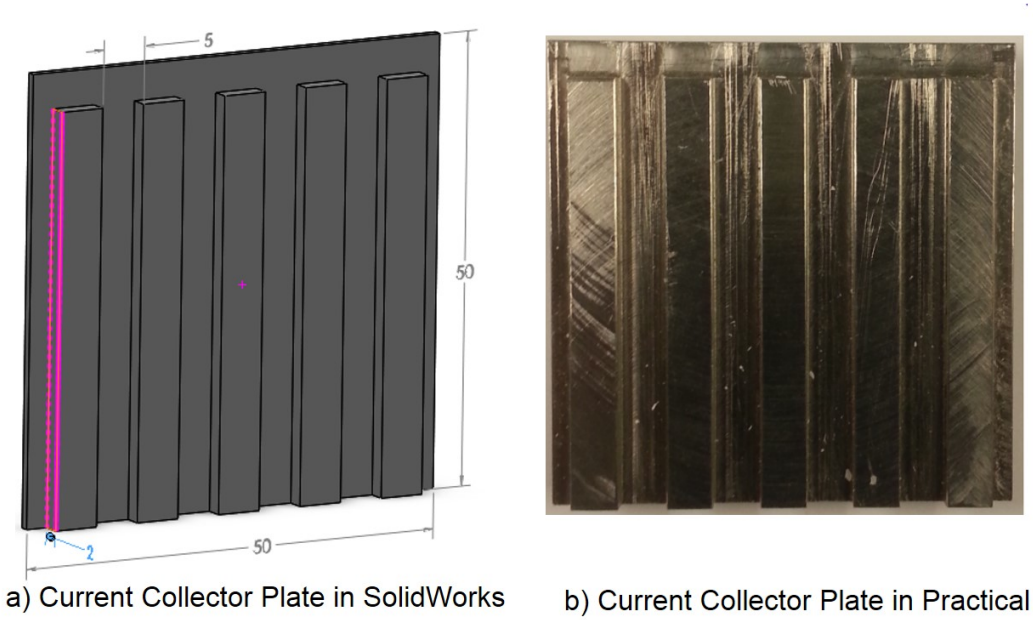

Figure 3.8: Current collector plate of the bipolar electrolysis stack

The standard drawing of bipolar alkaline electrolysis stack with relevant dimension is illustrated in Figure 3.9. The dimensions of each single cell are quite same as the dimensions of the second design of single cell alkaline electrolyser. Specially, in bipolar configuration, the thickness of all the parts are small compared with monopolar configuration. For example, in bipolar module the thickness of intermediate base plate is selected as 12 mm. Thus, in monopolar module that thickness was selected as 24 mm.

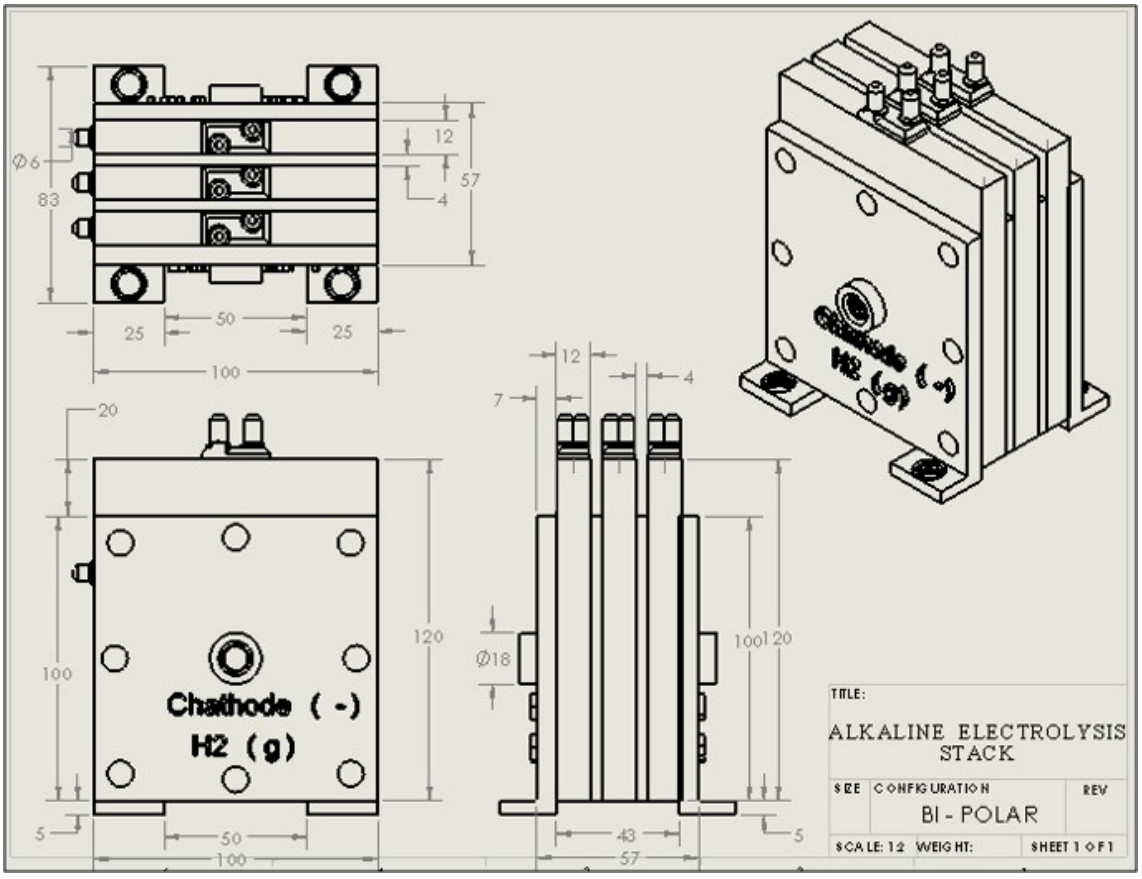

Figure 3.9: Standard drawing of the bipolar electrolysis stack

3.3.2 Fabrication of Bipolar Alkaline Electrolysis Stack

To analyze and observe the performance of electrolysis stack, the fabrication part is extremely important. As discussed in monopolar electrolysis stack, the gas impermeable plastic resin is used as a material for bipolar plates, intermediate base plates, anode and cathode end plates for bipolar electrolysis stack. Nylon mesh and filter papers are used as separating diaphragm. Moreover, the rubber is used as sealing gasket and porous nickel plates are used as a gas diffusion layer. Further, all the practical parts of bipolar alkaline electrolysis stack are shown in Figure 3.10.

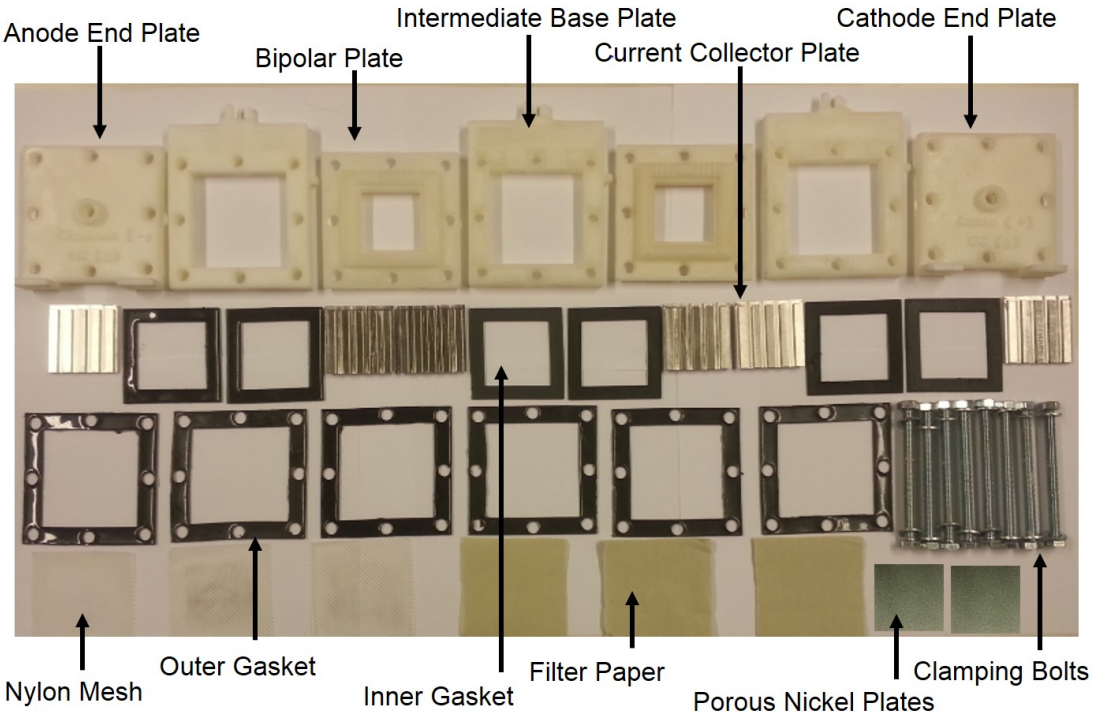

Figure 3.10: Basic practical parts of bipolar alkaline electrolysis stack

At last, all these practical parts are assembled together by keeping proper space between inside layers to form a bipolar electrolysis stack. Figure 3.11 is illustrated the proper arrangement of the inside parts of bipolar electrolysis stack using solidworks parts.

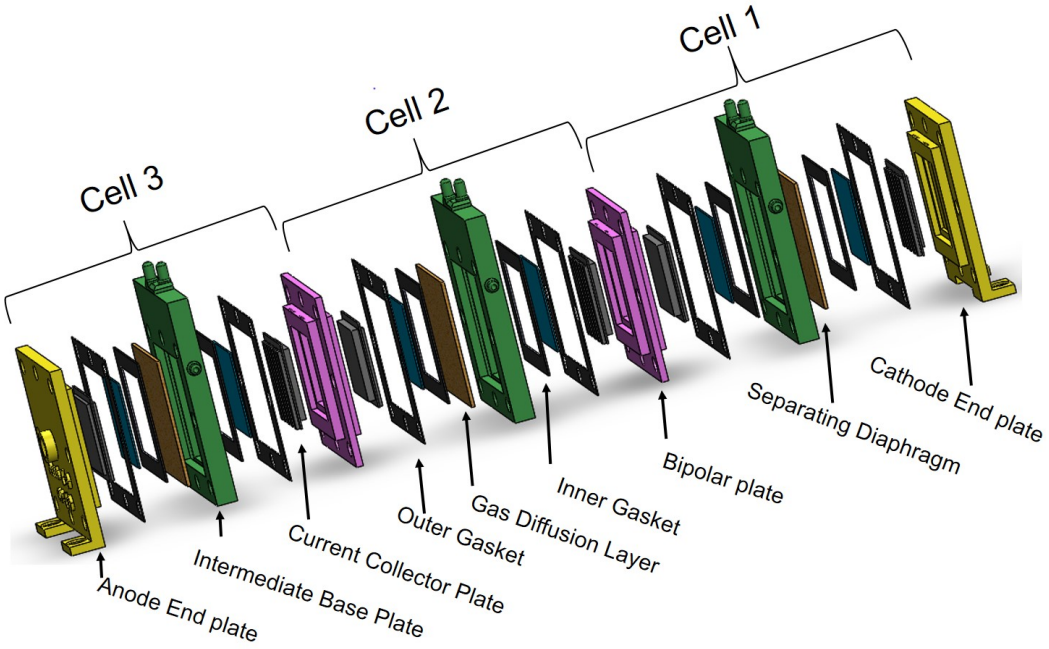

Figure 3.11: Basic SolidWorks parts of bipolar alkaline electrolysis stack

The final stage of bipolar alkaline electrolysis stack is shown in Figure 3.12.

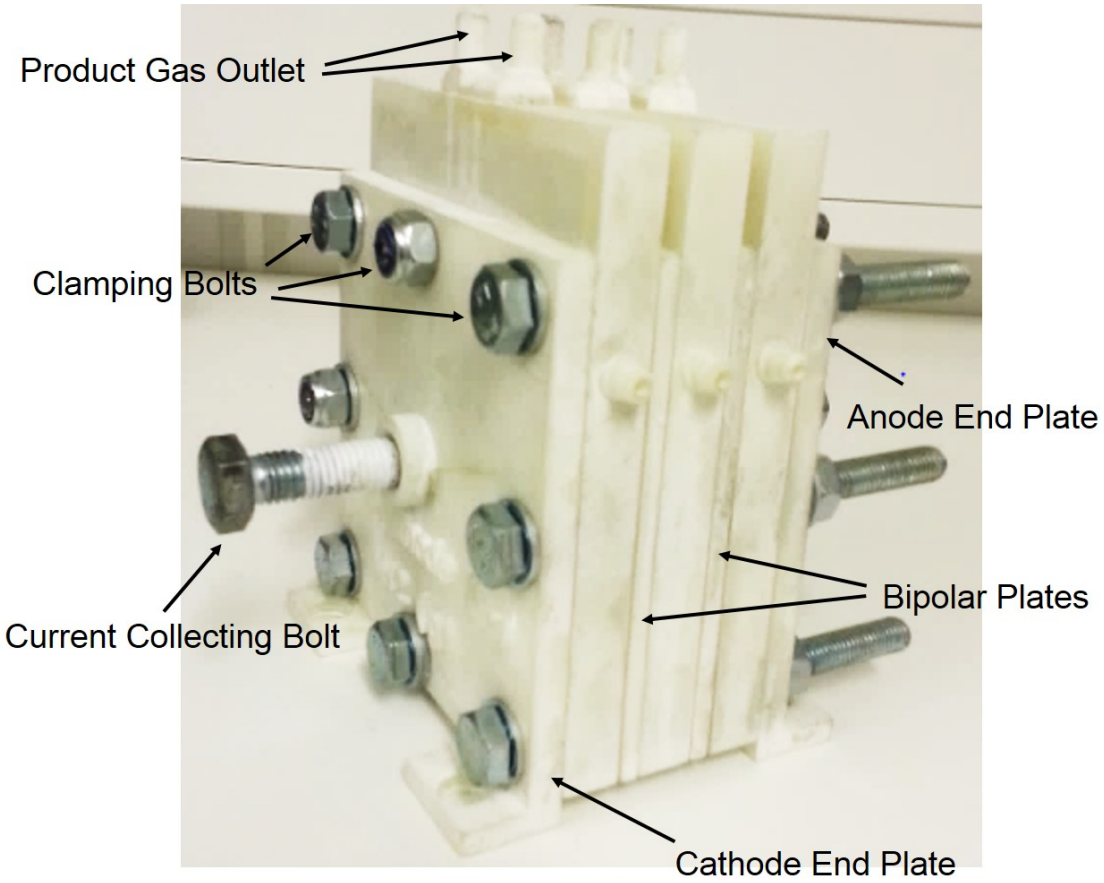

Figure 3.12: Final stage of the bipolar alkaline electrolysis stack

Chapter 4

Modeling of Alkaline Electrolyser

This chapter mainly presents the mathematical model of alkaline electrolyser. The electrochemical equations are the basic structure of the models, that take into consideration the main operational parameters of fuel cell such as the operational electrical current, voltage, temperature and cell area. The presented mathematical model has been implemented using MATLAB/SIMULINK and V-I and P-I characteristics are obtained for the relevant inputs.

4.1 Mathematical Model of Alkaline Electrolyser

The performance of alkaline electrolyser is typically compared by plotting its polarization curve (I-V characteristic curve), which is obtained by plotting the cell voltage against the current density. The polarization curve of typical alkaline electrolyser is shown in Figure 4.1.

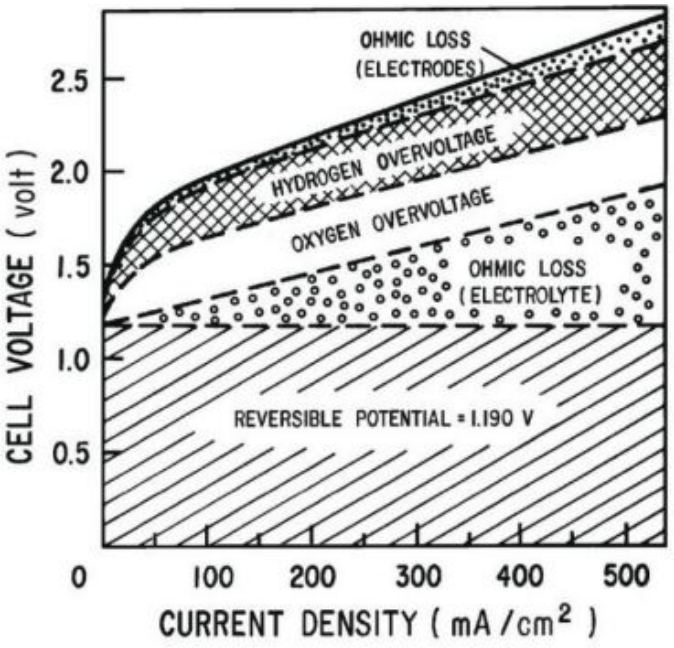

Figure 4.1: Polarization curves and distribution of cell voltage [3], [34]

According to the Figure 4.1, some primary sources are considered that increased the cell voltage (V_{cell}) over the reversible potential (V_{rev}). Hence it will cause the cell voltage to be higher than its reversible voltage. This is happened because of the irreversibly of the process. Such irreversibilities are mainly consisted in overvoltages that lower the efficiency of the cell [35]. Those primary sources can be listed as follows,

- Ohmic loss of electrolyte.
- Overvoltage associated with oxygen.
- Overvoltage associated with hydrogen.
- The ohmic loss caused by electric resistance of electrodes and circuitry.

The electrolysis cell voltage can be defined as the sum of the reversible voltage and the additional overvoltages that appear in the cell [11]. It defined as in equation 4.1.

$$V_{cell} = V_{rev} + V_{act} + V_{ohm} + V_{con} \tag{4.1}$$

Where, V_{rev} is the reversible cell voltage, V_{act} is activation overvoltage, V_{ohm} is the overvoltage caused by the ohmic losses and V_{con} is concentration overvoltage respectively.

4.1.1 Reversible Cell Voltage

The reversible cell voltage (V_{rev}) is the minimum voltage that required to take place the electrolysis. It can be determined by using the Gibbs equation which is given in equation 4.2 [36].

$$\Delta G = zFV_{rev} \tag{4.2}$$

Where ΔG is the Gibbs energy, z is number of electron and F is Faraday's Constant.

Gibbs equation can be rearranged to find reversible voltage as follows,

$$V_{rev} = \frac{\Delta G}{zF} \tag{4.3}$$

At standard condition (25 ° and 1 bar), the Gibbs energy for water splitting ($\Delta G°$) is equals to 237.2 kJ mol^{-1}[37] and Faraday's Constant equals to 96485 C mol^{-1}[36]. Moreover, the z is equals to 2. By substituting these values in the above equation, the V_{rev} can be calculated as in equation 4.5.

$$V_{rev} = \frac{237.2 \times 10^3}{2 \times 96485} \tag{4.4}$$

$$V_{rev} = 1.229V \tag{4.5}$$

4.1.2 Activation Overvoltage

The activation overvoltage (V_{act}) is generated owing to the electrochemical kinetics of the anode and cathode during simultaneous half-reactions. The electric charge transfer between the chemical species and the electrodes requires energy. This energy barrier that the charge has to overcome to go from the reactants to the electrodes or electrodes to reactants are highly depend on the catalytic properties of the electrode materials [11], [35]. It is generated an overvoltage across the electrode which is known as activation voltage. The V_{act} can be defined by following expression in equation 4.6.

$$V_{act} = slog\left(\frac{t_1 + \frac{t_2}{T} + \frac{t_3}{T^2}}{A} I + 1\right) \tag{4.6}$$

Where s, t_1, t_2, t_3 are the coefficient for overvoltage on electrodes, I is the current density, T is the temperature of the cell and A is the electrode area respectively [36], [37]. All the values and units of those constant are listed in Table 5.3.

4.1.3 Ohmic Phenomena

The overvoltage V_{ohm} is corresponded to the ohmic losses within the cell. These losses are produced by the resistance of cell elements such as electrodes, interconnection and separating diaphragm to the electrons flow [11], [35]. It can be reduced by shortening the distance between anode and cathode. Furthermore, V_{ohm} is mainly proportional to the electric current that flows through the cell. This overvoltage can be determined as in equation 4.7 [36].

$$V_{ohm} = \frac{r_1 + r_2 T}{A} I \tag{4.7}$$

Where r_1 and r_2 are parameter related to ohmic resistance of electrolyte [36], [37]. All the values and units of those constant are listed in Table 5.3.

4.1.4 Concentration Overvoltage

The concentration overvoltage (V_{con}), is caused by mass transport processes such as convection and diffusion. Usually in the case of alkaline electrolysis the V_{con} is much lower than V_{act} and V_{ohm}. Hence, in this modeling study the concentration overvoltage is neglected and the equation 4.1 can be rewritten as in equation 4.8.

$$V_{cell} = V_{rev} + V_{act} + V_{ohm} \tag{4.8}$$

4.1.5 Simulation Background

Table 5.3 is shown the values and units of all the constant parameters which is used in this modeling study. These data are taken from bibliography [36] and [37].

Table 4.1: Parameters for modeling study

CONSTANT PARAMETERS	SYMBOLS	UNITS	VALUE
Reversible Voltage	V_{rev}	V	1.229
Area of Electrode	A	cm^2	0.25
Faraday's Constant	F	$Cmol^{-1}$	96485
Number of Electrons	z		2
Coefficient for overvoltage on electrodes	s	V	0.185
Coefficient for overvoltage on electrodes	t_1	$A^{-1}m^2$	1.002
	t_2	$A^{-1}m^{2o}C$	8.424
	t_3	$A^{-1}m^{2o}C$	247.3
Parameter related to ohmic resistance of electrolyte	r_1	Ωm^2	$8.05e^{-5}$
	r_2	$\Omega m^{2o}C^{-1}$	$-2.5e^{-7}$

4.1.6 Mathematical Model in MATLAB SIMULINK

A mathematical model of the alkaline electrolyser has been developed in MATLAB/SIMULINK, based on the electrochemical characteristics of the electrolysis discussed in previous sections is shown in Figure 4.2. In this model, operating temperature (T)and cell area (A) are considered as inputs.

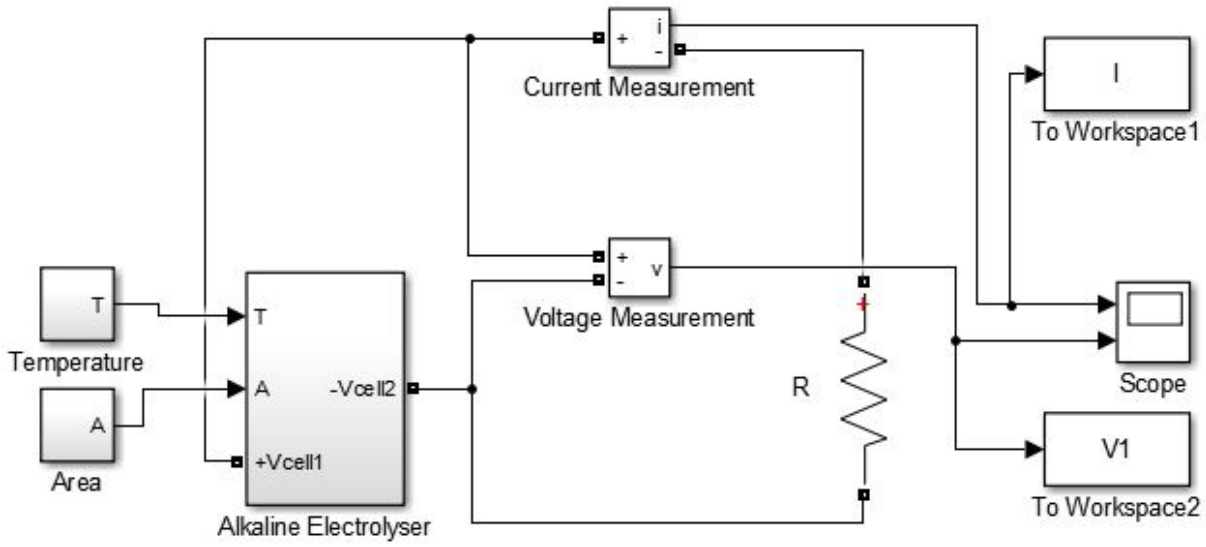

Figure 4.2: Mathematical model of alkaline electrolyser in SIMULINK

4.1.7 Characteristics of the Power and Voltage with Current of the Mathematical Model

The V-I characteristic of alkaline electrolyser is shown in Figure 4.3.

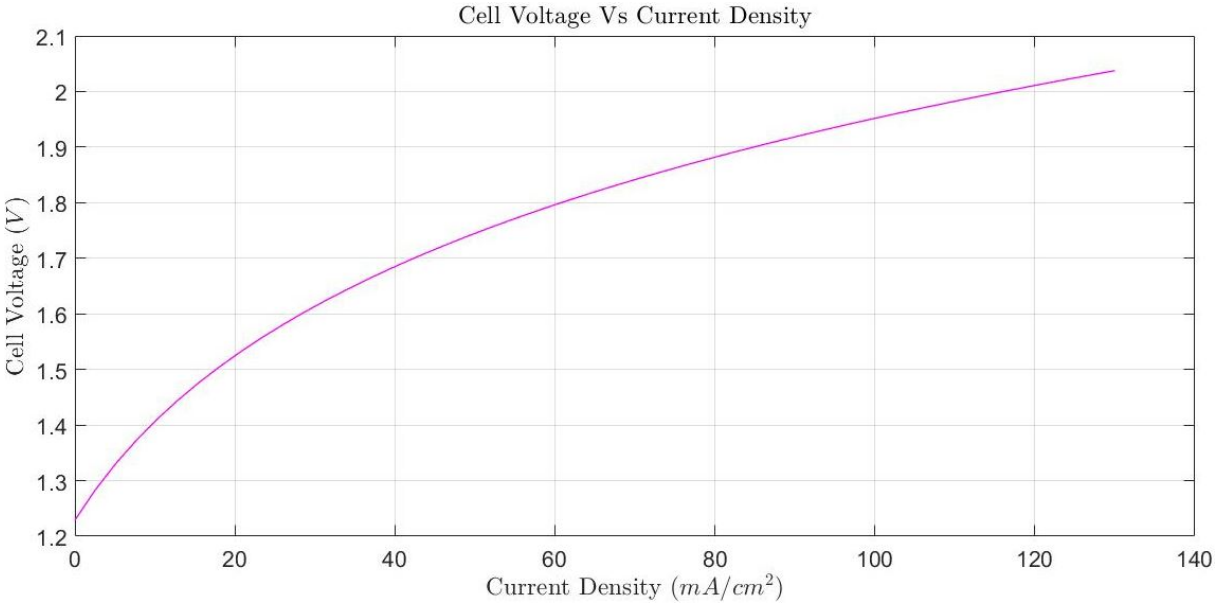

Figure 4.3: V-I characteristic of alkaline electrolyser

The P-I characteristic of alkaline electrolyser is shown in Figure 4.4.

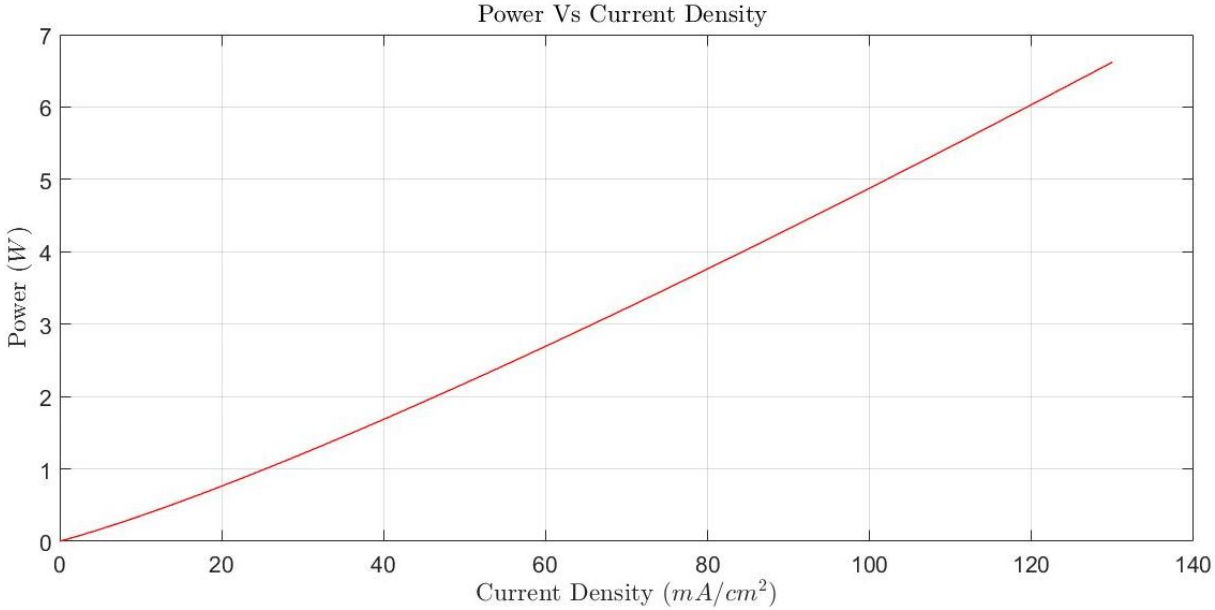

Figure 4.4: P-I characteristic of alkaline electrolyser

The cell voltage and overvoltage characteristics are illustrated in Figure 4.5. In order to get a better comparison between cell voltage and overvoltages, all the values of V_{ohm} are multiplied by a constant value of "-100". Since the V_{ohm} of this model are very small negative values.

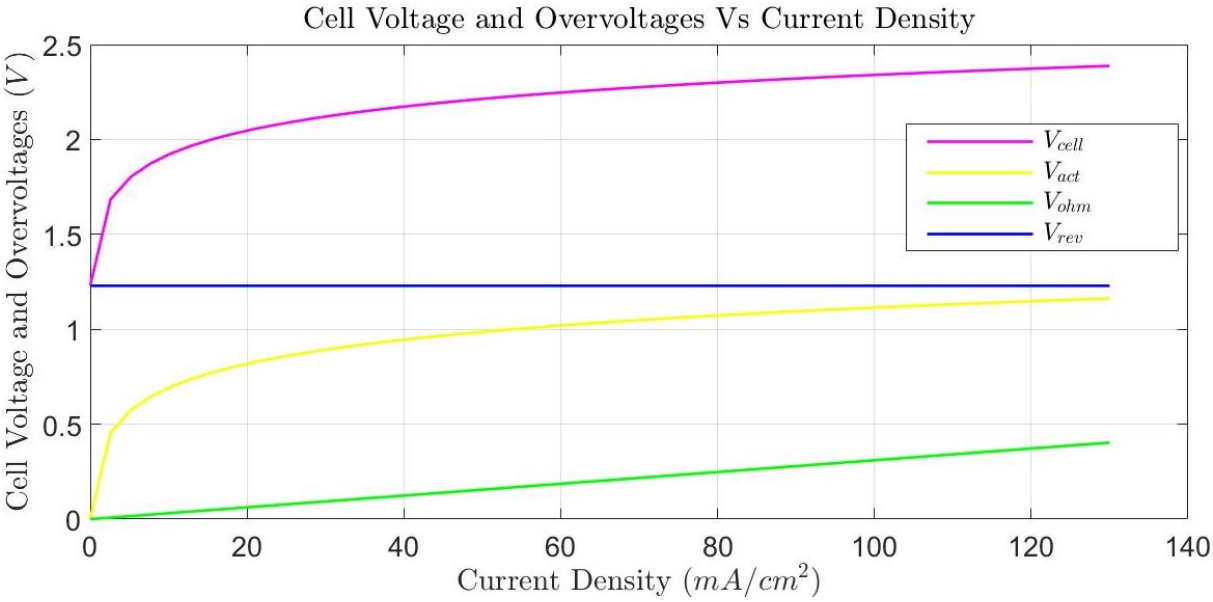

Figure 4.5: Cell voltage and overvoltages of alkaline electrolyser

Usually, the characteristics of electrolysis depend on the operating temperature. The polarization curves for different operating temperatures are illustrated in Figure 4.6.

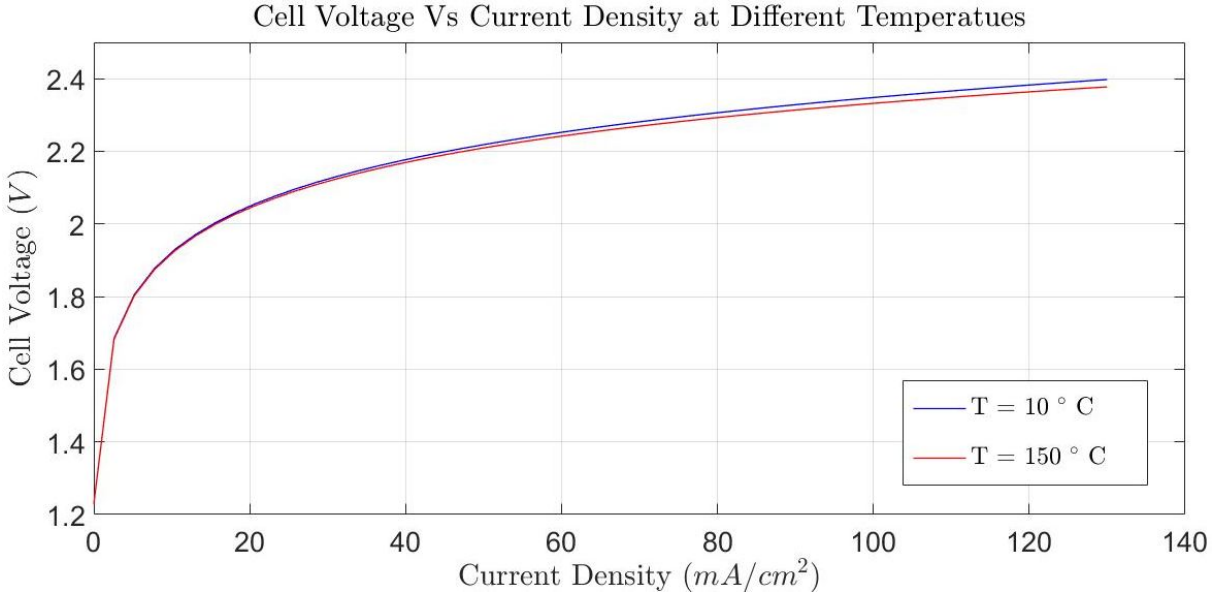

Figure 4.6: Polarization curves at different operating temperature

Chapter 5

Experiments and Results

This chapter illustrates the experimental results of the constructed single cell alkaline electrolyser, the monopolar electrolysis stack and the bipolar electrolysis stack. The apparatuses which are used for the experiments and the experimental procedures are described separately for each experiments in detail. Finally, the performances of both monopolar and bipolar alkaline electrolysis stack are compared with the mathematical model.

5.1 Experiment *I*: Model Start-up

Under this research project, several experiments have been done in order to fabricate a high performance compact alkaline electrolysis stack. Hence, the Experiment *I*, is done to examine the working principle of the electrolysis process. In this experiment, two porous nickel electrodes are immersed in the 30 wt% aqueous solutions of the KOH and the electric current is supplied through the power supply. Moreover, the experiment has been done without applying electrocatalyst to the electrodes. In the electrodes assembly, the separating paper and the nylon separator are placed in between the two electrodes and tied together to reduce the ohmic overvoltage. Figure 5.1 shows the electrodes assembly of the Experiment *I*.

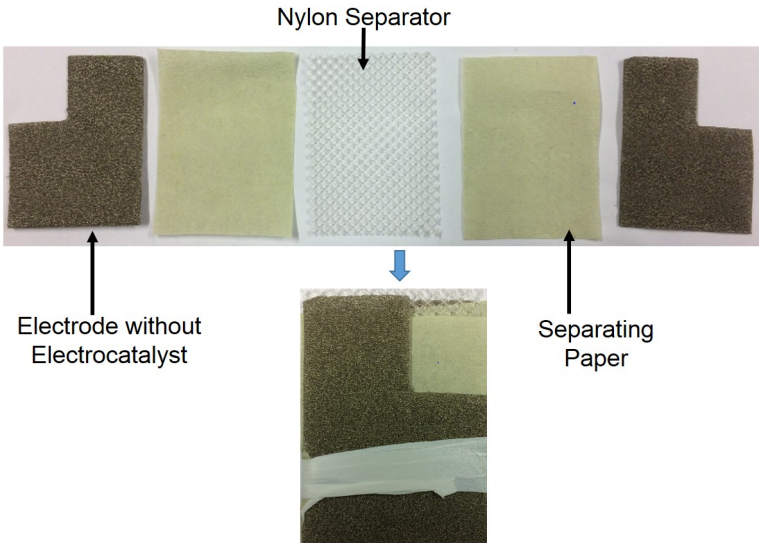

Figure 5.1: Electrodes assembly of the Experiment I

In order to take the results, the electrodes assembly is placed inside the KOH electrolyte solution which is prepared in the laboratory. The apparatuses that are used for the Experiment I is illustrated in Figure 5.2.

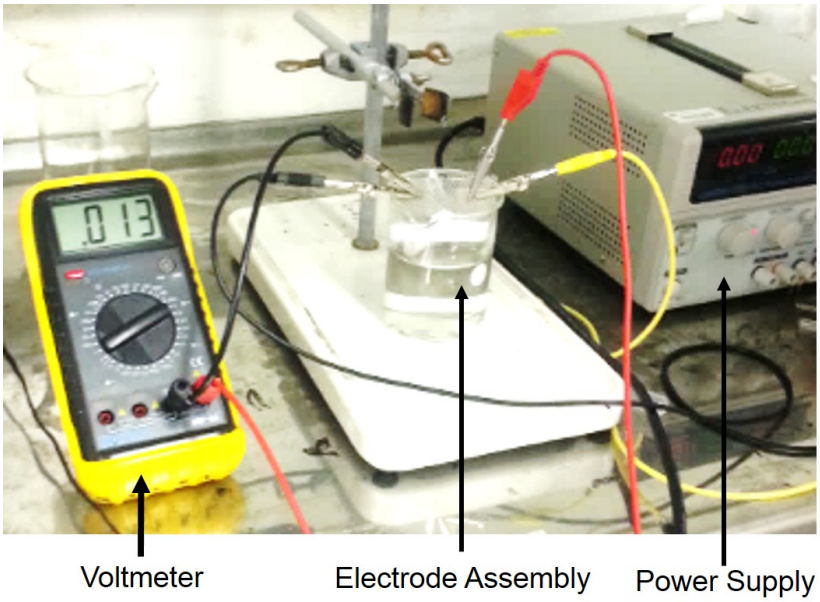

Figure 5.2: Bench setup of the Experiment I

5.1.1 I-V Characteristic Curve for Experiment *I*

The I-V characteristic curve of the Experiment I is presented in Figure 5.3 by using the voltage and the current values which are taken from the bench setup of Experiment I.

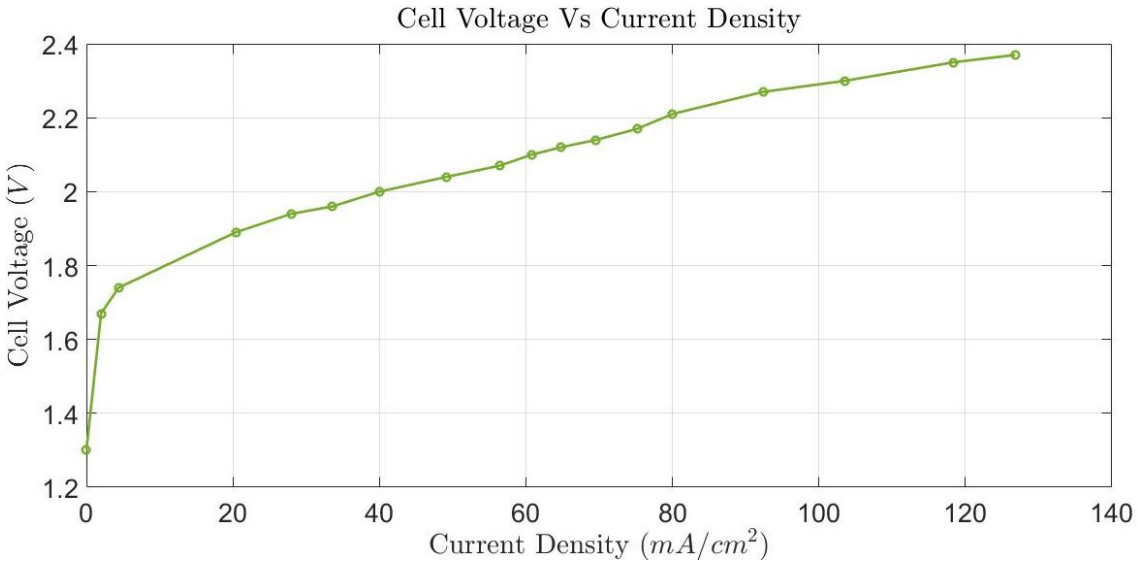

Figure 5.3: I-V characteristic curve of the Experiment I

5.2 Experiment *II*: Effect of Electrocatalyst for Electrochemical Reaction.

This experiment is almost similar to the Experiment *I*. In this experiment, the electrocatalyst is applied for the electrodes to increase the efficiency of the electrochemical process where it differs from Experiment *I*. The electrodes assembly which used in this experiment is shown in Figure 5.4.

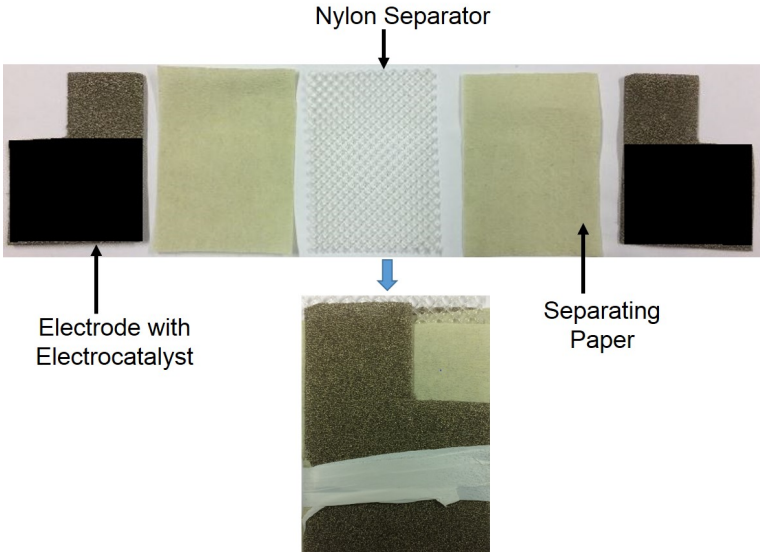

Figure 5.4: Electrodes assembly of the Experiment *II*

5.2.1 I-V Characteristic Curve for Experiment *II*

The I-V characteristic curve is drawn by using the voltage and the current values which are measured from the Experiment *II* as shown in Figure 5.5.

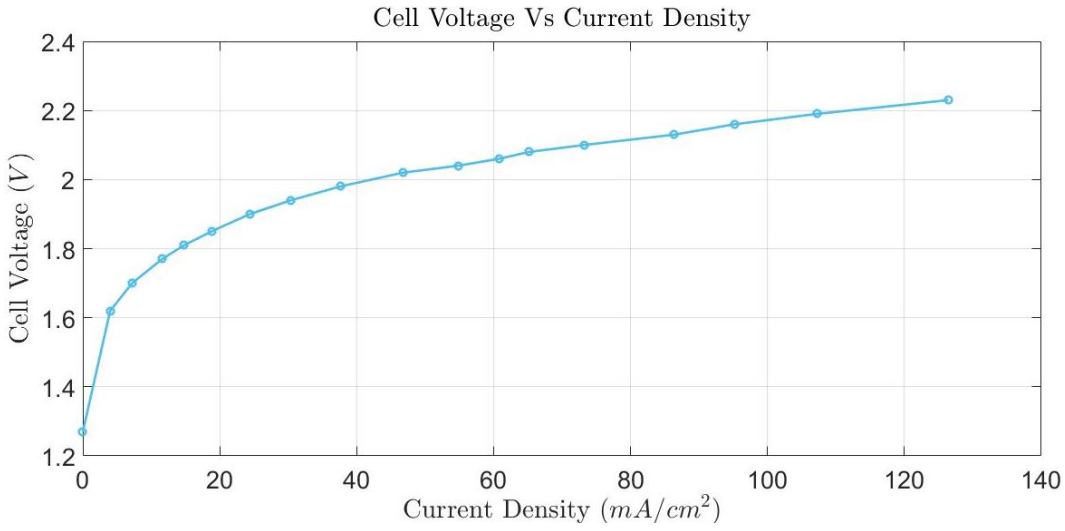

Figure 5.5: I-V characteristic curve of the Experiment *II*

5.2.2 Comparison of Results in Experiment *I* and Experiment *II* with Mathematical Model

The result comparison of the Experiment *I* and the Experiment *II* with the mathematical model is illustrated in Figure 5.6.

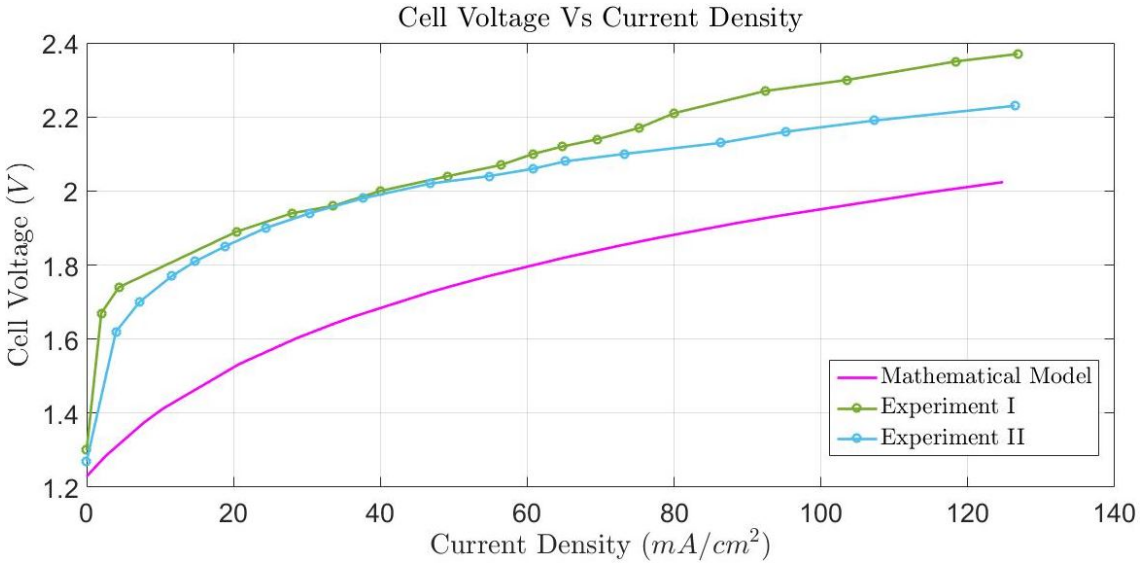

Figure 5.6: Comparison of the Experiment *I* and the Experiment *II* with the mathematical model

5.3 Important Theory Behind the Experimental Calculations

In this research study, several researches have been done in order to increase the performance of the electrolysis stack. Specially, the product gas flow rate, the power and the efficiency of the stack are considered to evaluate the performance of the stack. Hence, different equations are used to calculate these parameters and summarized in following subsections.

5.3.1 Equations for Flow Rate Calculation

Usually, the theoretical flow rate of the product gas can be calculated considering the Faraday's law of the electrolysis and the practical product gas flow rate can be calculated by using the measuring flask readings.

Faraday's Law of Electrolysis

The amount of substance (or number of moles) n can be defined by the following expression in Eq. 5.1 which is called as Faraday's law of electrolysis.

$$n = \frac{I \times t}{F \times z} \tag{5.1}$$

Where, I is the cell current in amperes, t is the time in seconds, F is the Faraday constant and z is the constant of proportionality called electrochemical equivalent (ECE). According to the electrochemical reaction of the alkaline electrolysis process, the value of z is taken as 2.

Ideal Gas Law

The theoretical product gas flow rate ($V_{H_2(g)}$ and $V_{O_2(g)}$) can be calculated by using the ideal gas law as in Eq. 5.2.

$$V_{H_2(g)} = V_{O_2(g)} = \frac{nRT}{P} \tag{5.2}$$

Where, R is the universal gas constant ($R = 0.082\,\mathrm{L\,atm\,K^{-1}\,mol^{-1}}$), P is operating pressure in atm and T is the operating temperature in K. The amount of substance "n" can be determined using Eq. 5.1 for both $H_2(g)$ and $O_2(g)$.

Equation for Practical Product Gas Flow Rate

The measuring flask reading can be used to measure the practical product gas flow rate as in Eq. 5.3.

$$V_{H_2(g)} = V_{O_2(g)} = \frac{v}{t} \times 60 \tag{5.3}$$

Where, v is the volume of measuring flask and t is the time required to fill the relevant volume of the measuring flask. Moreover, the 100 ml volume measuring flask is used throughout all the experiments to measure the product gas flow rate.

5.3.2 Equations for Power and Efficiency Calculation

The power and the efficiency calculation of the electrolysis cell is very important to observe the performance of the electrolysis cell. Thus, it is important to know the relevant equation for the power and the efficiency calculation.

Total Power

The power law can be used to calculate the total power of the cell as in Eq. 5.4.

$$P_{total} = V \times I \tag{5.4}$$

Where V is the cell voltage and I is the total current of the cell.

Ohmic Power

The power law can be rearranged to find the ohmic power (P_{ohmic}) by using the ohmic law. Hence, the ohmic power is defined as in Eq. 5.5.

$$V = I \times R$$

$$P_{ohmic} = I^2 \times R_{ohmic} \tag{5.5}$$

Where, R_{ohmic} is the ohmic resistance inside the cell. In general, the ohmic resistance is directly proportional to the distance between the anode and the cathode. Hence, it can be reduced by shortening the distance between the anode and the cathode. Moreover, the ohmic resistance of the cell can be determined by considering the gradient of the I-V characteristic curve.

Electrolysis Power

The electrolysis power can be calculated by taking the difference between the total power and the ohmic power. Thus, Eq. 5.6 represents the electrolysis power of the cell.

$$P_{electrolysis} = P_{total} - P_{ohmic} \tag{5.6}$$

Electrolysis Efficiency

At last, the electrolysis efficiency of the cell is determined as in Eq. 5.7.

$$\text{Elecrolysis Efficiency}(\eta) = \frac{P_{elecrolysis}}{P_{total}} \times 100\% \tag{5.7}$$

Energy Efficiency of the Cell

Even though, the energy efficiency of the electrolysis cell can be calculated by assuming theoretical Electromotive Force (EMF) value as 1.48 V. It is given in Eq. 5.8.

$$\text{Energy Efficiency of the Cell} = \frac{\text{Theoritycal EMF}}{\text{Cell Voltage}} \times 100\% \tag{5.8}$$

5.4 Experiment *III*: Collecting the Product Gas Using Designed Cell

In this experiment, the above mentioned electrodes (In Experiment *I* and Experiment *II*) are placed inside the cell frame to collect and measure the product gas flow rates. The experimental bench setup is shown in Figure 5.7.

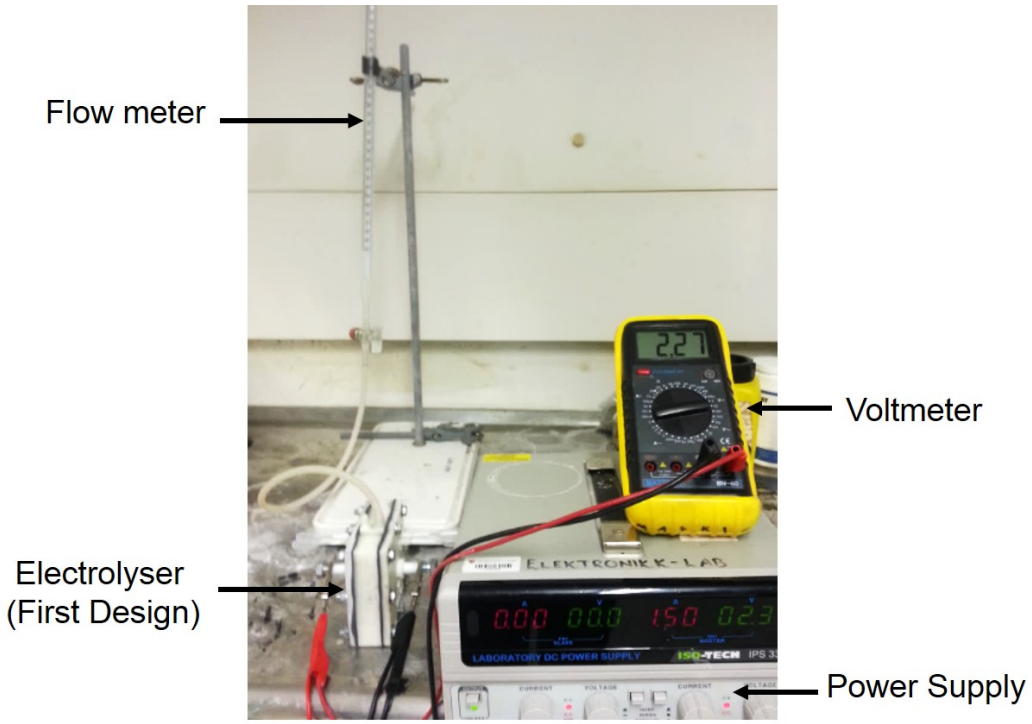

Figure 5.7: Test bench setup of the Experiment *III*

During the calculation, the flow meter reading is used to calculate the product gas flow rate instead of measuring flask reading as shown in the bench setup. The flow rate calculation data which are taken from the above test bench setup, are summarized in Table 5.1.

Table 5.1: Flow rate calculation data of the Experiment *III*

Product Gases	**Current Density(A)**	**Cell Voltage (V)**	**Time(s)**
Hydrogen ($H_2(g)$)	1.5	1.88	51
	2.5	2.07	30
	3.14	2.18	26
Oxygen ($O_2(g)$)	2.5	2.04	80
	3.14	2.18	66

5.4.1 Calculation of Hydrogen Gas Flow Rates ($V_{H_2}(g)$)

The maximum cell current value of 3.14 A is selected for the calculation. Moreover, Eq. 5.1 is used to calculate the number of hydrogen moles as follows.

$$n_{H_2(g)} = \frac{3.14\,\mathrm{C\,s^{-1}}}{96\,485\,\mathrm{C\,mol^{-1}} \times 2} = 9.7632 \times 10^{-4}\,\mathrm{mol\,min^{-1}}$$

Considering Eq. 5.2, assuming the pressure of 1 atm and the operating temperature of 27°C, the theoretical $V_{H_2(g)}$ can be determined as,

$$V_{H_2(g)} = \frac{n_{H_2(g)}RT}{P} = \frac{9.7632 \times 10^{-4}\,\mathrm{mol\,min^{-1}} \times 0.082\,\mathrm{L\,atm\,K^{-1}mol^{-1}} \times 1000\,\mathrm{ml\,L^{-1}} \times 300\,\mathrm{K}}{1\,\mathrm{atm}}$$

$$V_{H_2(g)} = 24.017\,\mathrm{cm^3\,min^{-1}}$$

The practical $V_{H_2(g)}$ again can be calculated considering the flow meter reading and using Eq. 5.3 as follows,

$$V_{H_2(g)} = \frac{10\,\mathrm{cm^3}}{27\,\mathrm{s}} \times \frac{60\,\mathrm{s}}{1\,\mathrm{min}} = 22.22\,\mathrm{cm^3\,min^{-1}}$$

5.4.2 Calculation of Oxygen Gas Flow Rate ($V_{O_2}(g)$)

The amount of substance for $O_2(g)$ can be determined by using either Eq. 5.1 or the electrochemical reaction of the alkaline electrolysis cell. According to the electrochemical reaction, the number of $O_2(g)$ moles should be half of $H_2(g)$ moles. Hence, the number of $O_2(g)$ moles can be easily determined as in Eq. 5.9.

$$n_{0_2(g)} = \frac{n_{H_2(g)}}{2} \tag{5.9}$$

$$n_{0_2(g)} = 4.8816 \times 10^{-4}\,\mathrm{mol\,min^{-1}}$$

Considering Eq. 5.2 and assuming the pressure of 1 atm and the operating temperature of 27°C , the theoretical $V_{O_2(g)}$ can be determined as follows.

$$V_{O_2(g)} = \frac{n_{O_2(g)}RT}{P} = \frac{4.8816 \times 10^{-4}\,\mathrm{mol\,min^{-1}} \times 0.082\,\mathrm{L\,atm\,K^{-1}mol^{-1}} \times 1000\,\mathrm{ml\,L^{-1}} \times 300\,\mathrm{K}}{1\,\mathrm{atm}}$$

$$V_{O_2(g)} = 12.01\,\mathrm{cm^3\,min^{-1}}$$

The experimental $V_{O_2(g)}$ again can be calculated considering the flow meter reading and using Eq. 5.3 as follows,

$$V_{O_2(g)} = \frac{10\,\mathrm{cm^3}}{66\,\mathrm{s}} \times \frac{60\,\mathrm{s}}{1\,\mathrm{min}} = 9.091\,\mathrm{cm^3\,min^{-1}}$$

5.4.3 Calculation of Power and Efficiency

The total power (P_{total}) of the single cell electrolyser can be calculated by considering the data in Table 5.1 and using an Eq. 5.4.

$$P_{total} = 2.18 \times 3.14 = 6.8452\,\mathrm{W}$$

According to the I-V characteristic curve of this experiment, the ohmic resistance can be determined as follows,

$$R_{ohm} = \frac{2.16 - 1.20}{3.0 - 0.1} = 0.331\,\Omega$$

Thus the ohmic power of the cell is given in Eq. 5.5.

$$P_{ohm} = I^2 \times R = 3.14^2 \times 0.331 = 3.264\,\mathrm{W}$$

Hence the electrolysis power of the cell can be defined as in Eq. 5.6.

$$P_{elecrolysis} = P_{total} - P_{ohm} = 3.5812\,\mathrm{W}$$

The electrolysis efficiency can be determined according to Eq. 5.7.

$$\text{Elecrolysis Efficiency}(\eta) = \frac{P_{elecrolysis}}{P_{total}} \times 100\% = 52.3\%$$

At last, the energy efficiency of the electrolysis cell can be calculated by assuming the theoretical EMF value as 1.48 V and using Eq. 5.8.

$$\text{Energy Efficiency of the Cell} = \frac{\text{Theoritycal EMF}}{\text{Cell Voltage}} \times 100\% = 67.9\%$$

5.4.4 I-V Characteristic Curve for Experiment *III*

The I-V characteristics curve for this experiment with measured data is illustrated in Figure 5.8.

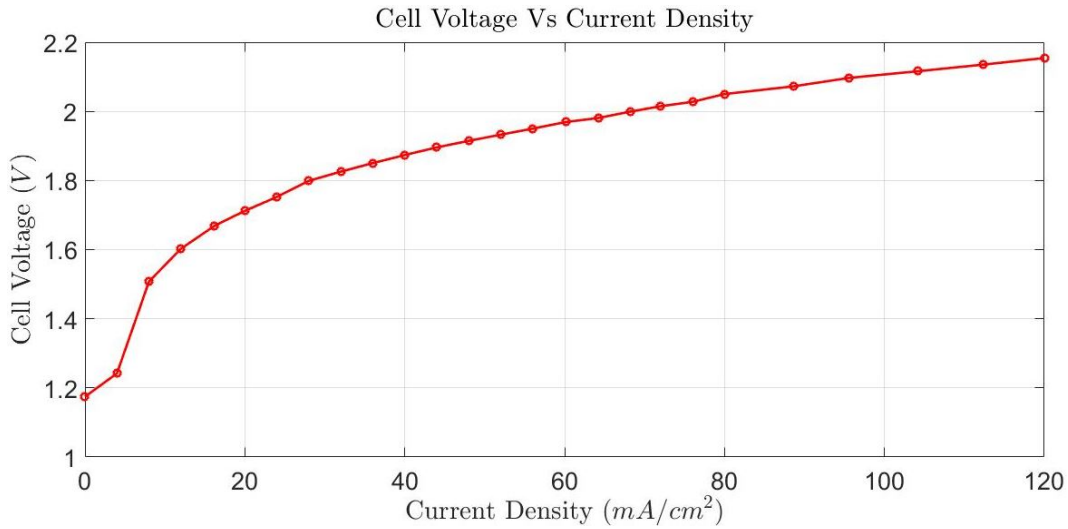

Figure 5.8: I-V characteristic of the Experiment *III*

5.5 Experiment *IV* : Increasing the Purity Level of Product Gas

The purity level of the product gas in the Experiment *III* is quite low owing to the water vapor. Hence, in this experiment, to increase the purity level of the product gases, the special storage tanks are designed top of the intermediate base plate. The apparatuses which are used for this experiment is shown in Figure 5.9.

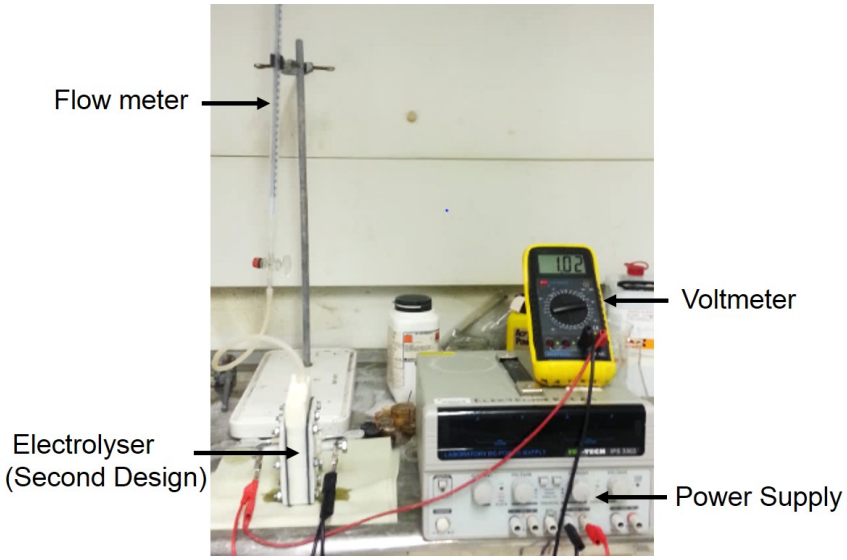

Figure 5.9: Test bench setup of the Experiment *IV*

In this experiment, the flow meter is used to measure the product gas flow rate instead of measuring flask as shown in the bench setup. The flow rate calculation data which are taken from the test bench setup, are given in Table 5.2.

Table 5.2: Flow rate calculation data of the Experiment *IV*

Product Gases	**Current Density(A)**	**Cell Voltage (V)**	**Time(s)**
Hydrogen ($H_2(g)$)	1.5	1.9	49
	2.5	2.07	28
	3.14	2.17	25
Oxygen ($O_2(g)$)	1.5)	1.9	113
	2.5	2.06	65
	3.14	2.13	55

5.5.1 Calculation of Hydrogen Gas Flow Rates ($V_{H_2(g)}$)

In this experiment also, the flow rate of the product gases can be determined by considering the Faraday's law of electrolysis and the flow meter reading as in Experiment *III*. Considering the cell current value as 3.14 A and using Eq. 5.1, the amount of substance n can be calculated as follows,

$$n_{H_2(g)} = \frac{3.14\,\mathrm{C\,s^{-1}}}{96\,485\,\mathrm{C\,mol^{-1}} \times 2} = 9.7632 \times 10^{-4}\,\mathrm{mol\,min^{-1}}$$

Considering Eq. 5.2 and assuming the pressure of 1 atm and the operating temperature of 27°C, the $V_{H_2(g)}$ can be determined as,

$$V_{H_2(g)} = \frac{n_{H_2(g)}RT}{P} = \frac{9.7632 \times 10^{-4}\,\mathrm{mol\,min^{-1}} \times 0.082\,\mathrm{L\,atm\,K^{-1}mol^{-1}} \times 1000\,\mathrm{ml\,L^{-1}} \times 300\,\mathrm{K}}{1\,\mathrm{atm}}$$

$$V_{H_2(g)} = 24.017\,\mathrm{cm^3\,min^{-1}}$$

The experimental $V_{H_2(g)}$ again can be calculated considering the flow meter reading and using Eq. 5.3 as follows,

$$V_{H_2(g)} = \frac{10\,\mathrm{cm^3}}{26\,\mathrm{s}} \times \frac{60\,\mathrm{s}}{1\,\mathrm{min}} = 23.07\,\mathrm{cm^3\,min^{-1}}$$

5.5.2 Calculation of Oxygen Gas Flow Rate ($V_{O_2(g)}$)

The amount of substance for $O_2(g)$ can be determined according to the Eq. 5.9 as in Experiment III.

$$n_{0_2(g)} = \frac{n_{H_2(g)}}{2} = 4.8816 \times 10^{-4}\,\mathrm{mol\,min^{-1}}$$

Considering the Eq. 5.2 and assuming the pressure of 1 *atm* and the operating temperature of 27°C, the theoretical $V_{O_2(g)}$ can be determined as follows,

$$V_{O_2(g)} = \frac{n_{O_2(g)}RT}{P} = \frac{4.8816 \times 10^{-4}\,\text{mol}\,\text{min}^{-1} \times 0.082\,\text{L}\,\text{atm}\,\text{K}^{-1}\text{mol}^{-1} \times 1000\,\text{ml}\,\text{L}^{-1} \times 300\,\text{K}}{1\,\text{atm}}$$

$$V_{O_2(g)} = 12.01\,\text{cm}^3\,\text{min}^{-1}$$

The experimental $V_{O_2(g)}$ again can be calculated considering flow meter reading and using Eq. 5.3 as follows,

$$V_{H_2(g)} = \frac{10\,\text{cm}^3}{55\,\text{s}} \times \frac{60\,\text{s}}{1\,\text{min}} = 10.91\,\text{cm}^3\,\text{min}^{-1}$$

5.5.3 Calculation of Power and Efficiency

The total power (P_{total}) of the single cell electrolyser can be calculated by considering the data in Table 5.2 and using Eq. 5.4.

$$P_{total} = 2.13 \times 3.14 = 6.6882\,\text{W}$$

According to the I-V characteristic curve of this experiment, the ohmic resistance can be determined as follows,

$$R_{ohm} = \frac{2.14 - 1.49}{3.14 - 0.3} = 0.229\,\Omega$$

Thus the ohmic power of the cell is given in Eq. 5.5.

$$P_{ohm} = I^2 \times R = 3.14^2 \times 0.229 = 2.257\,\text{W}$$

Hence the electrolysis power of the cell can be defined as in Eq. 5.6.

$$P_{elecrolysis} = P_{total} - P_{ohm} = 4.432\,\text{W}$$

The electrolysis efficiency can be determined according to the Eq. 5.7.

$$\text{Elecrolysis Efficiency}(\eta) = \frac{P_{elecrolysis}}{P_{total}} \times 100\% = 66.26\%$$

At last, the energy efficiency of the electrolysis cell can be calculated by assuming theoretical EMF value as 1.48 V and using Eq. 5.8.

$$\text{Energy Efficiency of the Cell} = \frac{\text{Theoritycal EMF}}{\text{Cell Voltage}} \times 100\% = 69.5\%$$

5.5.4 I-V Characteristic Curve of Experiment *IV*

The I-V characteristic curve for this experiment is illustrated in Figure 5.10.

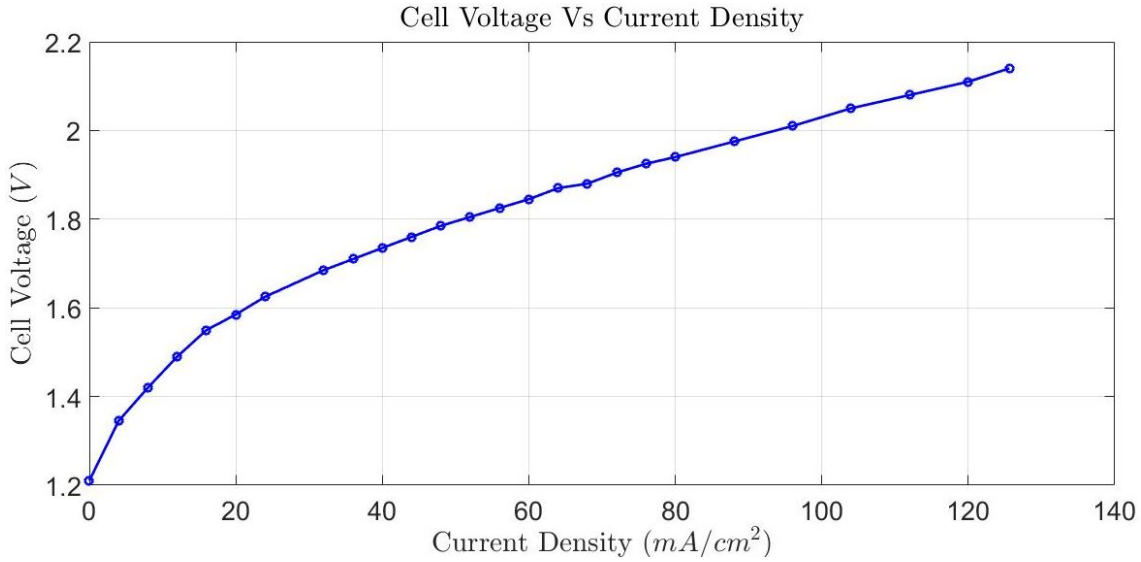

Figure 5.10: I-V characteristic of the Experiment *IV*

5.5.5 Comparison of Results in Experiment *III* and Experiment *IV* with Mathematical Model

In order to compare the results of the Experiment *III* and the Experiment *IV* with the mathematical model, all the I-V characteristic curves are drawn in the same graph as shown in Figure 5.11.

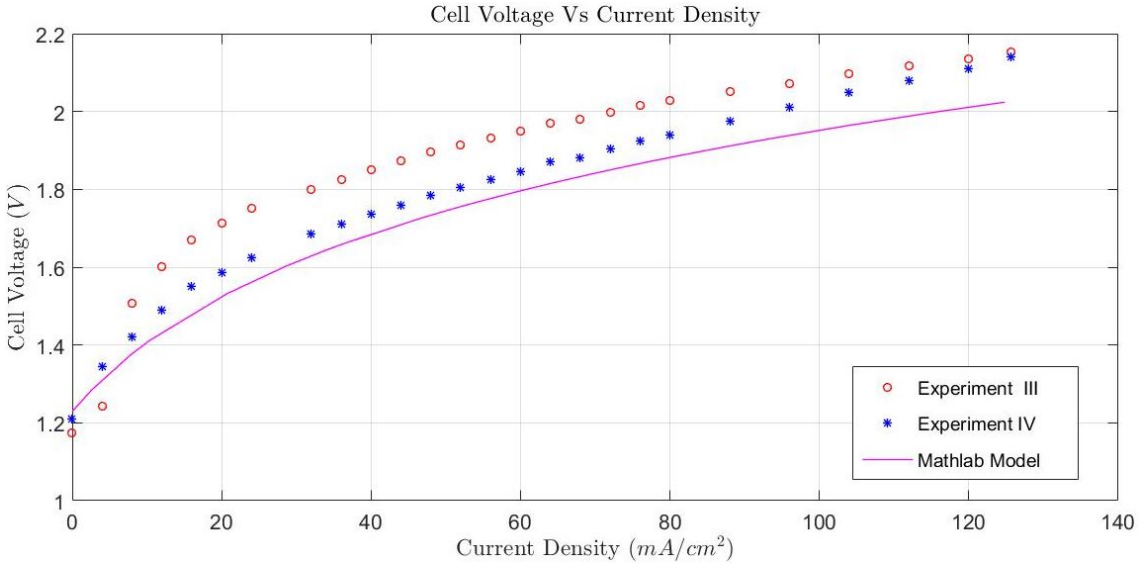

Figure 5.11: Comparison of the Experiment *III* and the Experiment *IV* with the mathlab model

5.6 Experiment *V* : Increasing Number of Electrodes in Anode and Cathode Side

According to the calculations of the Experiment *III* and the Experiment *IV*, the electrolysis cell which is used in the Experiment *IV* (Design 2) has a better performance than the Experiment *III* (design 1). Thus, the second design of the alkaline electrolyser is selected for the stack. Even though, the efficiency of that cell (66.26 %) is not enough for the stack. Hence, in order to increase the efficiency of the cell, few improvements have been done. Thus, those improvements will be explained in the Experiment *V* to the Experiment *IX* in detail.

Under this experiment, the number of porous nickel plates in the anode and the cathode side are increased as the first improvement. Thus, six porous nickel plates are adopted for both sides of the anode and the cathode. Figure 5.12 illustrates the bench setup of the Experiment *V*.

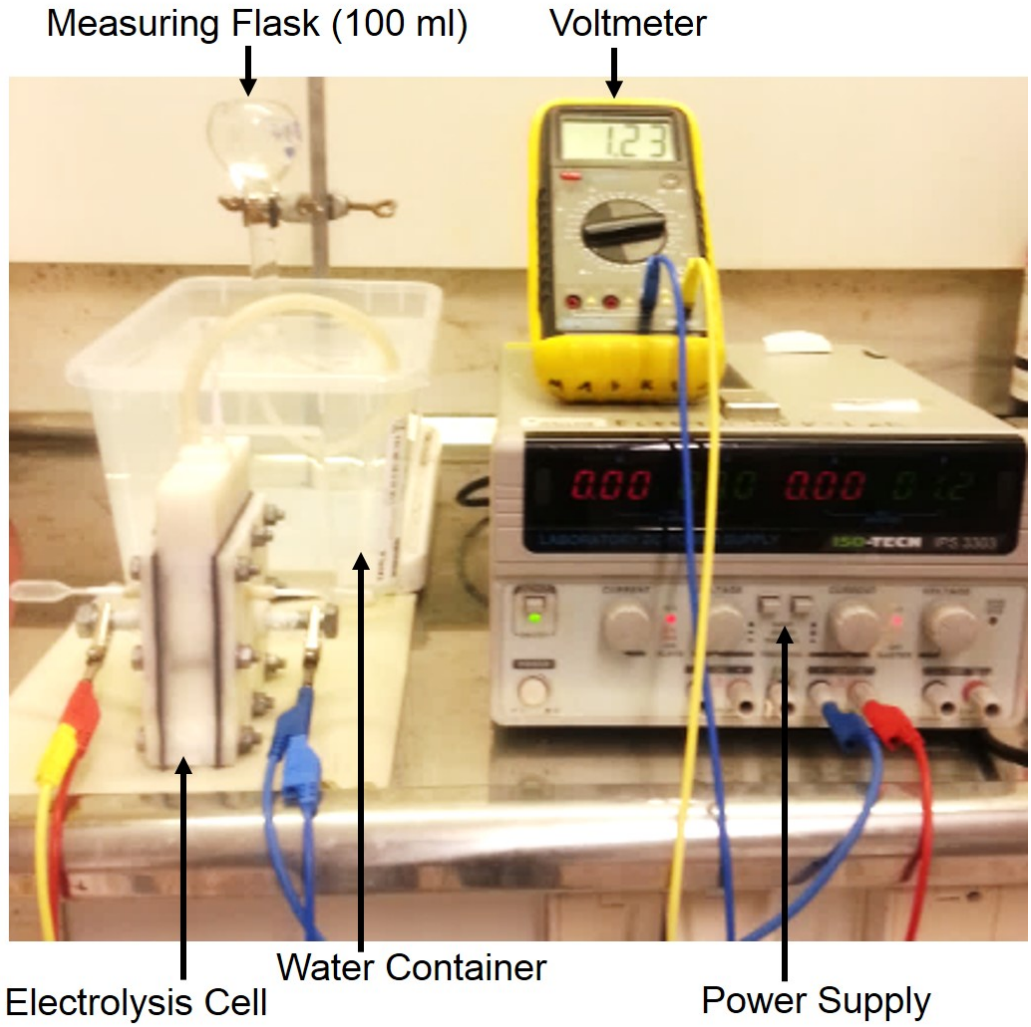

Figure 5.12: Bench setup of the Experiment *V*

The 100 ml volume measuring flask is selected for this experiment instead of the flow meter to increase the accuracy of the measurement. The flow rate calculation data which is obtained from the test bench setup, are given in Table 5.3.

Table 5.3: Flow rate calculation data of the Experiment *V*

Product Gases	**Current Density(A)**	**Cell Voltage (V)**	**Time(s)**
Hydrogen ($H_2(g)$)	2.5	2.03	301
	3.14	2.1	260
Oxygen ($O_2(g)$)	2.5	2.06	672
	3.14	2.1	554

5.6.1 Calculation of Product Gas Flow Rate

In this experiment, the calculation is done using the maximum cell current value of 3.14 A. Thus, the theoretical flow rates of $H_2(g)$ and $O_2(g)$ are remained unchanged as in the previous experiments. Hence, the theoretical hydrogen and oxygen gas flow rates can be determined by using Eq. 5.1 and Eq. 5.2 as $24.017\,\mathrm{cm^3\,min^{-1}}$ and $12.0085\,\mathrm{cm^3\,min^{-1}}$ respectively. Moreover, the experimental flow rates of $H_2(g)$ and $O_2(g)$ can be determined using the measuring flask readings and Eq. 5.3 as follows,

$$V_{H_2(g)} = \frac{100\,\mathrm{cm^3}}{260\,\mathrm{s}} \times \frac{60\,\mathrm{s}}{1\,\mathrm{min}} = 23.077\,\mathrm{cm^3\,min^{-1}}$$

$$V_{O_2(g)} = \frac{100\,\mathrm{cm^3}}{554\,\mathrm{s}} \times \frac{60\,\mathrm{s}}{1\,\mathrm{min}} = 10.83\,\mathrm{cm^3\,min^{-1}}$$

5.6.2 Calculation of Power and Efficiency

The total power of the cell can be determined considering Eq. 5.4.

$$P_{total} = 2.1 \times 3.14 = 6.594\,\mathrm{W}$$

According to the I-V characteristic curve of the Experiment *V*, the ohmic resistance of the cell can be calculated as follows,

$$R_{ohm} = \frac{2.1 - 1.47}{3.14 - 0.1} = 0.207\,\Omega$$

Eq. 5.5 can be used to calculate the ohmic power of the cell.

$$P_{ohm} = I^2 \times R = 3.14^2 \times 0.207 = 2.0433\,\mathrm{W}$$

Hence the electrolysis power of the cell can be defined as in Eq. 5.6.

$$P_{elecrolysis} = P_{total} - P_{ohm} = 4.5507\,\mathrm{W}$$

The electrolysis efficiency of the cell can be determined by considering Eq. 5.7.

$$\text{Elecrolysis Efficiency}(\eta) = \frac{P_{elecrolysis}}{P_{total}} \times 100\% = 69.01\%$$

At last, the energy efficiency of the electrolysis cell can be calculated by assuming the theoretical EMF value as 1.48 V and using Eq. 5.8.

$$\text{Energy Efficiency of the Cell} = \frac{\text{Theoritycal EMF}}{\text{Cell Voltage}} \times 100\% = 70.5\%$$

5.6.3 I-V Characteristic Curve of Experiment *V*

The I-V characteristic curve of the Experiment V is illustrated in Figure 5.13.

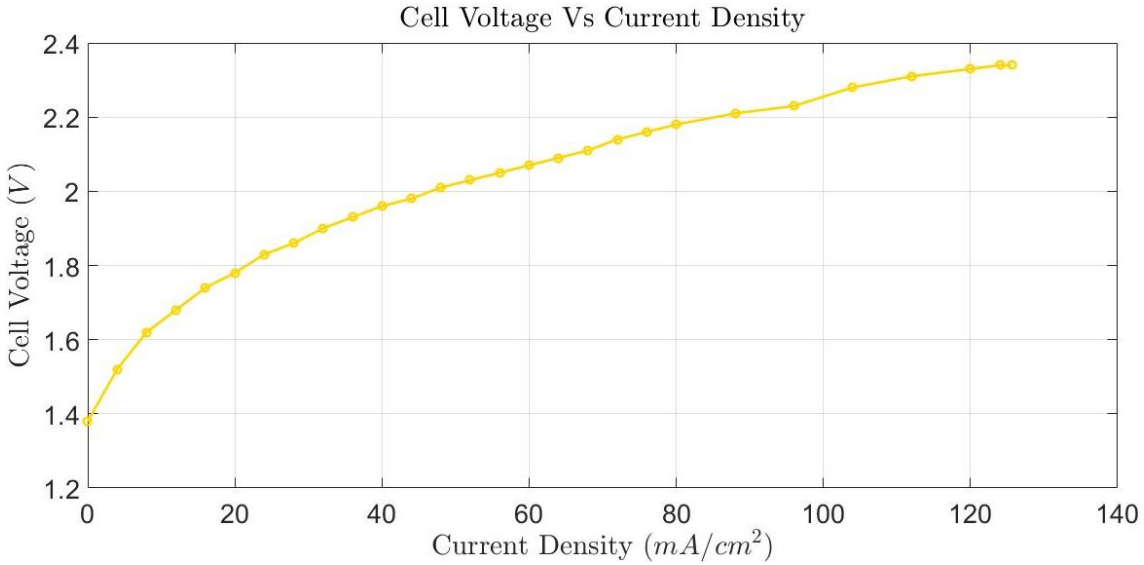

Figure 5.13: I-V characteristic of the Experiment V

5.7 Experiment *VI* : Effect of Anode and Cathode Distance for Electrolysis process

The distance between the anode and the cathode is a significant fact to change the power and the efficiency of the electrolysis cell. Usually, by shortening the distance between the anode and the cathode, the power and the efficiency can be increased while reducing the ohmic loss. Hence, few experiments have been done by changing the gap between the anode and the cathode to observe the effect of the anode and the cathode distance for the electrolysis process.

5.7.1 Experiment *A* : Separating Diaphragm with 2.5 mm Thickness

Usually, in this experiment, the separating diaphragm consists of nylon mesh with a 1 mm thickness and 0.15 mm thick filter papers. In this experiment one nylon mesh and ten filter papers are used as the separating diaphragm. Hence, the whole thickness of the separating diaphragm becomes 2.5 mm. This thickness is directly equal to the anode and the cathode distance.

Moreover, the same bench setup is used in this experiment as in the Experiment V and the flow rate calculation data of the Experiment A is given in Table 5.4.

Table 5.4: Flow rate calculation data of the Experiment A

Product Gases	**Current Density(A)**	**Cell Voltage (V)**	**Time(s)**
Hydrogen ($H_2(g)$)	3.14	2.34	244
Oxygen ($O_2(g)$)	3.14	2.34	512

The same calculations are repeated as in the previous experiments. Hence, all the calculated parameters are illustrated in Table 5.5.

Table 5.5: Calculated parameters of the Experiment A

Flow Rates Calculation		**Power and Efficiency Calculation**	
Cell Current (A)	3.14	Cell Voltage(V)	2.34
$n_{H_2(g)}(mol/min)$	9.7632×10^{-4}	$P_{total}(W)$	7.0336
$n_{O_2(g)}(mol/min)$	4.8816×10^{-4}	$R_{ohmic}(\Omega)$	0.27
$V_{H_2(g)(Theo)(cm^3/min)}$	24.017	$P_{ohmic}(W)$	2.66
$V_{O_2(g)(Theo)(cm^3/min)}$	12.01	$P_{electrolysis}(W)$	4.3741
$V_{H_2(g)(Exp)(cm^3/min)}$	22.73	$\eta_{electrolysis}(\%)$	62.18
$V_{O_2(g)(Exp)(cm^3/min)}$	11.72	$\eta_{energy}(\%)$	63.25

At last, the I-V characteristic curve of the Experiment A is given in Figure 5.14.

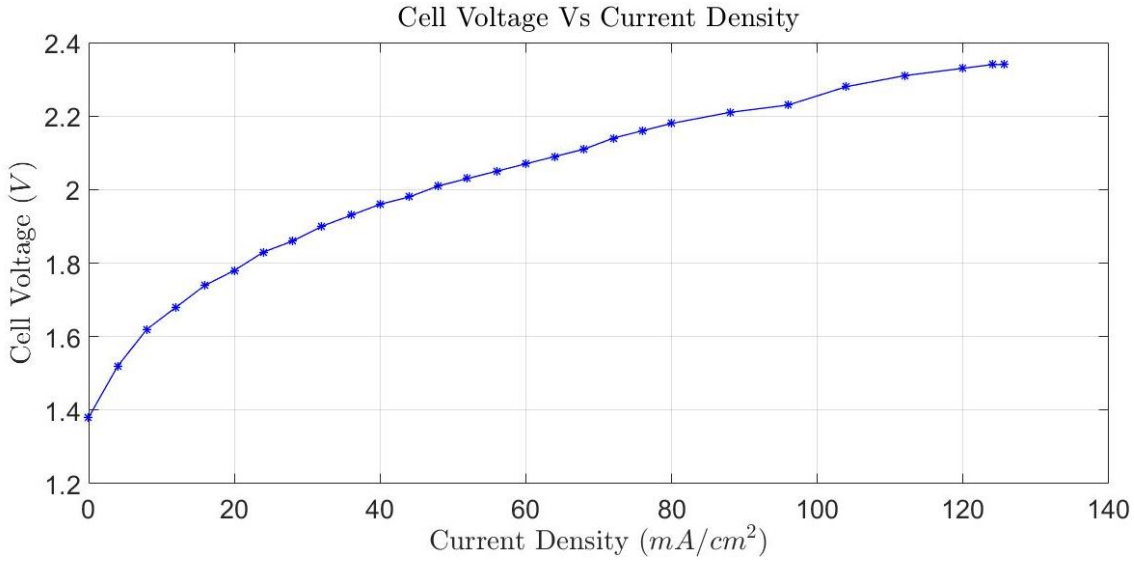

Figure 5.14: I-V characteristic of the Experiment A

5.7.2 Experiment *B* : Separating Diaphragm with 1.9 mm Thickness

In this experiment, the separating diaphragm consists of one nylon mesh and six filter papers. Thus, the entire thickness of the separating diaphragm becomes 1.9 mm. Further, the same bench setup is adopted for this experiment as in the Experiment *V* and the flow rate calculation data of the Experiment *B* is shown in Table 5.6.

Table 5.6: Flow rate calculation data of the Experiment *B*

Product Gases	**Current Density(A)**	**Cell Voltage (V)**	**Time(s)**
Hydrogen ($H_2(g)$)	2.5	2.02	310
	3.14	2.12	251
Oxygen ($O_2(g)$)	2.5	2.02	627
	3.14)	2.12	494

The same calculation steps are repeated in this experiment. Thus, all the calculated parameters are given in Table 5.7.

Table 5.7: Calculated parameters of the Experiment *B*

Flow Rates Calculation		**Power and Efficiency Calculation**	
Cell Current (A)	3.14	Cell Voltage(V)	2.12
$n_{H_2(g)}(mol/min)$	9.7632×10^{-4}	$P_{total}(W)$	6.6568
$n_{O_2(g)}(mol/min)$	4.8816×10^{-4}	$R_{ohmic}(\Omega)$	0.234
$V_{H_2(g)(Theo)(cm^3/min)}$	24.017	$P_{ohmic}(W)$	2.303
$V_{O_2(g)(Theo)(cm^3/min)}$	12.01	$P_{electrolysis}(W)$	4.3541
$V_{H_2(g)(Exp)(cm^3/min)}$	23.9	$\eta_{electrolysis}(\%)$	65.4
$V_{O_2(g)(Exp)(cm^3/min)}$	11.76	$\eta_{energy}(\%)$	69.8

Figure 5.15 is illustrated the I-V characteristic curve of Experiment *B*.

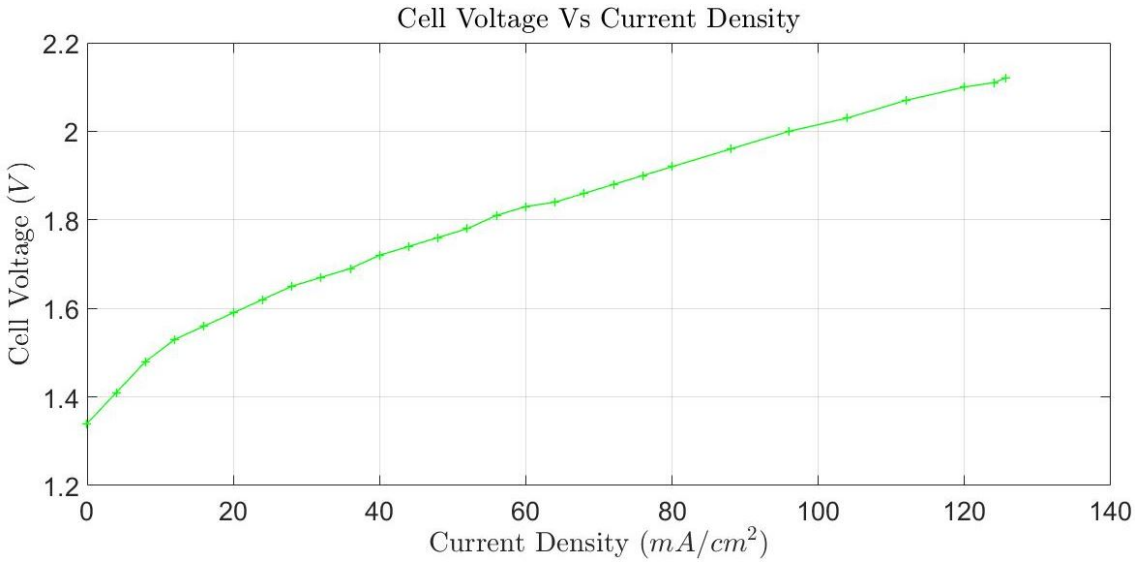

Figure 5.15: V-I characteristic of the Experiment *B*

5.7.3 Experiment *C* : Separating Diaphragm with 1.3 mm Thickness

The separating diaphragm of this experiment consists of one nylon mesh and two filter papers. Hence, the thickness of the separating diaphragm becomes 1.3 mm. Moreover, the same bench setup is used in this experiment as in the Experiment *V* and the flow rate calculation data of the Experiment *C* is illustrated in Table 5.8.

Table 5.8: Flow rate calculation data of the Experiment *C*

Product Gases	**Current Density(A)**	**Cell Voltage (V)**	**Time(s)**
Hydrogen ($H_2(g)$)	2.5	1.98	300
	3.14	2.04	250
Oxygen ($O_2(g)$)	2.5	1.98	588
	3.14)	2.04	505

In this experiment, same calculations are repeated. Hence, all the calculated parameters are listed in Table 5.9.

Table 5.9: Calculated parameters of the Experiment C

Flow Rates Calculation		**Power and Efficiency Calculation**	
Cell Current (A)	3.14	Cell Voltage(V)	2.04
$n_{H_2(g)}(mol/min)$	9.7632×10^{-4}	$P_{total}(W)$	6.4056
$n_{O_2(g)}(mol/min)$	4.8816×10^{-4}	$R_{ohmic}(\Omega)$	0.194
$V_{H_2(g)(Theo)(cm^3/min)}$	24.017	$P_{ohmic}(W)$	1.914
$V_{O_2(g)(Theo)(cm^3/min)}$	12.01	$P_{electrolysis}(W)$	4.4921
$V_{H_2(g)(Exp)(cm^3/min)}$	24	$\eta_{electrolysis}(\%)$	70.13
$V_{O_2(g)(Exp)(cm^3/min)}$	11.88	$\eta_{energy}(\%)$	72.5

At last, the I-V characteristic curve of the Experiment C is shown in Figure 5.16.

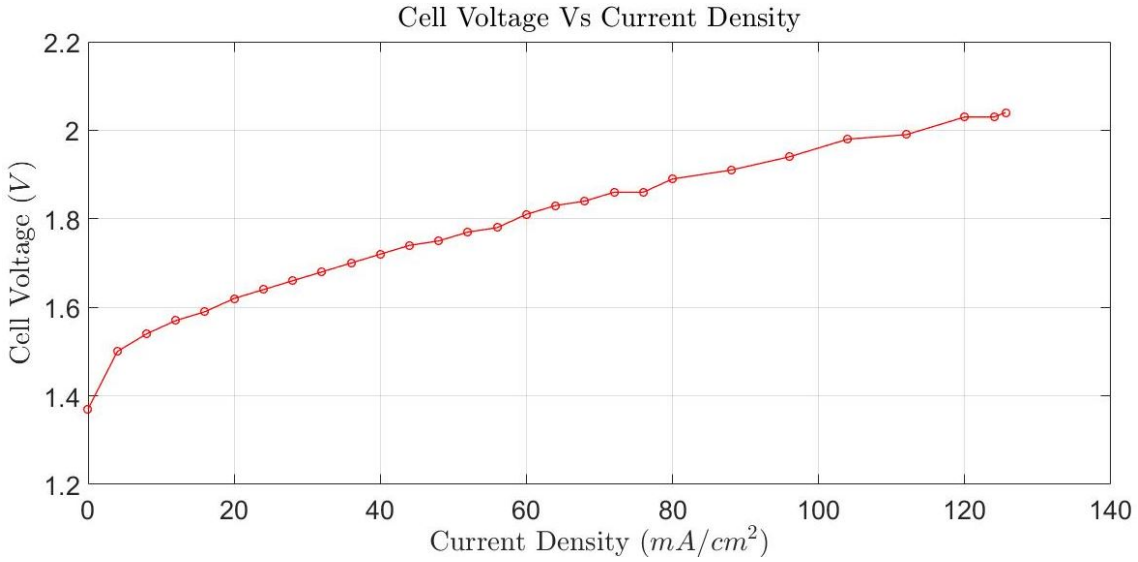

Figure 5.16: I-V characteristic of the Experiment C

5.7.4 Comparison of Experiments *A*, *B* and *C* with Matlab Model

To compare the results of the Experiments A, B and C with the Matlab model, all the I-V characteristic curves are illustrated in the same graph as shown in Figure 5.17.

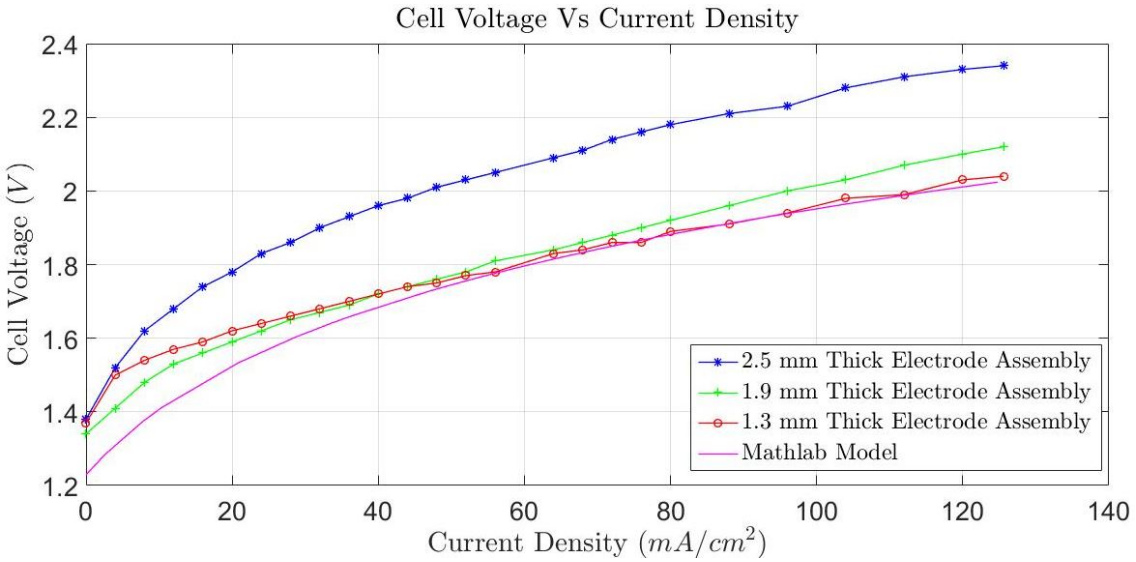

Figure 5.17: Comparison of the Experiments *A*, *B* and *C* with the matlab model

5.8 Experiment *VII*: Electrolysis Cell with Polymeric Membrane Separator

In this experiment, only one polymeric membrane is employed as a separating diaphragm. The same bench setup is used to observe the flow rate calculation data as in the Experiment *V*. Moreover, the same experiment is conducted for both Nafion 115 (N 115) and Nafion 117 (N 117) membranes separately.

5.8.1 Electrolysis cell with N 115 Membrane

The N 115 membrane is used as a separating diaphragm in this experiment. The flow rate, the power and the efficiency calculation data are given in Table 5.10.

Table 5.10: Flow rate calculation data of the N 115 membrane

Product Gases	**Current Density(A)**	**Cell Voltage (V)**	**Time(s)**
Hydrogen ($H_2(g)$)	3.1	3.73	278
Oxygen ($O_2(g)$)	3.1	3.73	553

The calculated parameters of this experiment are illustrated in Table 5.11. Since, the same calculation steps are repeated in this experiment as in the previous experiments.

Table 5.11: Calculated parameters of the N 115 membrane

Flow Rates Calculation		**Power and Efficiency Calculation**	
Cell Current (A)	3.1	Cell Voltage(V)	3.73
$n_{H_2(g)}(mol/min)$	9.6388×10^{-4}	$P_{total}(W)$	11.563
$n_{O_2(g)}(mol/min)$	4.8194×10^{-4}	$R_{ohmic}(\Omega)$	0.782
$V_{H_2(g)(Theo)(cm^3/min)}$	23.71	$P_{ohmic}(W)$	7.512
$V_{O_2(g)(Theo)(cm^3/min)}$	11.86	$P_{electrolysis}(W)$	4.0512
$V_{H_2(g)(Exp)(cm^3/min)}$	21.58	$\eta_{electrolysis}(\%)$	35.04
$V_{O_2(g)(Exp)(cm^3/min)}$	10.85	$\eta_{energy}(\%)$	37.4

The I-V characteristic curve of the experiment is shown in Figure 5.18.

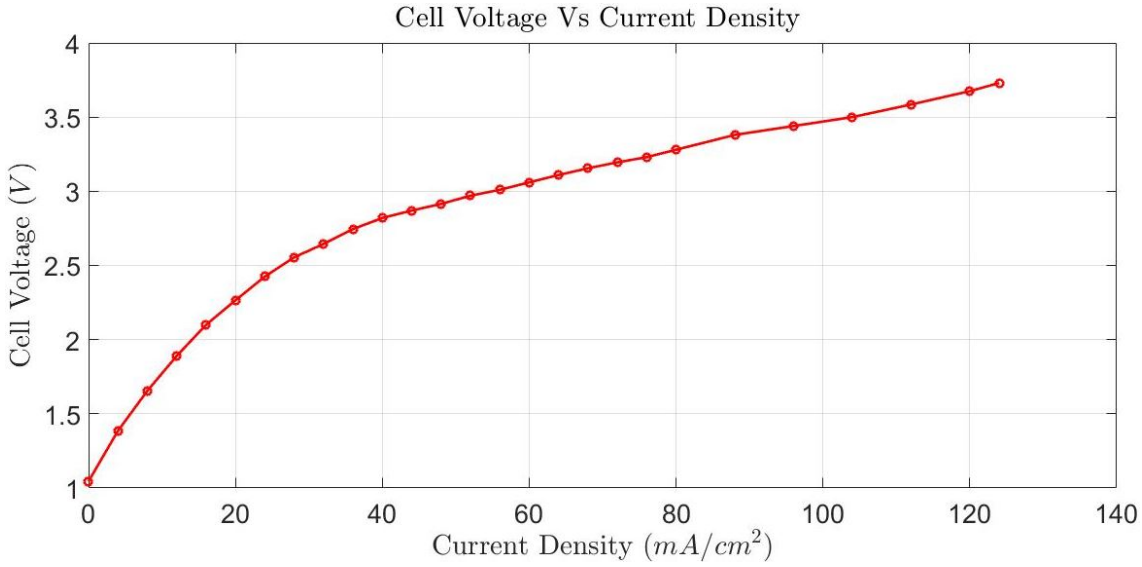

Figure 5.18: I-V characteristic curve of the N 115 membrane

5.8.2 Electrolysis cell with N 117 Membrane

The N 117 membrane is used as a separating diaphragm in this experiment. Furthermore, the flow rate, the power and the efficiency calculation data are listed in Table 5.12.

Table 5.12: Flow rate calculation data of the N 117 membrane

Product Gases	**Current Density(A)**	**Cell Voltage (V)**	**Time(s)**
Hydrogen $(H_2(g))$	3.14	3.96	290
Oxygen $(O_2(g))$	3.14	3.96	580

The calculated parameters of this experiment are illustrated in Table 5.13. Since, the same calculation steps are repeated in this experiment as in previous experiments.

Table 5.13: Calculated parameters of the N 117 membrane

Flow Rates Calculation		**Power and Efficiency Calculation**	
Cell Current (A)	3.14	Cell Voltage(V)	3.96
$n_{H_2(g)}(mol/min)$	9.7632×10^{-4}	$P_{total}(W)$	12.4344
$n_{O_2(g)}(mol/min)$	4.8816×10^{-4}	$R_{ohmic}(\Omega)$	0.8257
$V_{H_2(g)(Theo)(cm^3/min)}$	24.017	$P_{ohmic}(W)$	8.141
$V_{O_2(g)(Theo)(cm^3/min)}$	12.01	$P_{electrolysis}(W)$	4.2937
$V_{H_2(g)(Exp)(cm^3/min)}$	20.7	$\eta_{electrolysis}(\%)$	34.53
$V_{O_2(g)(Exp)(cm^3/min)}$	10.35	$\eta_{energy}(\%)$	37.4

Figure 5.19 illustrates the I-V characteristic of the experiment.

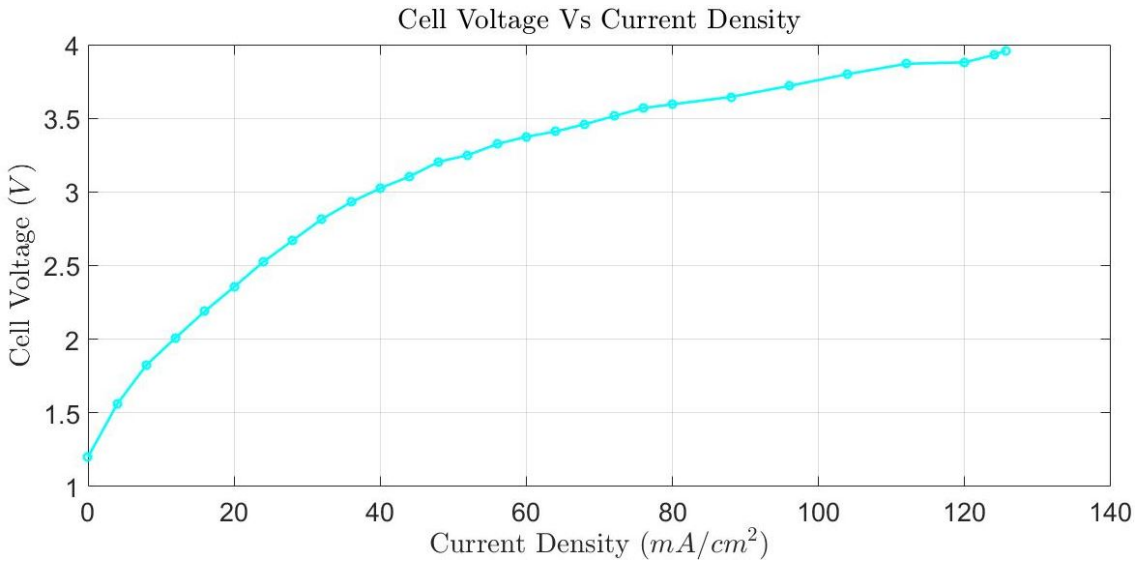

Figure 5.19: I-V characteristic curve of the N 117 membrane

5.8.3 Comparison of Experiment *VII* with Mathematical Model

To compare the results of the Experiment *VII* with the mathematical model, all the I-V characteristic curves are presented in Figure 5.20.

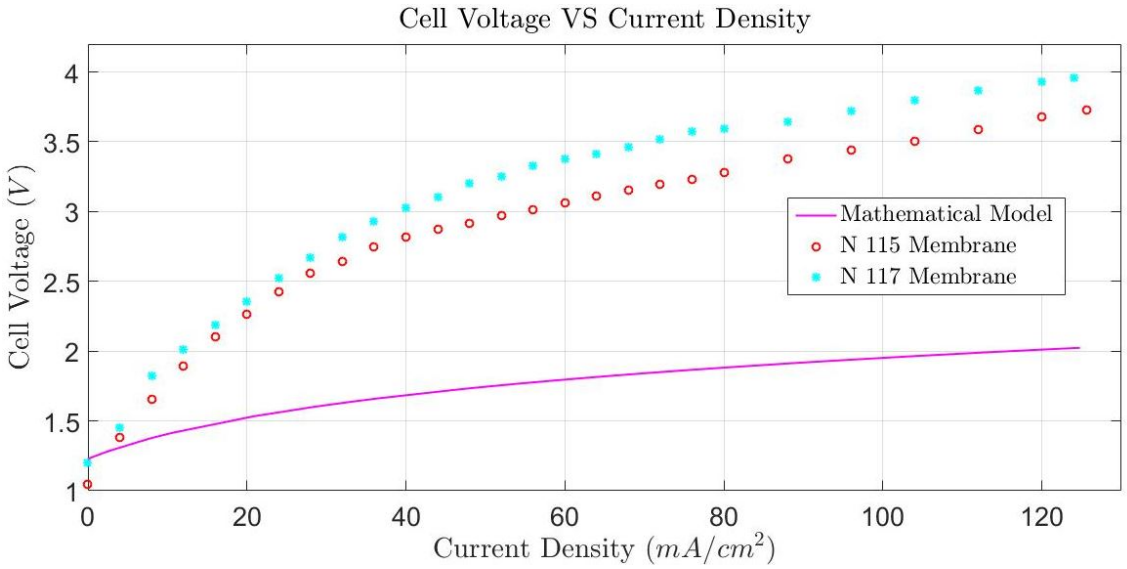

Figure 5.20: Comparison of the Experiment *VII* with the mathematical model

5.9 Experiment *VIII* : Using Porous Stainless Steel Plates as a Electrodes

In order to reduce the ohmic overvoltage, the porous stainless steel plate is used as an electrode instead of the normal stainless steel plate. Moreover, the separating diaphragm of this experiment consists of one nylon mesh and two filter papers. The same bench setup is used to observe the flow rate calculation data as in the Experiment *V*. The important parameters which are used to calculate the flow rate, the power and the efficiency of the cell are given in Table 5.14.

Table 5.14: Flow rate calculation data of the Experiment *VIII*

Product Gases	**Current Density(A)**	**Cell Voltage (V)**	**Time(s)**
Hydrogen ($H_2(g)$)	2.5	1.98	300
	3.14	2.04	250
Oxygen ($O_2(g)$)	2.5	1.98	588
	3.14)	2.04	505

In this experiment, same calculations are repeated. Hence, all the calculated parameters are listed in Table 5.15.

Table 5.15: Calculated parameters of the Experiment *VIII*

Flow Rates Calculation		**Power and Efficiency Calculation**	
Cell Current (A)	3.14	Cell Voltage(V)	2.04
$n_{H_2(g)}(mol/min)$	9.7632×10^{-4}	$P_{total}(W)$	6.4056
$n_{O_2(g)}(mol/min)$	4.8816×10^{-4}	$R_{ohmic}(\Omega)$	0.194
$V_{H_2(g)(Theo)(cm^3/min)}$	24.017	$P_{ohmic}(W)$	1.914
$V_{O_2(g)(Theo)(cm^3/min)}$	12.01	$P_{electrolysis}(W)$	4.4921
$V_{H_2(g)(Exp)(cm^3/min)}$	24	$\eta_{electrolysis}(\%)$	70.13
$V_{O_2(g)(Exp)(cm^3/min)}$	11.88	$\eta_{energy}(\%)$	72.5

At last, the I-V characteristic curve of the Experiment *VIII* is shown in Figure 5.21.

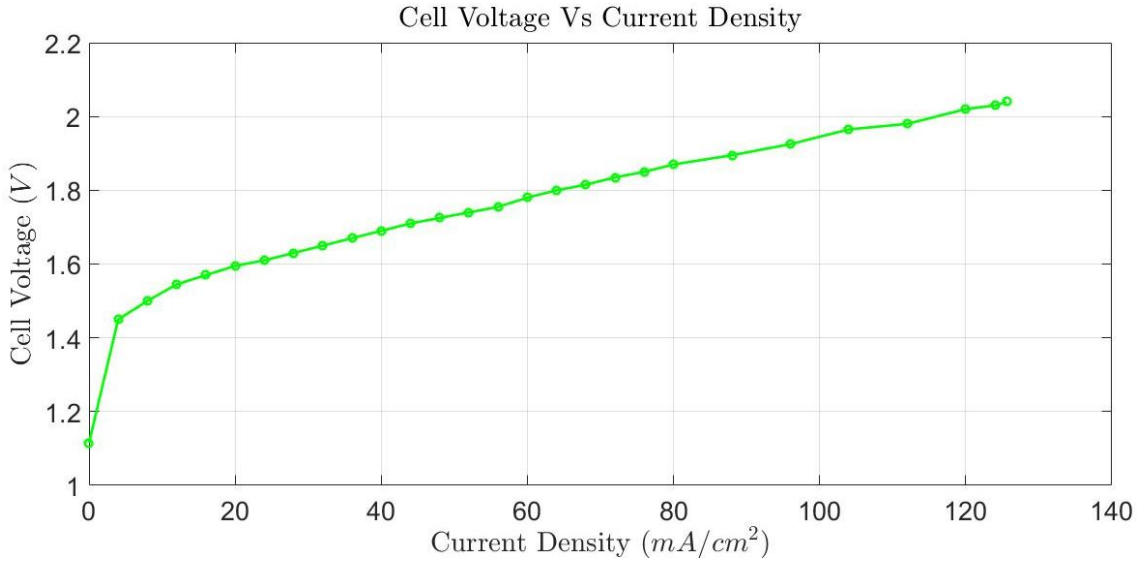

Figure 5.21: I-V characteristic of the Experiment *VIII*

5.10 Experiment *IX* : Electrolysis Cell with Fine Nylon Mesh

The separating diaphragm of this experiment consists of one nylon mesh and two filter papers. The same bench setup is used to observe the flow rate calculation data as in the Experiment *V*. The important parameters which are used to calculate the flow rate, the power and the efficiency of the cell are given in Table 5.16.

Table 5.16: Flow rate calculation data of the Experiment *IX*

Product Gases	**Current Density(A)**	**Cell Voltage (V)**	**Time(s)**
Hydrogen ($H_2(g)$)	2.5	2	334
	3.1	2.05	254
Oxygen ($O_2(g)$)	2.5	2	613
	3.14)	2.05	551

In this experiment, same calculations are repeated. Hence, all the calculated parameters are listed in Table 5.17.

Table 5.17: Calculated parameters of the Experiment *IX*

Flow Rates Calculation		**Power and Efficiency Calculation**	
Cell Current (A)	3.1	Cell Voltage(V)	2.05
$n_{H_2(g)}(mol/min)$	9.6388×10^{-4}	$P_{total}(W)$	6.355
$n_{O_2(g)}(mol/min)$	4.8194×10^{-4}	$R_{ohmic}(\Omega)$	0.2
$V_{H_2(g)(Theo)(cm^3/min)}$	23.71	$P_{ohmic}(W)$	1.922
$V_{O_2(g)(Theo)(cm^3/min)}$	11.86	$P_{electrolysis}(W)$	4.433
$V_{H_2(g)(Exp)(cm^3/min)}$	23.62	$\eta_{electrolysis}(\%)$	69.8
$V_{O_2(g)(Exp)(cm^3/min)}$	10.89	$\eta_{energy}(\%)$	72.2

At last, the I-V characteristic curve of the Experiment *IX* is shown in Figure 5.22.

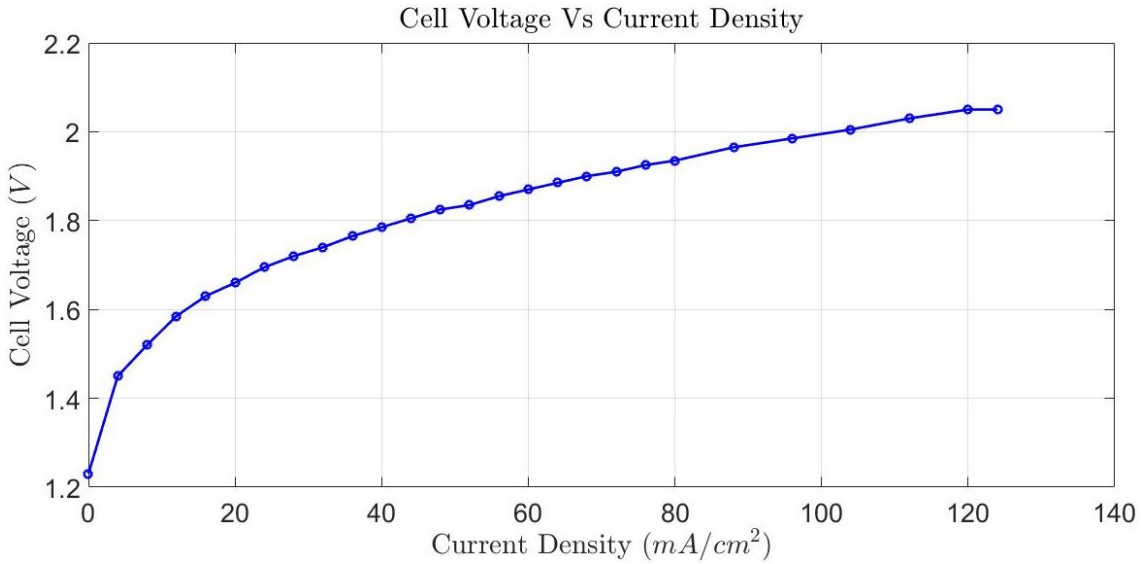

Figure 5.22: I-V characteristic of the Experiment *IX*

5.10.1 Comparison of Experiment *V*, *VIII* and *IX* with Mathematical Model

In order to compare the results of the Experiments *V*, *VIII* and *IX* with the mathematical model, all the I-V characteristic curves are drawn in the same graph as shown in Figure 5.23.

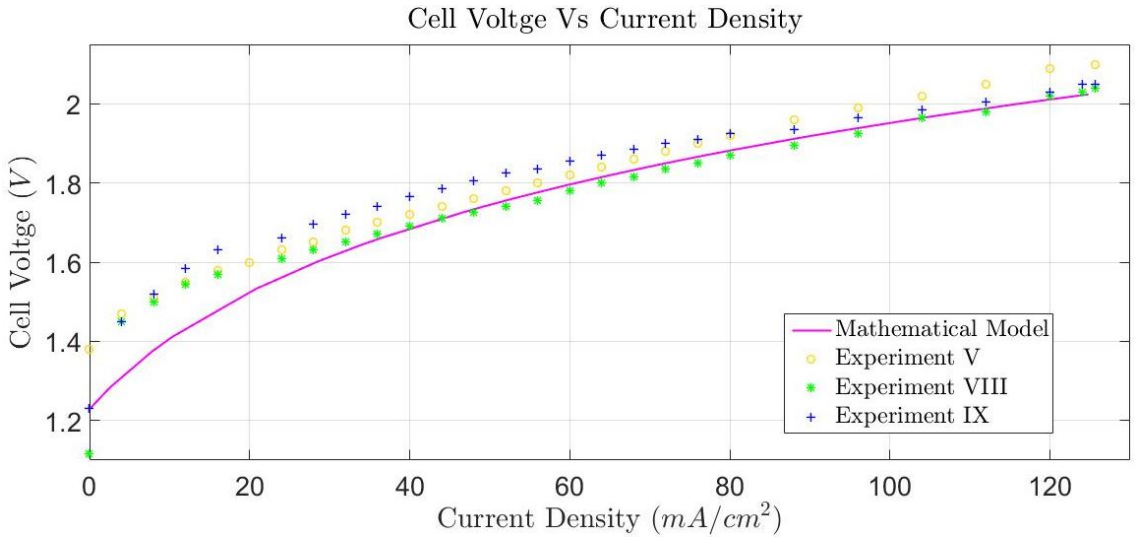

Figure 5.23: Comparison of the Experiment *V*, *VIII* and *IX* with the mathematical model

According to the comparison of the Experiments *V*, *VIII* and *IX* with the mathematical model, the Experiment *VIII* implies a great performance than the other experiments. Since, the cell which is used in the Experiment *VIII* have a small distance between the anode and the cathode. Moreover, the conductivity of the inside material is also high when compared with the other experiments.

5.11 Experiment *X* : Testing of Monopolar Alkaline Electrolysis Stack

The electrolysis cell in the Experiment *VIII* is used to build the monopolar electrolysis stack due to the great performance compared with the other experiments. Hence, the electrodes assembly of each single cell consists of two porous stainless steel plates, two filter papers and one nylon mesh. Furthermore, the stack consists of three single cells. Figure 5.24 illustrates the test bench setup of the Experiment *X*.

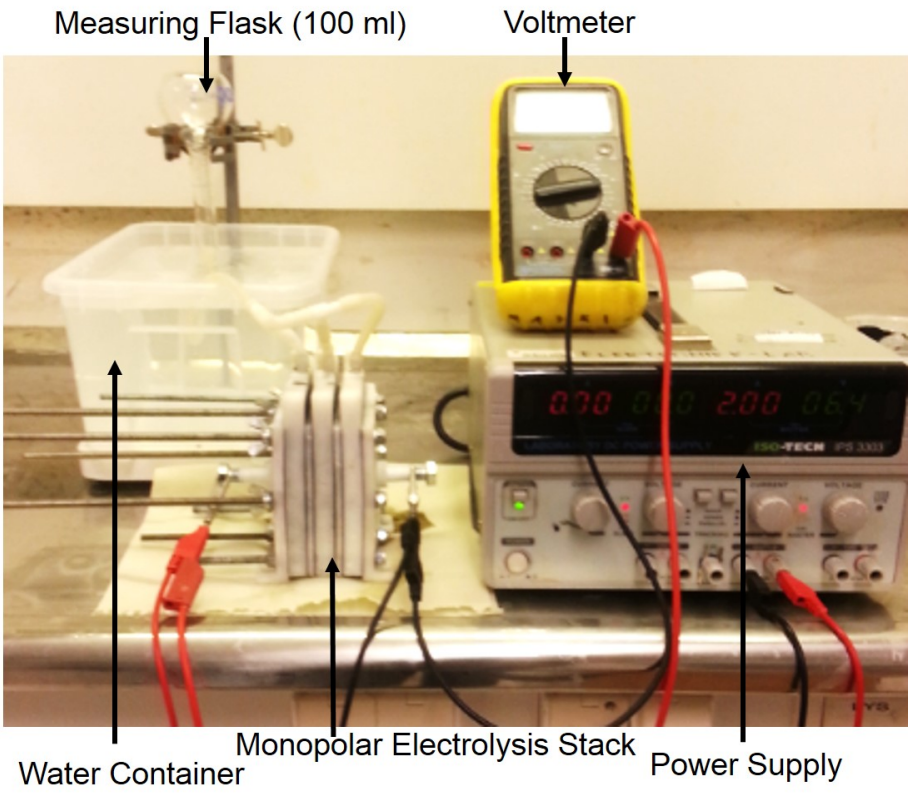

Figure 5.24: Bench setup of the Experiment X

The important parameters which are obtained from above test bench setup are given in Table 5.18.

Table 5.18: Flow rate calculation data of the Experiment X

Product Gases	**Current Density(A)**	**Cell Voltage (V)**	**Time(s)**
Hydrogen ($H_2(g)$)	2.5	6.3	100
	3.14	6.49	86
Oxygen ($O_2(g)$)	2.5	6.4	250
	3.14)	6.5	190

The same calculation steps are repeated in this experiment as in the previous experiments. Thus, all the calculated parameters that are used to analyze the performance of the stack are listed in Table 5.19.

Table 5.19: Calculated parameters of the Experiment X

Flow Rates Calculation		**Power and Efficiency Calculation**	
Cell Current (A)	3.14	Cell Voltage(V)	2.04
$n_{H_2(g)}(mol/min)$	9.7632×10^{-4}	$P_{total}(W)$	20.3786
$n_{O_2(g)}(mol/min)$	4.8816×10^{-4}	$R_{ohmic}(\Omega)$	0.6655
$V_{H_2(g)(Theo)(cm^3/min)}$	72.051	$P_{ohmic}(W)$	6.5615
$V_{O_2(g)(Theo)(cm^3/min)}$	36.03	$P_{electrolysis}(W)$	13.82
$V_{H_2(g)(Exp)(cm^3/min)}$	69.76	$\eta_{electrolysis}(\%)$	67.8
$V_{O_2(g)(Exp)(cm^3/min)}$	30.46	$\eta_{energy}(\%)$	68.413

At last, the I-V characteristic curve of the monopolar electrolysis stack is shown in Figure 5.25.

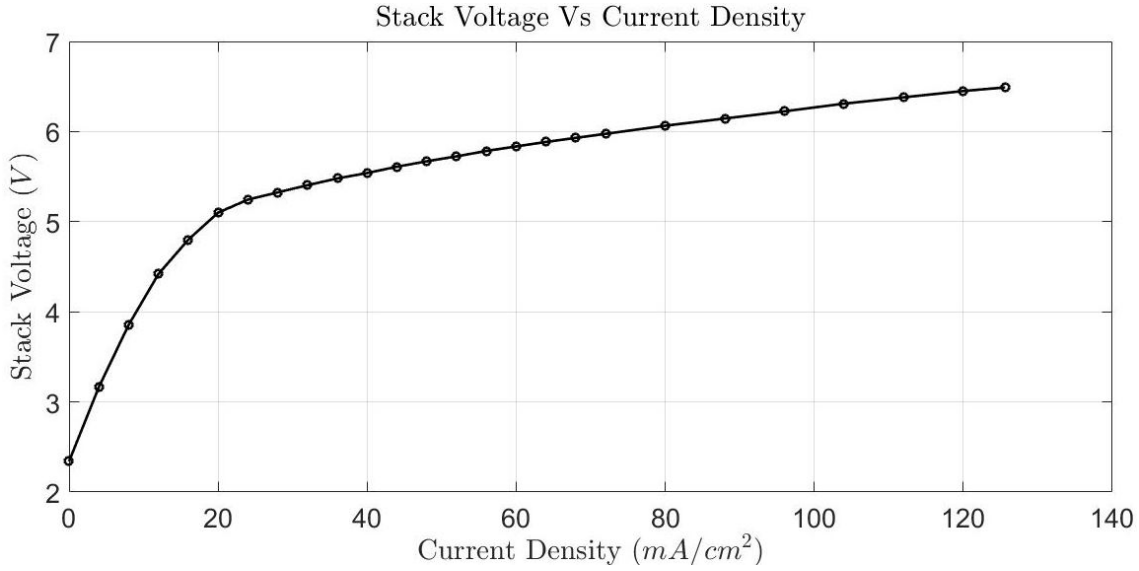

Figure 5.25: I-V characteristic of the monopolar electrolysis stack

5.12 Experiment *XI* : Testing of Bipolar Alkaline Electrolysis Stack

The electrolysis cell in the Experiment *VIII* is used to build the bipolar electrolysis stack similarly in the Experiment X owing to the great performance. Hence, the electrodes assembly of each single cell consists of two porous stainless steel plates, two filter papers and one nylon mesh. Furthermore, the stack consists of three single cells. The test bench setup of the Experiment *XI* is shown in Figure 5.26.

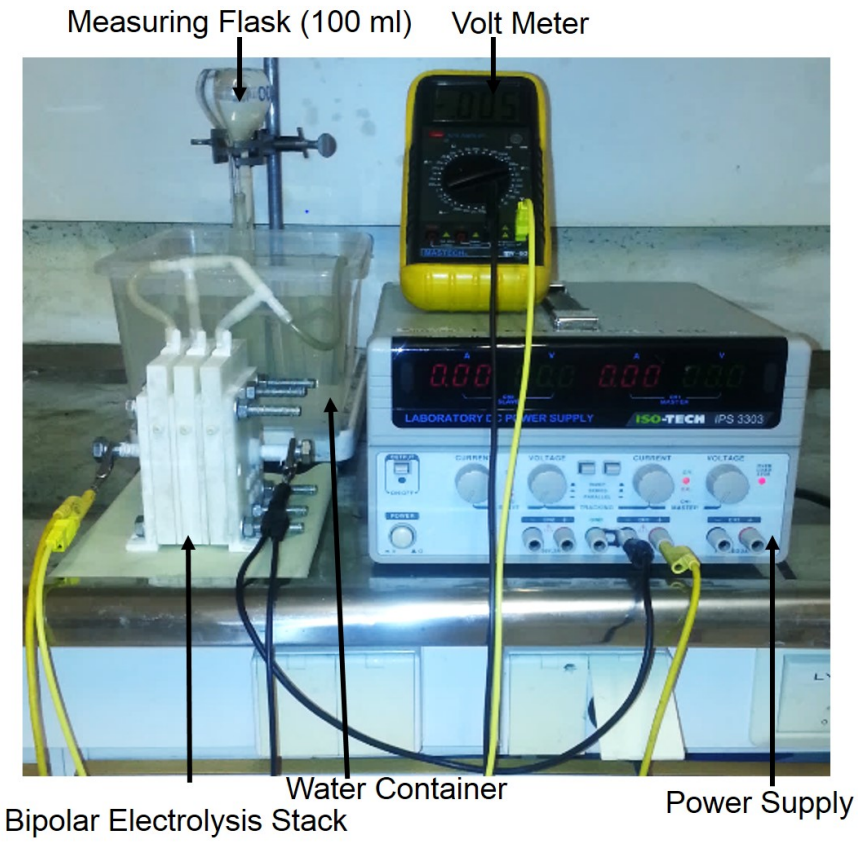

Figure 5.26: Bench setup of the Experiment *XI*

The flow rate calculation data which are obtained from above test bench setup are given in Table 5.20.

Table 5.20: Flow rate calculation data of the Experiment *XI*

Product Gases	**Current Density(A)**	**Cell Voltage (V)**	**Time(s)**
Hydrogen ($H_2(g)$)	2.5	6.0	96
	3.14	6.17	84
Oxygen ($O_2(g)$)	2.5	5.9	191
	3.14	6.17	167

The same calculation steps are repeated in this experiment. Thus, all the calculated parameters that are used to analyze the performance of the stack are listed in Table 5.21.

Table 5.21: Calculated parameters of the Experiment *XI*

Flow Rates Calculation		**Power and Efficiency Calculation**	
Cell Current (A)	3.14	Cell Voltage(V)	2.04
$n_{H_2(g)}(mol/min)$	9.7632×10^{-4}	$P_{total}(W)$	19.3738
$n_{O_2(g)}(mol/min)$	4.8816×10^{-4}	$R_{ohmic}(\Omega)$	0.592
$V_{H_2(g)(Theo)(cm^3/min)}$	72.051	$P_{ohmic}(W)$	5.835
$V_{O_2(g)(Theo)(cm^3/min)}$	36.03	$P_{electrolysis}(W)$	13.538
$V_{H_2(g)(Exp)(cm^3/min)}$	71.43	$\eta_{electrolysis}(\%)$	69.88
$V_{O_2(g)(Exp)(cm^3/min)}$	35.93	$\eta_{energy}(\%)$	71.96

The I-V characteristic curve of the Experiment *XI* is shown in Figure 5.27.

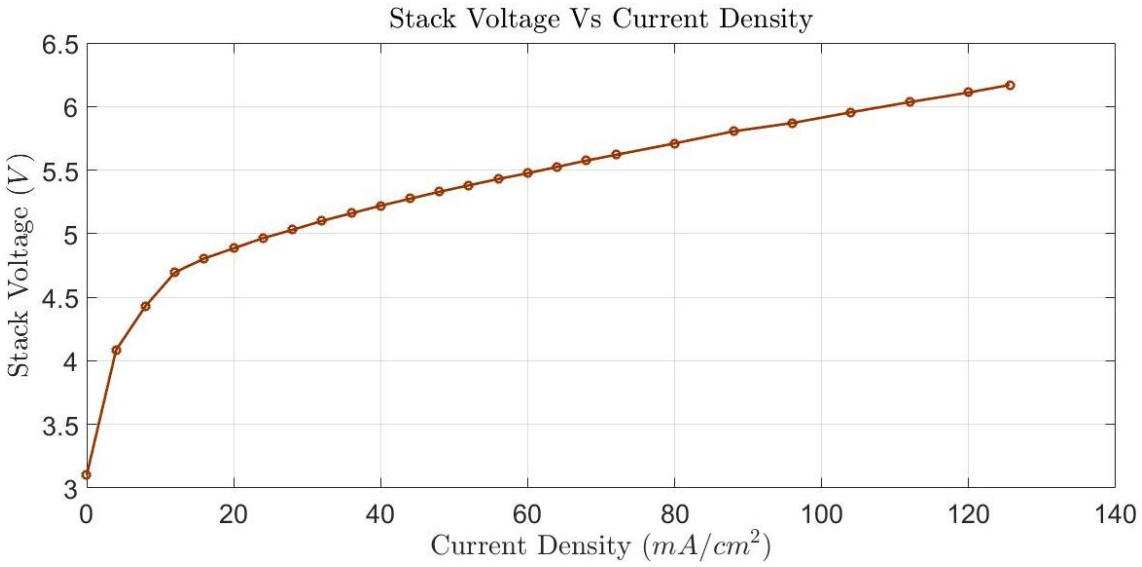

Figure 5.27: I-V characteristic of the bipolar electrolysis stack

5.12.1 Comparison of Monopolar and Bipolar Configuration of Alkaline Electrolysis Stack

The comparison of the monopolar and the bipolar configurations of the alkaline electrolysis stack is one of the main objectives of this research study. Thus, to compare the results of the monopolar alkaline electrolysis stack and the bipolar alkaline electrolysis stack with the mathematical model, all the I-V characteristic curves are shown in Figure 5.28.

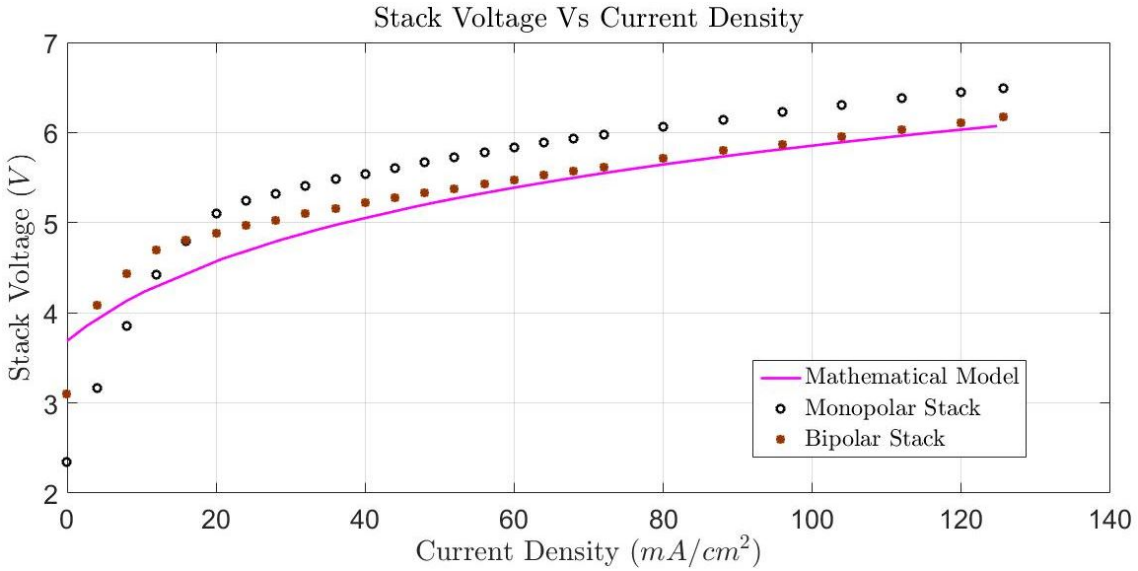

Figure 5.28: I-V characteristic curves of the Experiments *X*, *XI* with the mathematical model

According to the comparison graph of the monopolar and the bipolar electrolysis stack, the bipolar electrolysis stack exhibits a great performance (low overvoltage and high efficiency) than the monopolar stack since the bipolar electrolysis stack have a low ohmic loss inside the stack compared with the monopolar stack. Thus, the most manufacturers are using the bipolar electrolysis stack to produce hydrogen from electrolysis process than the monopolar electrolysis stack. Figure 5.29 illustrates the final stage of both monopolar and bipolar alkaline electrolysis stack.

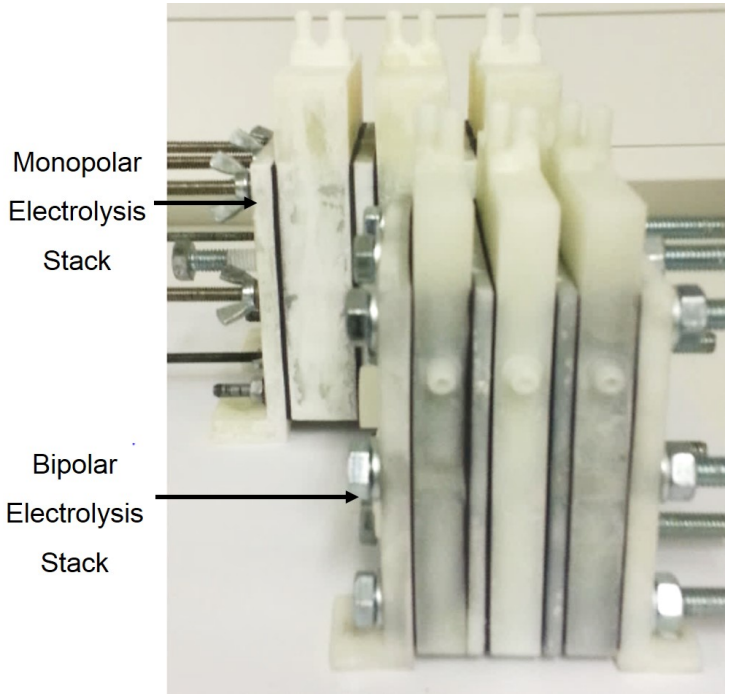

Figure 5.29: Comparison of the monopolar and the bipolar electrolysis stack

Moreover, from the manufacturing point of view, the bipolar electrolysis modules are complicated in designing, fabricating and maintaining. The bipolar electrolysis stack is more compact than the monopolar electrolysis stack. Consequently, it reduces the ohmic overvoltage inside the stack while increasing the performance. Hence, it has a lower unit cell voltage and a higher current density. Usually, the bipolar stack can be operated at a higher pressure and temperature.

5.13 Experiment *XII* : AC Impedance Test

In this research study, it is extremely important to obtain the impedance and the ohmic resistance of the cell. There are several methods available to analyze the AC impedance of the electrolysis cell such as the electrochemical impedance spectroscopy (EIS), the current sweep and the current interruption. Normally, the current sweep and the current interruption method cannot be used to determine the impedance of the cell during operation [38]. Consequently, the EIS is used to measure the ohmic resistance of the cell during the operation in this research study. Moreover, the EIS is widely used to study the harmonic responses of an electrochemical system. The test bench setup of the AC impedance test is shown in Figure 5.30.

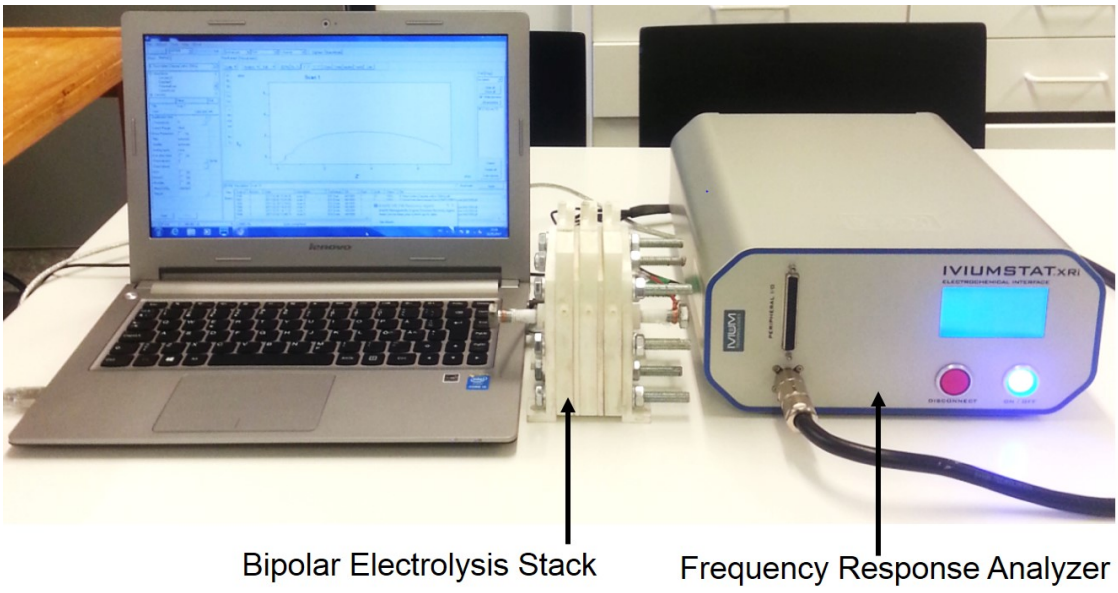

Figure 5.30: Bench setup of the AC impedance test

During the AC impedance test, the anode and the cathode are selected as the research and reference electrodes respectively. The impedance data are collected using a IVIUMASTAT frequency response analyzer, and IviumSoft is employed to post process the results. Further, the test operates under the open circuit voltage. At the beginning, a small sinusoidal signal is applied to the anode and the cathode while selecting appropriate frequency values for the test. Finally, the resulting current is analyzed in the frequency domain in terms of impedance.

In general, the impedance is a complex quantity with a real and imaginary part. The real part of the impedance is directly proportional to the ohmic resistance of the electrolysis cell. The Nyquist plot is commonly used to display the impedance of the system.

5.13.1 The Nyquist Plot of Electrolysis Stack

In nyquist plot, the negative value of the imaginary part of the impedance is plotted against the real part of the impedance. Figure 5.31 shows the nyquist plot for a single porous electrode.

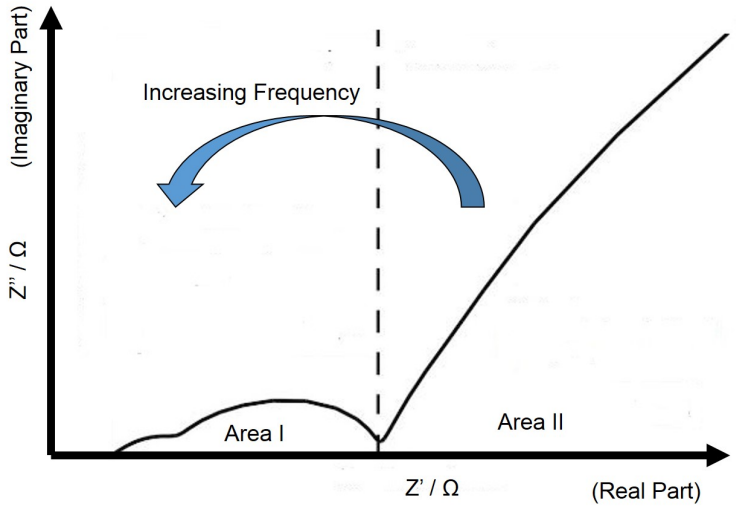

Figure 5.31: Nyquist plot of the single porous electrode

The Area *I* represents the charge transfer reaction and the double layer capacitance effect. Moreover, the Area *II* is affected by the diffusion within the electrolyte and active electrode materials [39]. The nyquist plot of the alkaline electrolysis cells is illustrated in Figure 5.32.

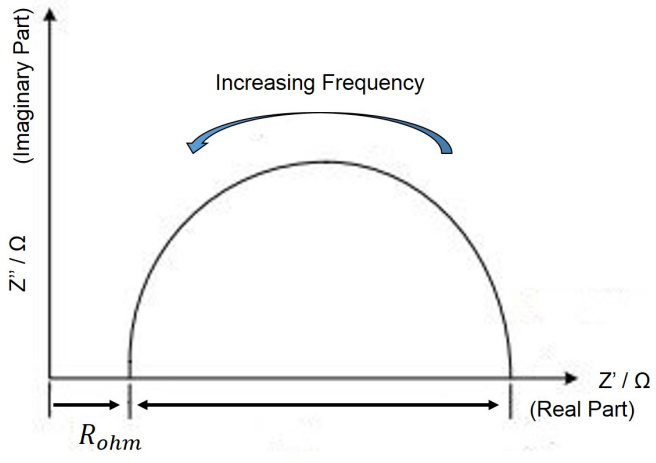

Figure 5.32: Nyquist plot of the electrolysis cells

Where, R_{ohm} is the ohmic resistance of the cell and R_{pol} is the polarization resistance of the cell.

5.13.2 Calculation of Ohmic Resistance

The objective of this test is to calculate the exact value of the ohmic resistance. Hence, the equivalent circuit of the electrolysis stack can be used to calculate the value of ohmic resistance. Nevertheless, by taking the difference between the highest frequency and the lowest frequency intercepts with the real axis on a nyquist plot, the ohmic resistance can be obtained very easily.

In general the equivalent circuit of the electrochemical device can be illustrated as in Figure 5.33.

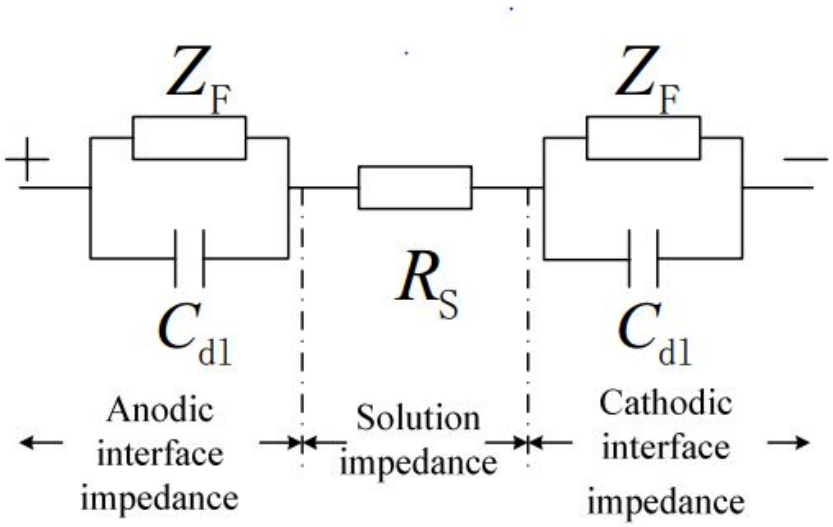

Figure 5.33: Equivalent circuit for the electrochemical device [40]

Normally, this kind of equivalent circuit can be deployed to fit the experimental impedance plots. Even though, during this experiment many logical series and parallel combination of electric circuit components is tried to fit the experimental impedance plots because of different equivalent circuits can results similar impedance plot [40]. Consequently, Root Mean Square Error (RMSE) values are used to evaluate the goodness of the fit.

5.13.3 AC Impedance Test of Monopolar Electrolysis Stack

The AC impedance test of the monopolar electrolysis stack is implemented under a constant current condition. The constant current amplitude of the test is selected as 10 mA and the frequency range is selected as $1mHz \leq f \leq 100kHz$. The AC impedance plot of the monopolar electrolysis stack is shown in Figure 5.34.

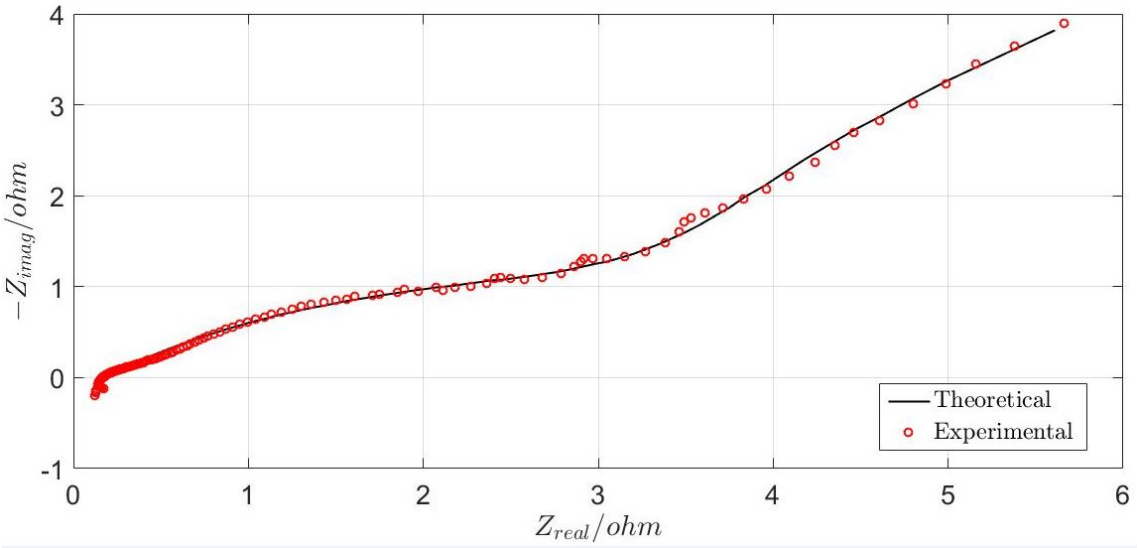

Figure 5.34: AC - impedance plot of the monopolar electrolysis stack

According to the impedance plot of the monopolar electrolysis stack, the ohmic resistance of the stack is observed as 0.714 Ω. Moreover, the equivalent circuit which is used to fit the experimental impedance plot of monopolar stack is illustrated in Figure 5.35 and the RMSE value is calculated as 0.04552 for this fit.

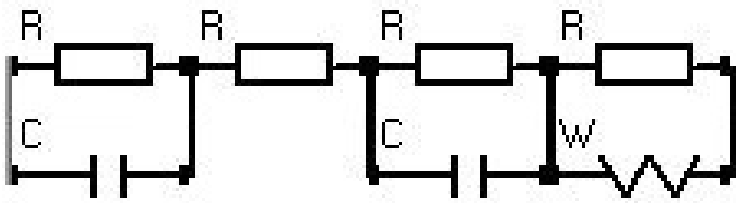

Figure 5.35: Equivalent circuit of AC impedance test for the monopolar stack

5.13.4 AC Impedance Test of Bipolar Electrolysis Stack

The AC impedance test of the bipolar electrolysis stack is implemented under the constant current condition same as in the monopolar electrolysis stack. The constant current amplitude of the test is selected as 10 mA and the frequency range is selected as $10mHz \leq f \leq 100kHz$. Figure 5.36 illustrates the AC impedance plot of the bipolar electrolysis stack.

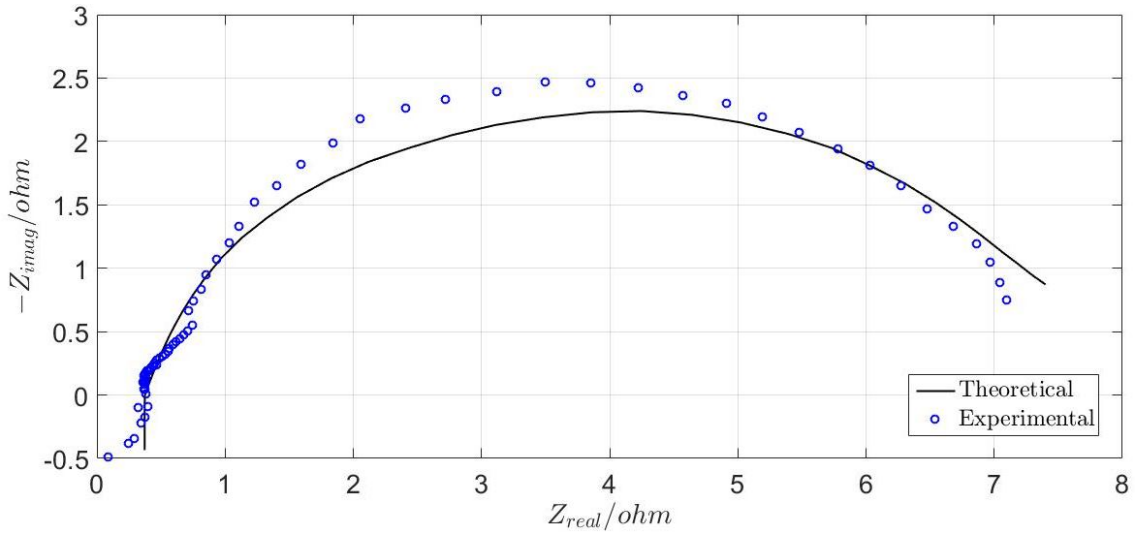

Figure 5.36: AC - impedance plot of the bipolar electrolysis stack

According to the impedance plot of the bipolar electrolysis stack, the ohmic resistance of the stack is observed as 0.621 Ω. Moreover, the equivalent circuit which is used to fit the experimental impedance plot is shown in Figure 5.37 and the RMSE value is calculated as 0.1961 for this fit.

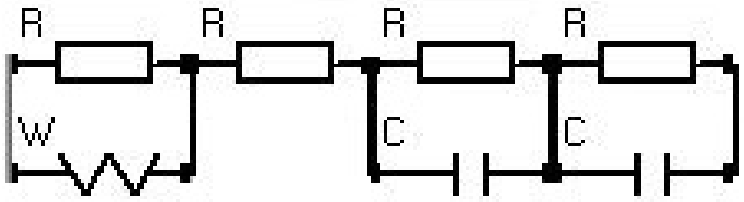

Figure 5.37: Equivalent circuit of AC impedance test for the bipolar stack

5.14 Discussion

The main focus of this research study is to construct an alkaline electrolysis stack to observe the stack performance. Moreover, the mathematical model of the alkaline electrolyser was developed in MATLAB Simulink environment, with selected parameters and obtained an I-V characteristic curve to compare with the practical polarization curves. At last, the designed electrolysis stacks were fabricated in order to collect the gas and measure the flow rates of the product gases while calculating the electrolysis power and efficiency.

In this study, both monopolar and bipolar configurations of the alkaline electrolysis stack were developed to compare the performance of each electrolysis stack with the mathematical model. At the beginning, two different single cell alkaline electrolysers were fabricated and obtained the performance to select the best cell for the stack.

Thereafter, the several experiments were carried out to increase the performance of the selected cell. Finally, the electrolysis cell in the Experiment *VIII* was selected for the stack implementation since it exhibits a great performance compared with the other experiments. Throughout the design process, the Solidworks was used as the design software and the 3D print of the designed cell was taken from the 3D printing machine in the lab. The base plates, the electrodes, the separating diaphragm, the electrolyte, the bipolar plate, the connecting rods and the sealing gasket were used for the fabrication process. Hence, all these components were deployed to fabricate two different configurations of the electrolysis stack as shown in Figures 3.7 and 3.12 respectively. At last, the performance of both monopolar and bipolar configurations of the electrolysis stacks were analyzed and compared with the mathematical model as shown in Figure 5.28.

5.14.1 Selecting the Best Design of Single Cell Alkaline Electrolyser

Specially, the Experiments *I, II, III*, and *IV* were the benchmark test to select a better performing single cell alkaline electrolyser for the stack implementation. In Experiments *I* and *II*, the effect of the electrocatalyst for the electrolysis process was examined. Thus, the Experiment *II* exhibits good performance than the Experiment *I* owing to the effect of electrocatalyat (Figure 5.6). Normally, the electrocatalyst is able to increase the rate of the electrochemical reaction by reducing the overvoltages. The first and second design of the single cell alkaline electrolyser was used in the Experiment *III* and the Experiment *IV* respectively to collect and measure the product gas flow rate. Moreover, the product gas purity level of the Experiment *III* is low due to the presence of water vapor. Thus, in the Experiment *IV*, the special storage tank was designed top of the intermediate base plate to increase the purity level. The important calculated parameters of the Experiments *III* and *IV* are given in Table 5.22.

Table 5.22: Comparison of the Experiment *III* and *IV*

Calculated Parameters	**Experiment *III***	**Experiment *IV***
$V_{H_2(g)(The.)(cm^3/min)}$	24.017	24.017
$V_{H_2(g)(Exp.)(cm^3/min)}$	22.22	23.07
$V_{O_2(g)(The.)(cm^3/min)}$	12.01	12.01
$V_{O_2(g)(Exp.)(cm^3/min)}$	9.091	10.91
$\eta_{electrolysis}(\%)$	52.3	66.26
$\eta_{energy}(\%)$	67.9	69.5

According to the calculation of the Experiment *IV*, there is a small difference between the experimental and theoretical values of flow rates, the electrolysis efficiency and the energy efficiency. Thus, the cell in Experiment *IV* should have a small energy loss compared with the cell in Experiment *III* due to the low space between the anode and the cathode in the cell of Experiment *IV* which reduces the ohmic loss inside the cell. Moreover, the Table 5.22 and Figure 5.11 reveal that the Experiment *IV* has a

better performance than Experiment *III*. Thus, the electrolysis cell in the Experiment *IV* (second design of single cell alkaline electrolyser) is deployed for the electrolysis stack implementation.

5.14.2 Improving the Selected Cell

As mentioned early, the second design of the single cell alkaline electrolyser was selected for the stack because of the good performance than the first design. Even though, the efficiency of the second design (66.26 %) was not enough for a stack implementation. Thus, the Experiments *V, VI, VII, VIII* and *IX* were carried out to improve the performance of the selected cell. In Experiment *V*, the six porous nickel plates were employed for both anode and cathode sides as a first improvement. Moreover, the electrolysis efficiency of the Experiment *V* was quite better than the Experiment *IV*. As a consequence, the porous nickel plates can reduce the flow resistance inside the cell by reducing the ohmic overvoltage. The materials of the separating diaphragm was changed in the Experiment *VII* as a second improvement. Hence, the N 115 and N 117 polymeric membrane were used as the separating diaphragm. Even though, those experiments presented the abnormal result with a higher overvoltage value as shown in Figure 5.20 due to the very low conductivity of the polymeric membrane. Thus, the membrane enhances the ohmic resistance inside the cell by reducing the electrolysis efficiency. Nevertheless, the electrolysis cell with the N 115 showed a good performance compared with cell with the N 117 membrane since the conductivity of the N 115 is higher than the N 117 and the thickness is lower than the N 117. The detailed description of Nafion membrane property is presented in Appendix D.

The porous stainless steel plates were used as the electrodes in the Experiment *VIII* with the 1.3 mm thick diaphragm. The diaphragm consists of two filter papers and one nylon mesh. At last, in the Experiment *IX*, the fine nylon mesh was used as a the separating diaphragm. The important calculated parameters of the Experiments *V, VII, VIII* and *IX* are listed in Table 5.23.

Table 5.23: Comparison of the Experiment *V*, *VII*, *VIII* and *IX*

Calculated Parameters	**Exp. *V***	**Exp. *VII* (N 115)**	**Exp. *VII* (N 117)**	**Exp. *VIII***	**Exp. *IX***
$V_{H_2(g)(The.)(cm^3/min)}$	24.017	23.71	24.017	24.017	23.71
$V_{H_2(g)(Exp.)(cm^3/min)}$	23.077	21.58	20.7	24	23.62
$V_{O_2(g)(The.)(cm^3/min)}$	12.01	11.86	12.01	12.01	11.86
$V_{O_2(g)(Exp.)(cm^3/min)}$	10.83	10.85	10.35	11.88	10.89
$\eta_{electrolysis}(\%)$	69.01	35.04	34.53	70.13	69.8
$\eta_{energy}(\%)$	70.5	37.4	37.4	72.5	72.2

According to the calculations of the Experiment *VIII*, there is a very small difference between the experimental and theoretical values of flow rates, and the electrolysis efficiency and the energy efficiency. Thus, this cell should have very small energy

loss compared with the other experiments, since the separating diaphragm in the Experiment *VII* is extremely thinner than the other experiments. Moreover, the conductivity of the filter paper also very high value which reduces the ohmic loss inside the cell. Furthermore, Table 5.23 and Figure 5.23 imply that the Experiment *VIII* has the better performance than the other experiments. Thus, the electrolysis cell in the Experiment *VIII* is selected for the final electrolysis stack implementation.

5.14.3 Effect of Anode and Cathode Distance for Electrolysis Process

The Experiment *VI* was based on the effect of the electrodes distance for the electrolysis process. In this experiment, three different experiments (Experiment *A*, *B* and *C*) were carried out by changing the distance between the anode and the cathode. The 2.5 mm separating diaphragm was employed for the Experiment *A*. Consequently, the calculated electrolysis efficiency of this experiment was 62.18 %. Thus, the 1.9 mm thick separating diaphragm was selected for the Experiment *B* and the calculated efficiency was 65.4 %. Thereafter, the Experiment *C* was conducted by using the 1.3 mm diaphragm and the electrolysis efficiency was obtained as 70.13 %. Further, the calculated ohmic resistance of the Experiments *A, B* and *C* were 0.27 Ω, 0.234 Ω and 0.194 Ω respectively.

The results of the Experiment *VI* exhibit that the efficiency of the cell increases when decreasing the distance between the anode and cathode since it reduces the ohmic overvoltage by increasing the electrolysis efficiency. Moreover, according to Figure 5.17, the Experiment *C* (1.3 mm thick separating diaphragm) has the low overvoltage compared with the other two experiments.

5.14.4 Comparison of Monopolar and Bipolar Configuration Alkaline Electrolysis Stack

The electrolysis cell in Experiment *VIII* was deployed to fabricate electrolysis stack. The Experiments *X* and *XI* were based on testing of monopolar and bipolar electrolysis stacks respectively. The calculated parameters of both Experiments *X* and *XI* are illustrated in Table 5.24.

Table 5.24: Comparision of the Experiment *X* and *XI*

Calculated Parameters	**Experiment *X***	**Experiment *XI***
$V_{H_2(g)(The.)(cm^3/min)}$	72.051	72.051
$V_{H_2(g)(Exp.)(cm^3/min)}$	69.76	71.43
$V_{O_2(g)(The.)(cm^3/min)}$	36.03	36.03
$V_{O_2(g)(Exp.)(cm^3/min)}$	30.46	35.93
$\eta_{electrolysis}(\%)$	67.8	69.88
$\eta_{energy}(\%)$	68.413	71.96

Figure 5.28 and Table 5.24 showed that the bipolar stack have the great performance than monopolar electrolysis stack due to the bipolar electrolysis stack is more compact than the monopolar electrolysis stack. Consequently, it reduces the ohmic overvoltage inside the stack while increasing the performance. Hence, it has the lower unit cell voltage and higher current density compared with the monopolar electrolysis stack.

5.14.5 AC Impedance Test

The AC impedance test was implemented under constant current condition since it is important to know the exact value of the ohmic loss inside the cell. Moreover, the results of the impedance test were used to verify the calculated ohmic loss under the relevant experiments. Nevertheless, the results of the AC impedance test imply that the bipolar electrolysis stack has the low ohmic loss compared with the monopolar electrolysis stack.

Chapter 6

Conclusion

This research work presents the design, testing and modeling of two compact alkaline electrolysis stacks base on both monopolar and bipolar configurations and a comparison of their relative performances. In both cases the design was limited to three individual cells in each stack module due to time restrictions on the project. The main focus of this project was to construct a compact alkaline electrolysis stack and to observe the electrolysis performance both in I-V characteristics and the volume of hydrogen and oxygen produced. To achieve the objectives of this research work twelve different experiments have been implemented.

The first four experiments were benchmark tests to determine the best single cell configuration to adopt in the stack design. As a result of this stage, two different single cell designs were (Chapter 2) adopted for the experiments. Among that two designs, the second design of the single cell alkaline electrolyser was selected for the stack fabrication since that design gave a better performance than the first design. Moreover, throughout the design process, Solidworks was used as the design software. Even though, the efficiency of the selected single cell was not enough for the stack. Thus, in the first design, improvements were made in an iterative fashion. Consequently, the Experiments *V, VI, VII, VIII,* and *IX* were carried out to improve the performance of the selected stack design. At last, the Experiment *VIII* gave the best results compared with the other experiments. Hence, the single cell electrolyser in the Experiment *VIII* was deployed for the final electrolysis stack implementation.

The monopolar and bipolar configurations of the electrolysis stack have been developed (Chapter 3) from the knowledge gained in the single cell development phase. In the final stage of the project, mathematical modelling of the alkaline electrolyser stacks and cells was developed in the MATLAB Simulink environment to provide theoretical current voltage curves that were then compared with the experimental data. The performances of the designed stacks were determined in the Experiment *X* and the Experiment *XI*. The bipolar electrolysis stack exhibited better performance than the monopolar electrolysis stack (Figure 5.28 and Table 5.24). According to the observations from Experiment *IX*, the hydrogen gas flow rate, the oxygen gas flow rate and the electrolysis efficiency were calculated as $71.43\,\mathrm{cm^3\,min^{-1}}$, $35.96\,\mathrm{cm^3\,min^{-1}}$ and 69.88 % respectively. Moreover, the AC impedance tests were used to obtain the exact values of the ohmic loss inside both stacks.

All the observations of this research study indicate that the designed bipolar stack has a better performance in terms of the efficiency, power and the flow rates than the monopolar equivalent. Moreover, the bipolar stack is more compact than the monopolar stack. Finally, we propose the following aspect for future work:

- Optimization of the stack performance by using different material for the electrodes,s,
- Design of a mechanism to increase the product gases pressure by allowing the gas to build up to useful application pressures such as 10 bar.

Appendix A

Detailed Dimention of First Design

This chapter is explained all the detail about the dimension of first SolidWorks model in details.

A.1 Dimension of Anode and Cathode Side Base Plates

The dimensions of base plate is selected as 100 mm x 100 mm width and height respectively.

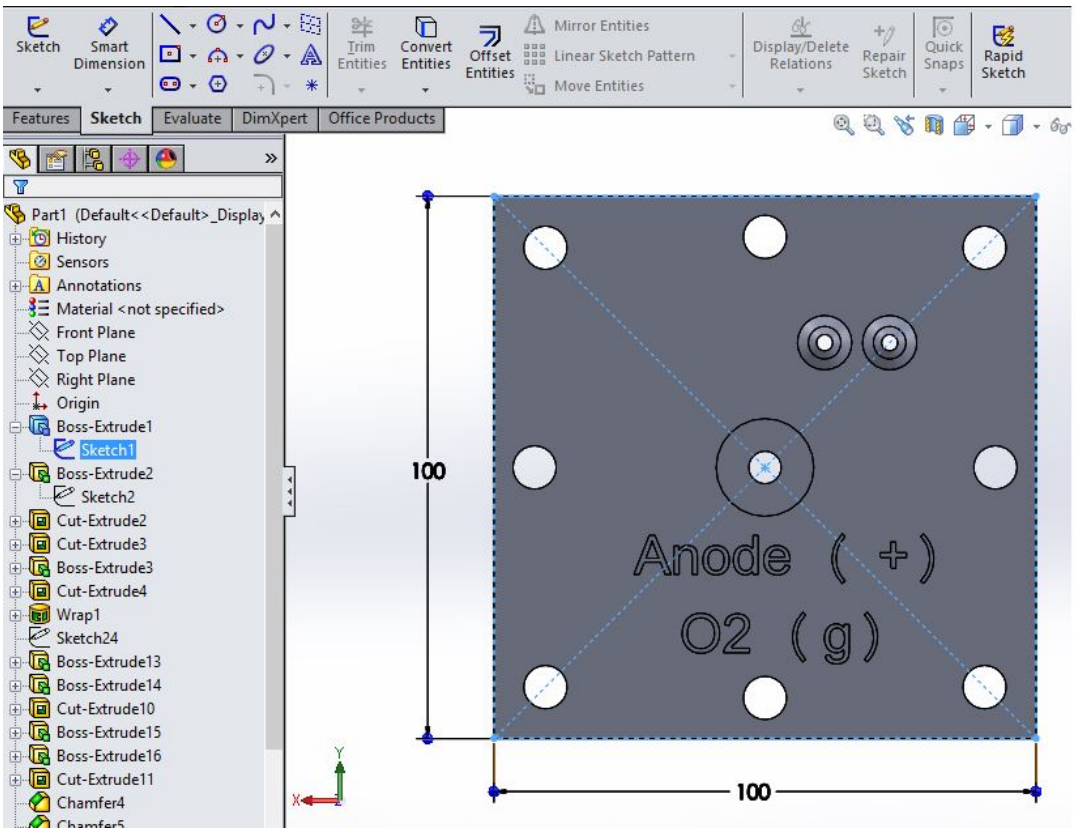

Figure A.1: Anode side base plate dimension

The diameter of each clamping hole is selected as 8 mm.

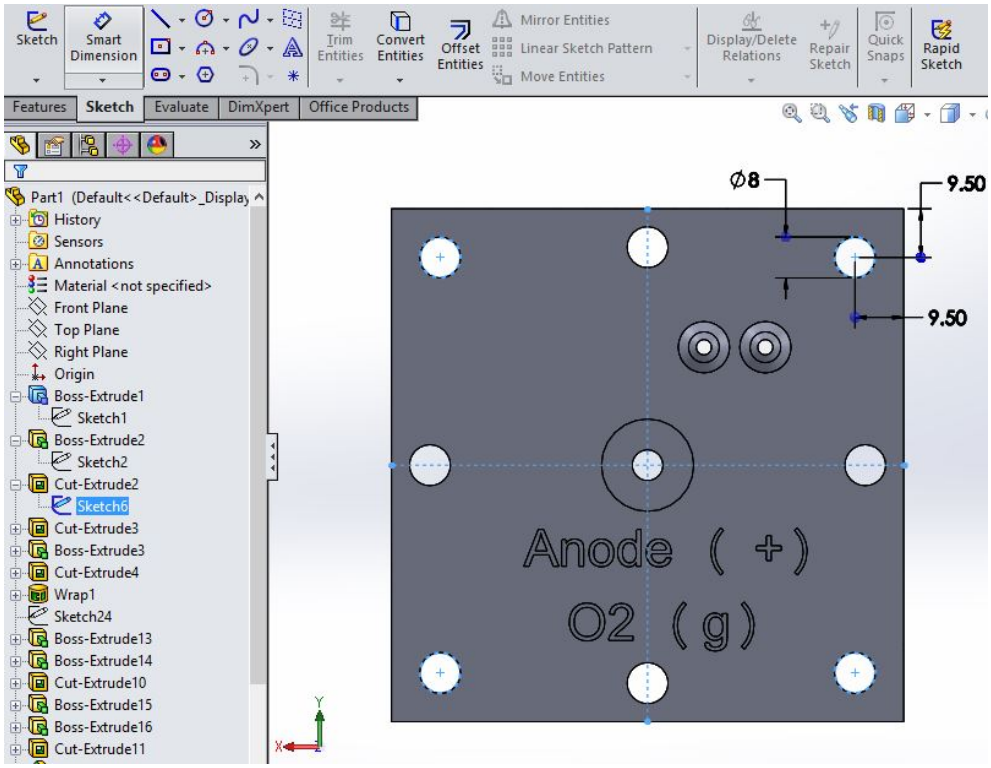

Figure A.2: Diameter of clamping holes

The outer diameter of electrolyte supply tube is selected as 6 mm.

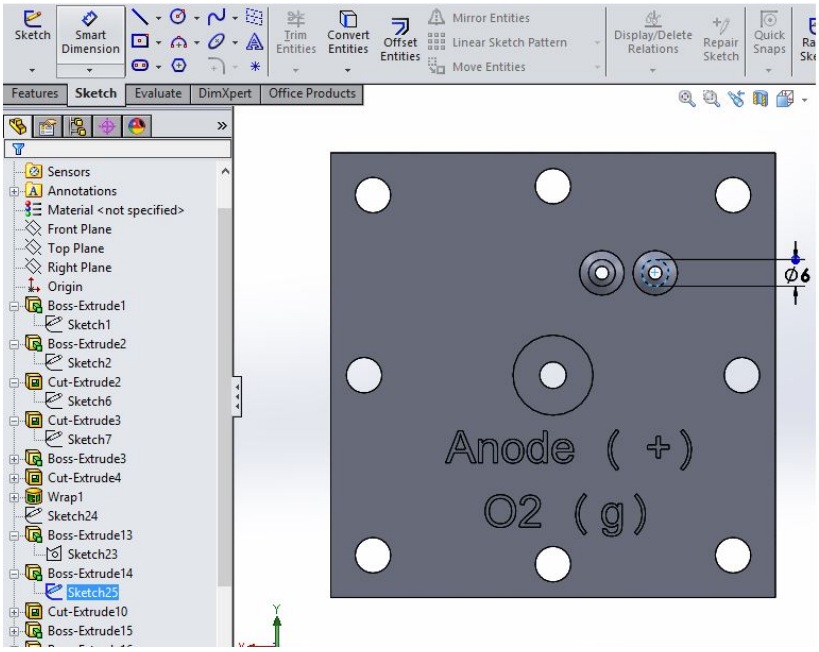

Figure A.3: Outer diameter of electrolyte supply tube

The inner diameter of electrolyte supply tube is selected as 3 mm.

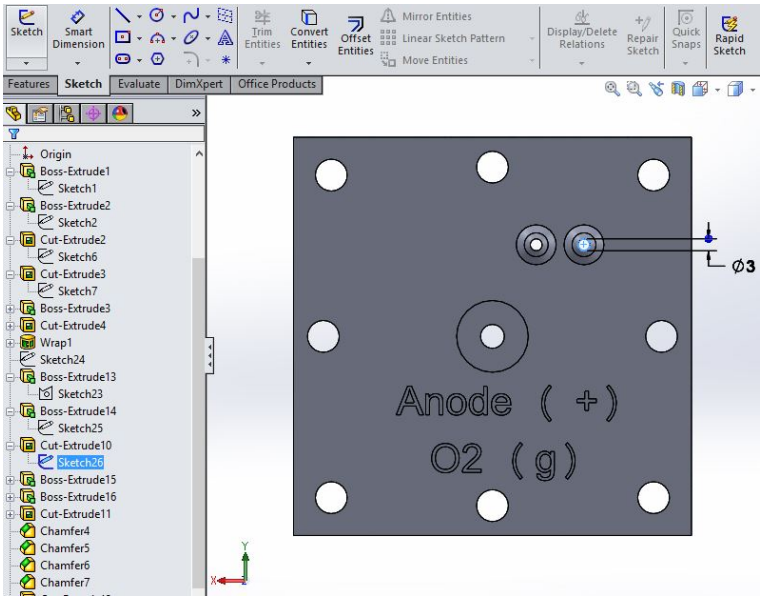

Figure A.4: Inner diameter of electrolyte supply tube

The cathode side base plate is completely identical to the anode side base plate.

A.2 Dimension of Intermediate Base Plate

The dimensions of intermedeate base plate are selected as 100 mm X 100 mm width and height respectively.

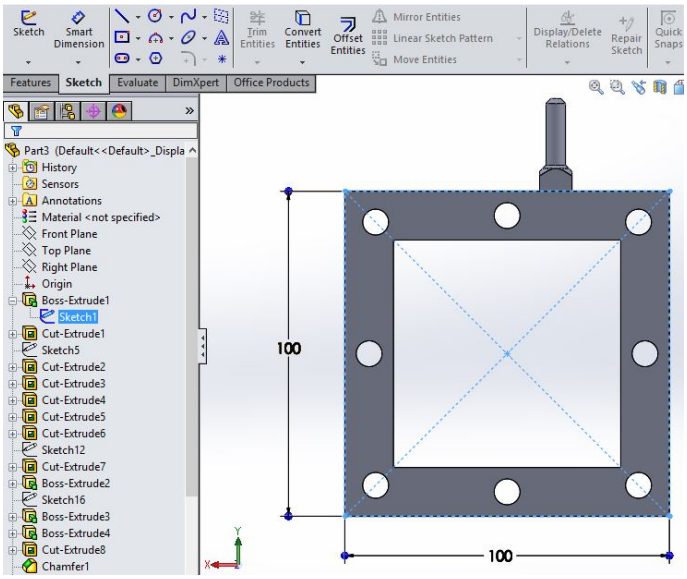

Figure A.5: Dimension of intermediate base plate

The air outlet tube have 6 mm outer diameter and 3 mm inner diameter. The length of air outlet tube is selected as 28.94 mm.

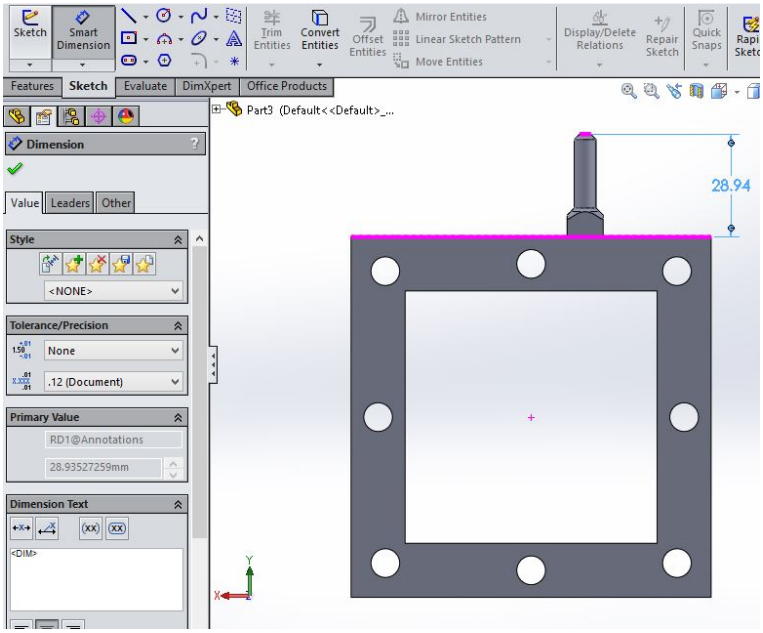

Figure A.6: Length of air outlet tube

The electrode space of the electrolyser is selected as 3 mm width.

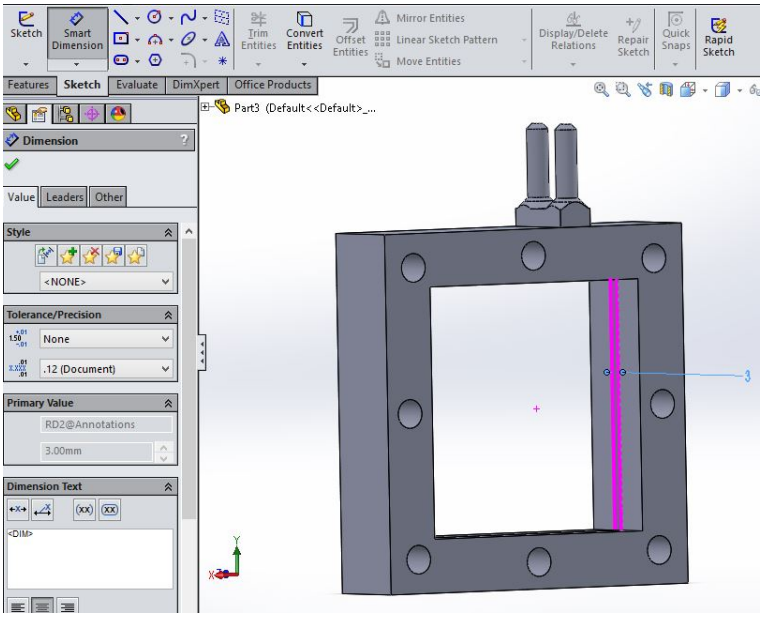

Figure A.7: Electrode space of electrolyser

A.3 Section Views of the Electrolyser

The section view of anode and cathode side base plate are identical.

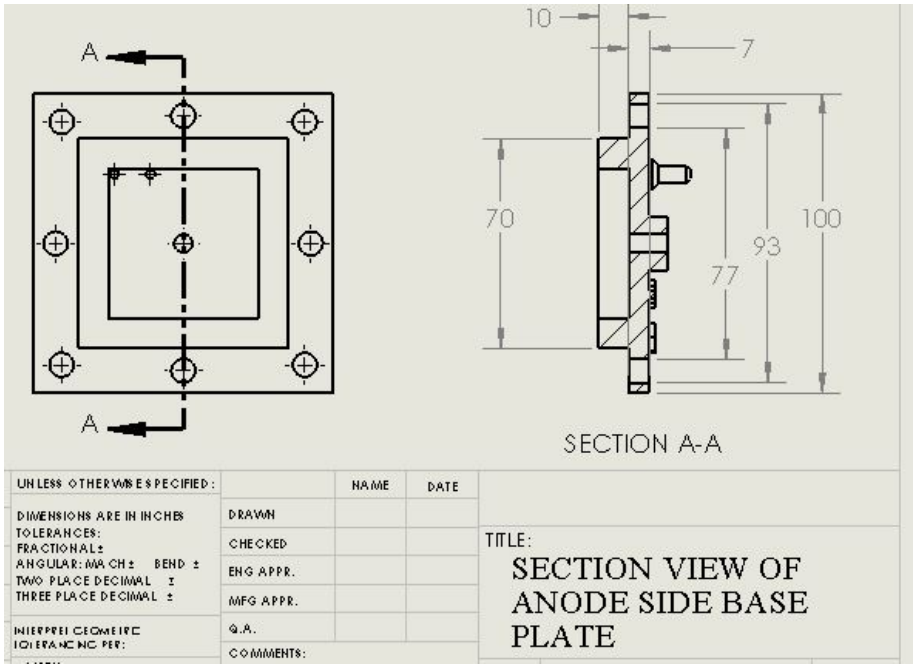

Figure A.8: Section view of anode side base plate

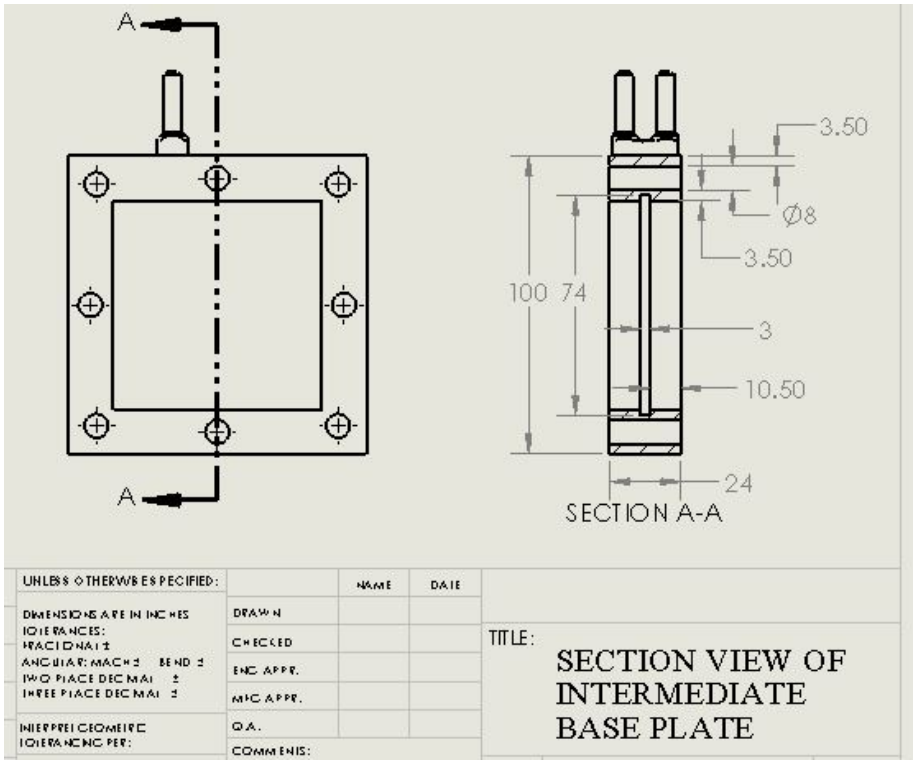

Figure A.9: Section view of intermediate base plate

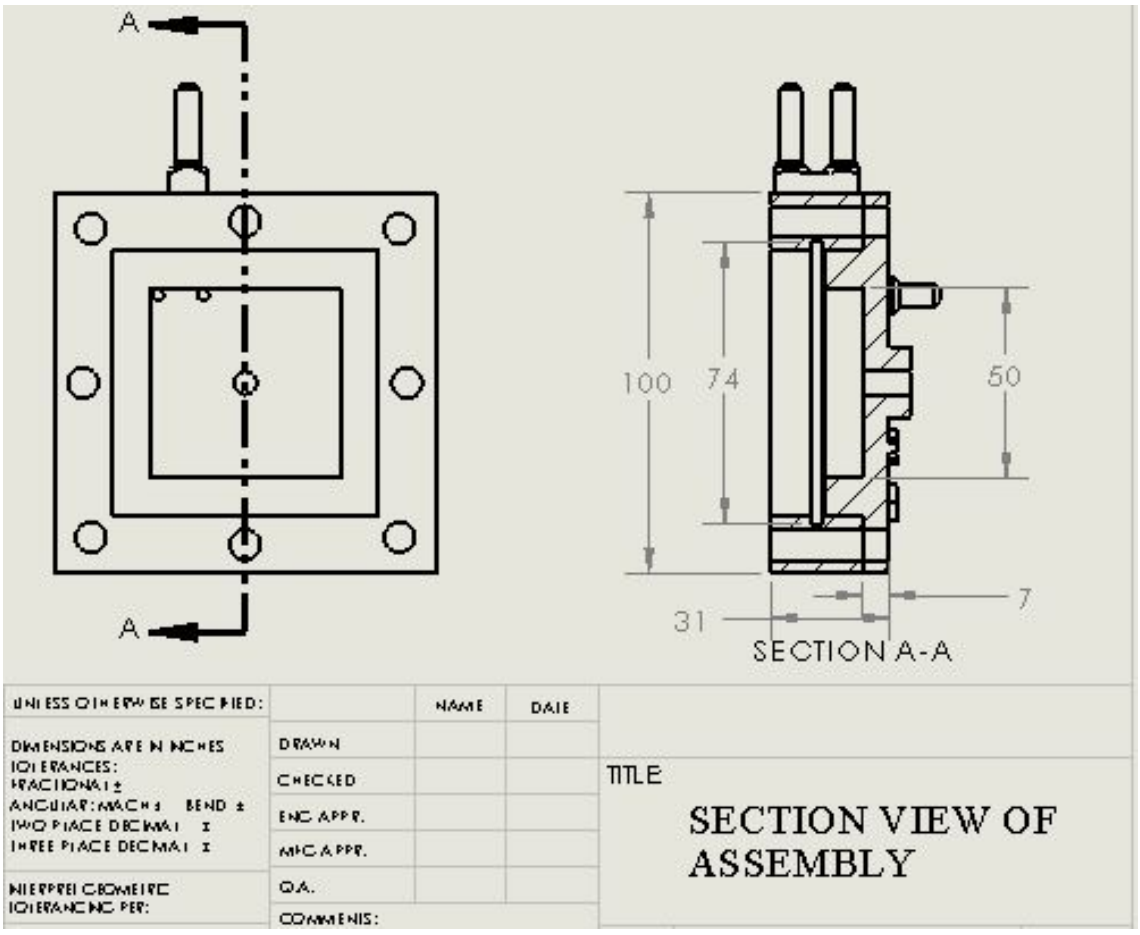

Figure A.10: Section view of assembly

Appendix B

Detailed Dimention of Second Design

This chapter is explained all the detail about the dimension of second SolidWorks model in details.

B.1 Dimension of Anode and Cathode Side Base Plates

The dimensions of base plate is selected as 100 mm x 100 mm width and height respectively.

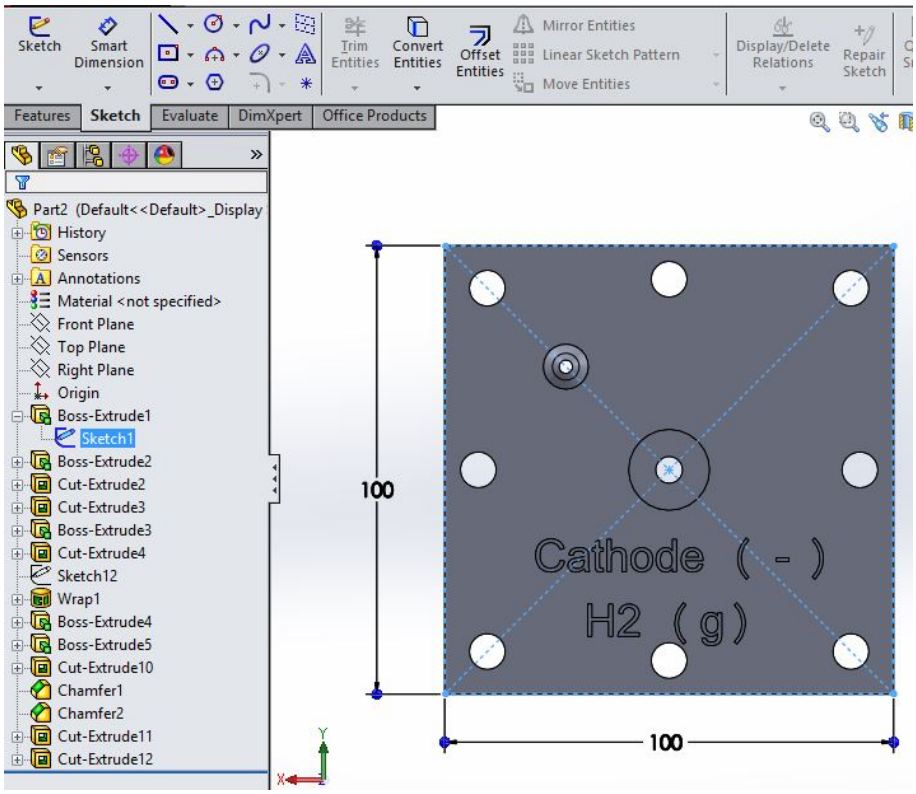

Figure B.1: Cathode side base plate dimension

The diameter of each clamping hole is selected as 8 mm.

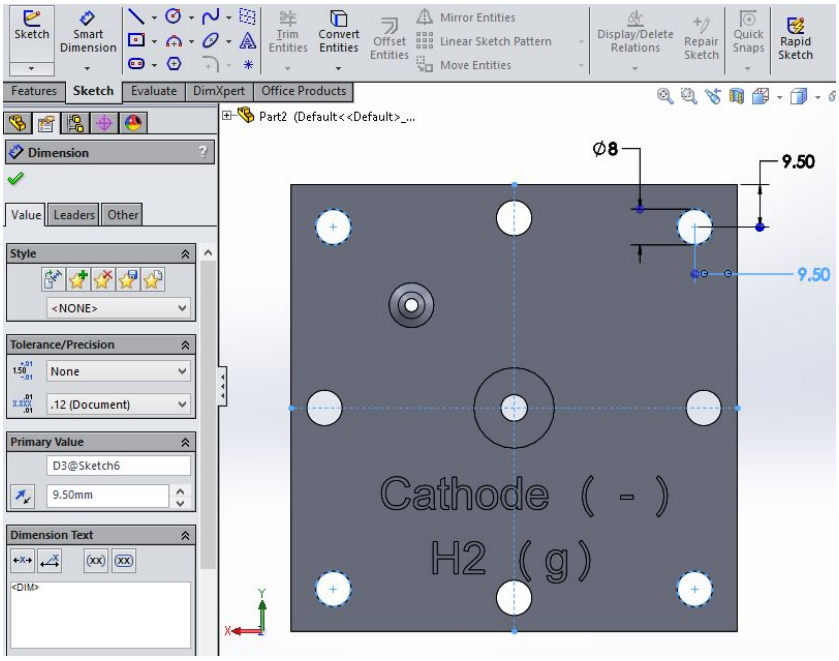

Figure B.2: Diameter of clamping holes

The outer diameter of electrolyte supply tube is selected as 6 mm.

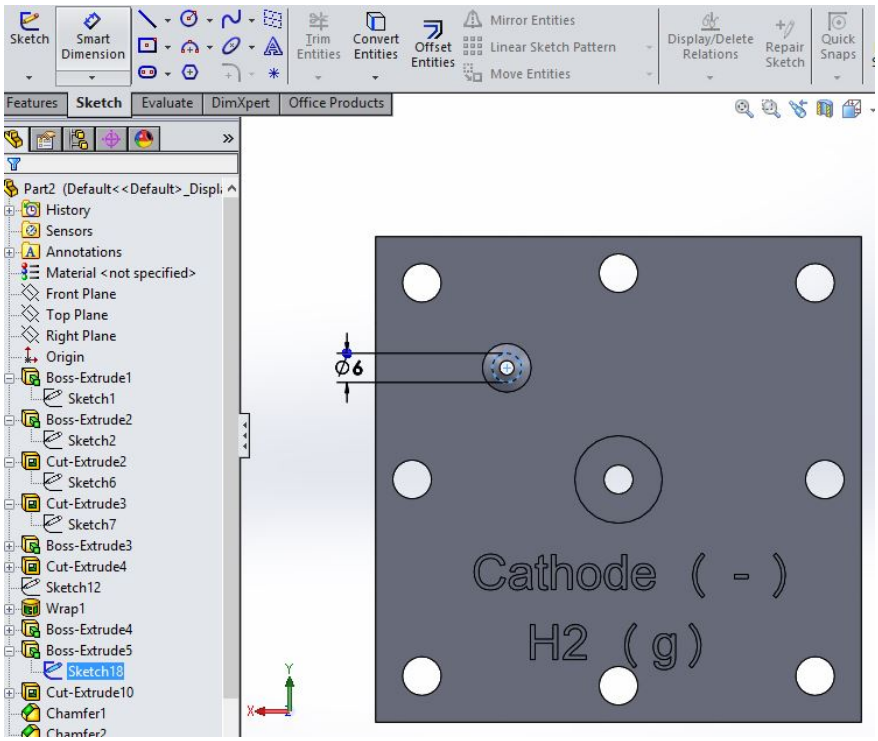

Figure B.3: Outer diameter of electrolyte supply tube

The inner diameter of electrolyte supply tube is selected as 3 mm.

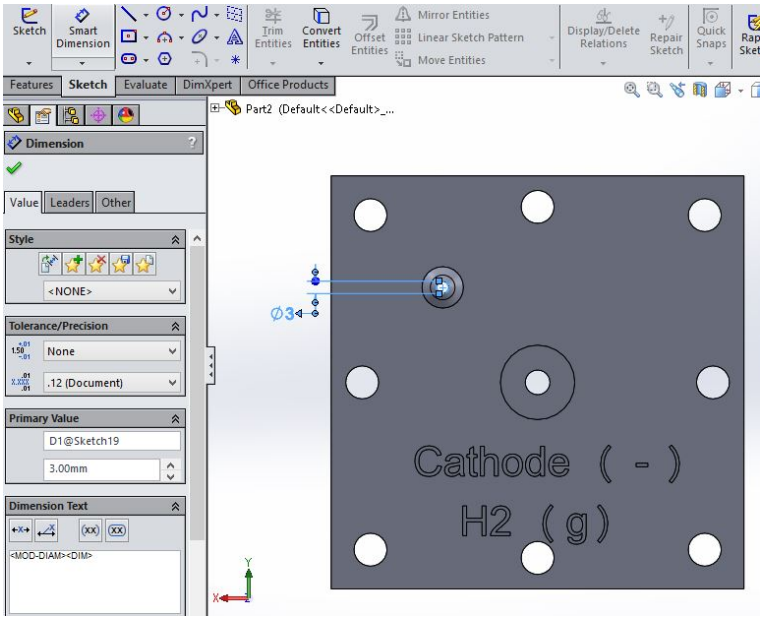

Figure B.4: Inner diameter of electrolyte supply tube

The anode side base plate is completely identical to the cathode side base plate.

B.2 Dimension of Intermediate Base Plate

The dimensions of intermediate base plate are selected as 100 mm X 130 mm width and height respectively.

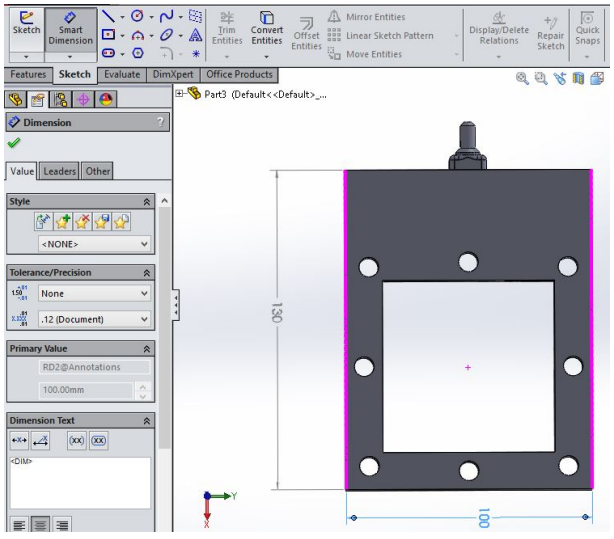

Figure B.5: Dimension of intermediate base plate

The air outlet tube have 6 mm outer diameter and 3 mm inner diameter. The length of air outlet tube is selected as 19.5 mm.

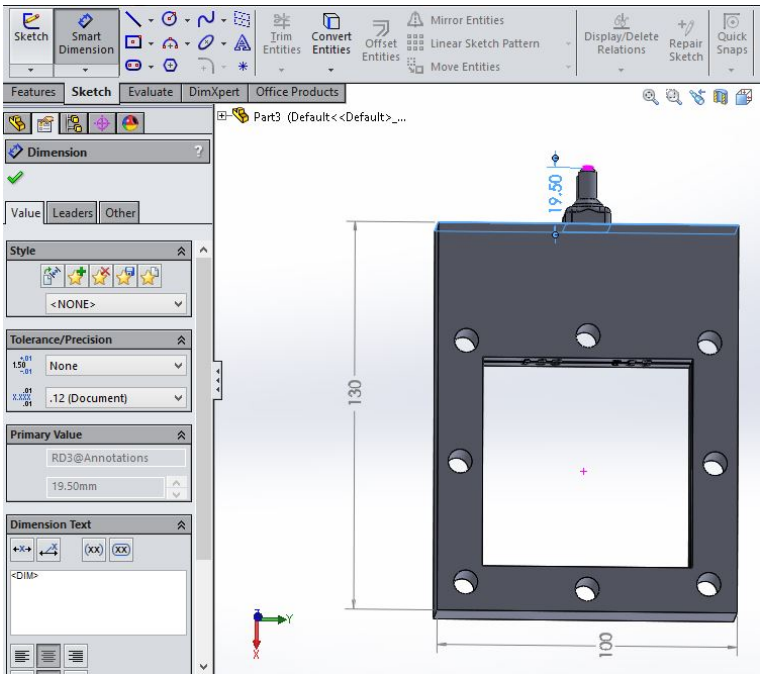

Figure B.6: Length of air outlet tube

The electrode space of the electrolyser is selected as 3 mm width.

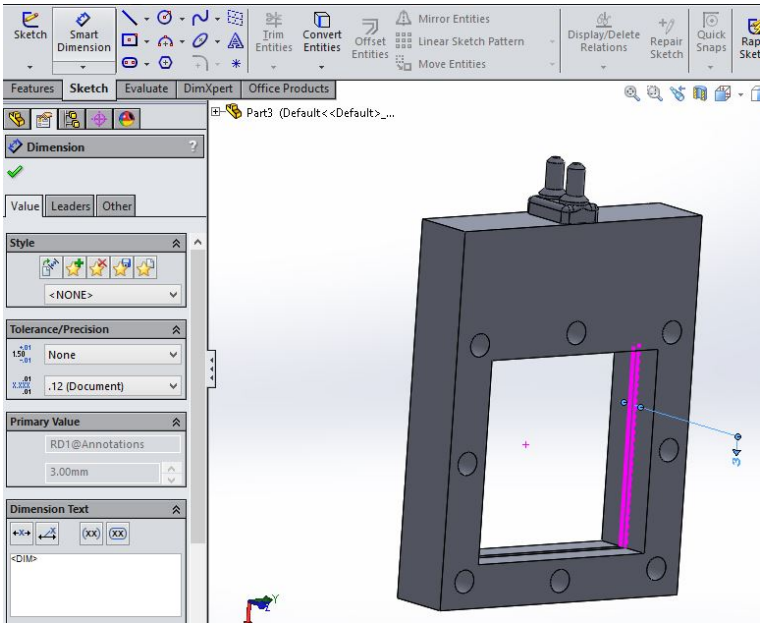

Figure B.7: Electrode space of electrolyser

B.3 Section Views of the Electrolyser

The section view of anode and cathode side base plate are identical.

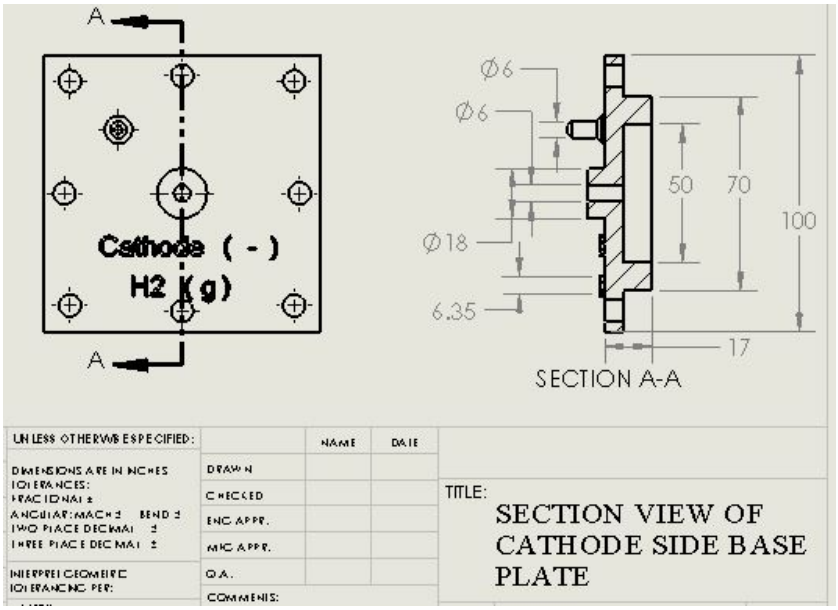

Figure B.8: Section view of cathode side base plate

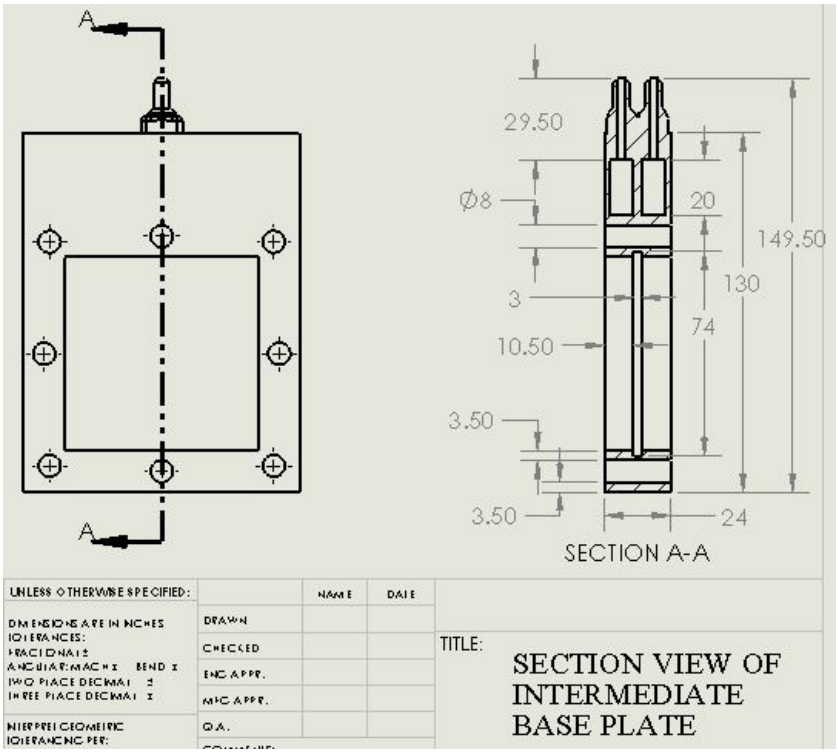

Figure B.9: Section view of intermediate base plate

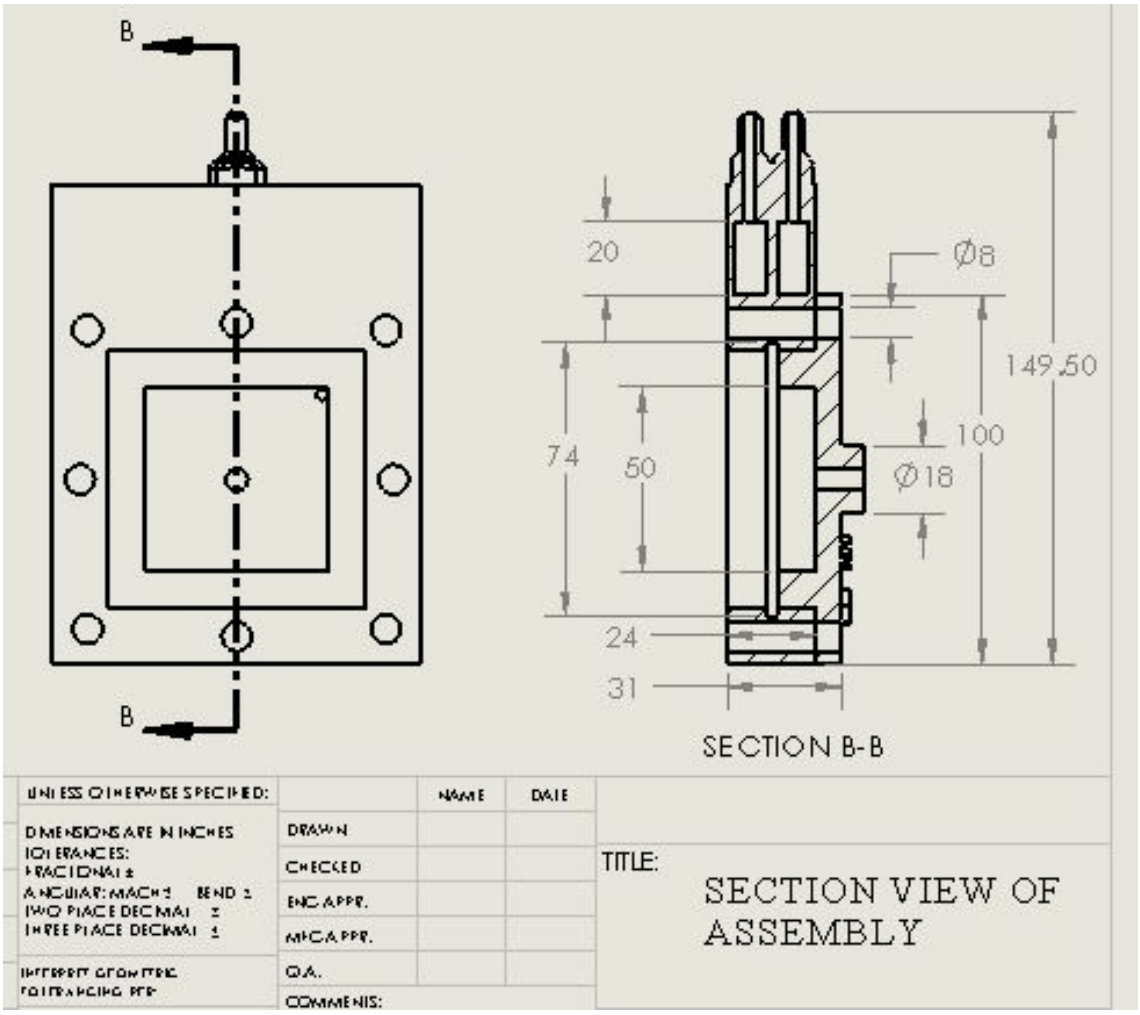

Figure B.10: Section view of assembly

Appendix C

Detailed Dimention of Electrolysis Stack

This chapter is presented all the detail about the dimension of both monopolar and bipolar configuration of alkaline electrolysis stack in details.

C.1 Section View of Monopolar Electrolysis Stack

Figure C.1 is exhibited the section view of monopolar electrolysis stack. Moreover, the dimensions of each single cell are dramatically same as the dimensions of second design of single cell alkaline electrolyser. The detailed dimension of second design of single cell alkaline electrolyser is available in Appendix B.

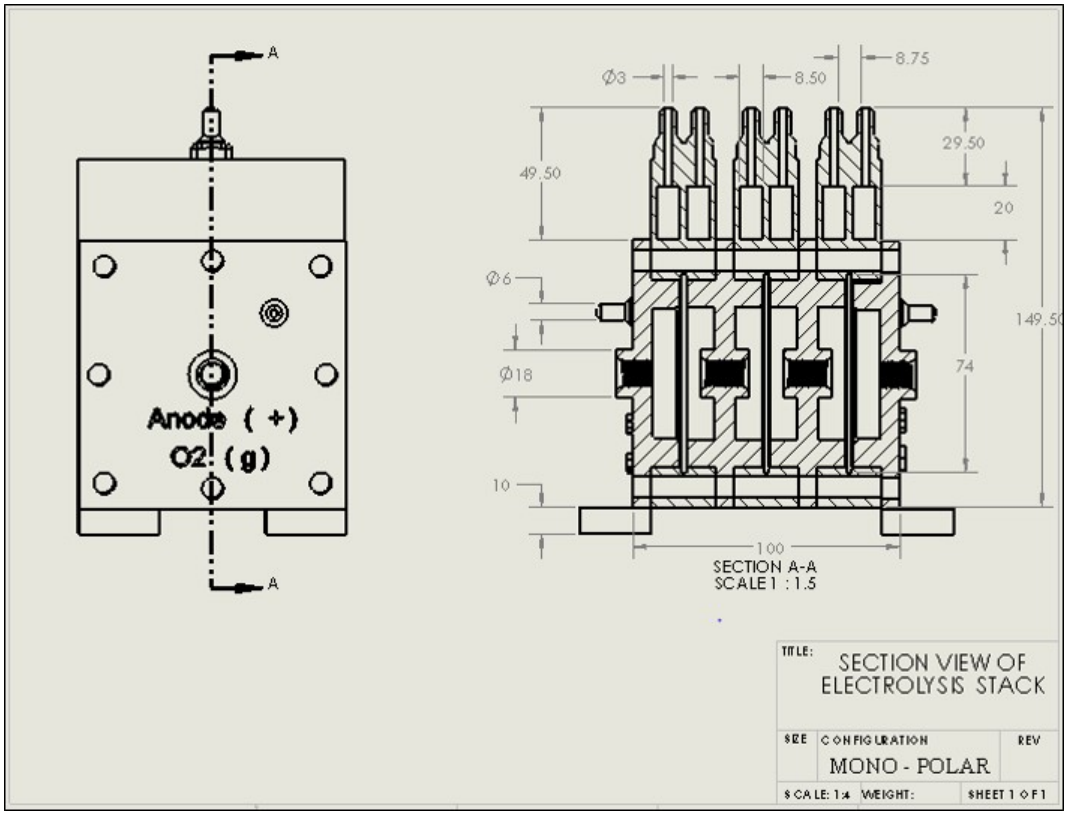

Figure C.1: Section view of monopolar electrolysis stack

C.2 Section View of Bipolar Electrolysis Stack

The section view of bipolar electrolysis stack is shown in Figure C.2. Moreover, the dimensions of each single cell are dramatically same as the dimensions of second design of single cell alkaline electrolyser. The detailed dimension of second design of single cell alkaline electrolyser is available in Appendix B.

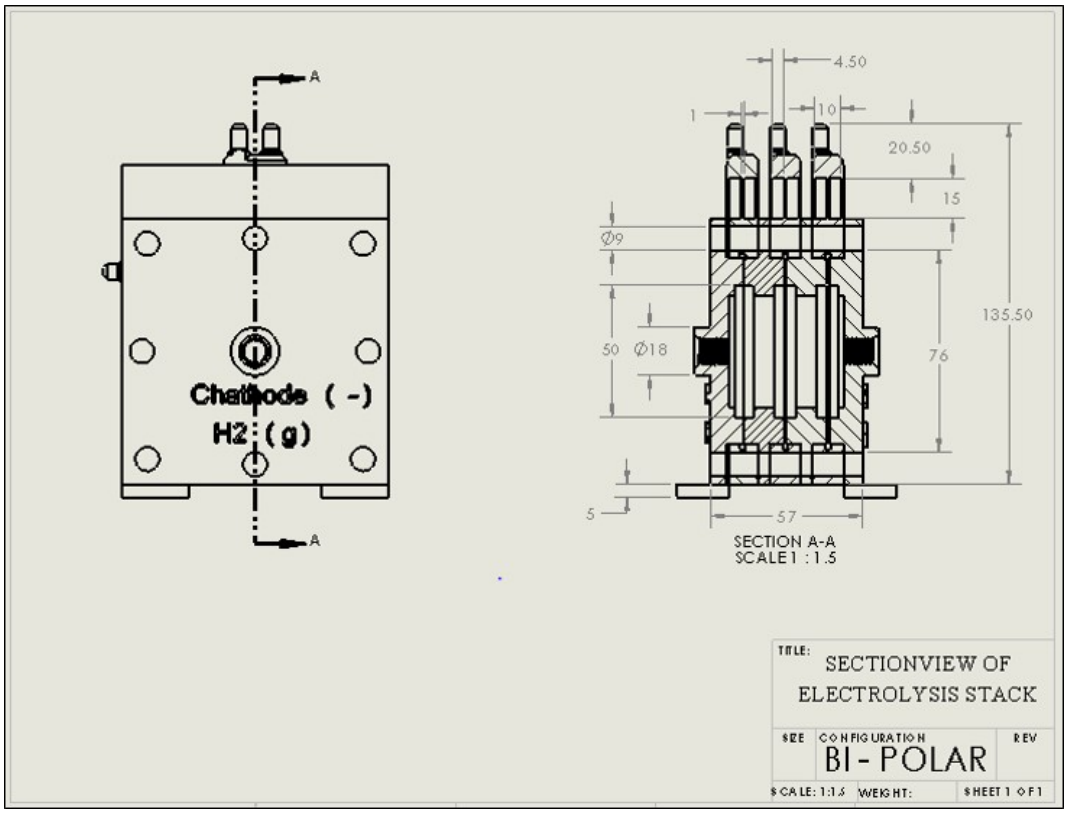

Figure C.2: Section view of bipolar electrolysis stack

Appendix D

Detailed Description of Nafion Membrane Property

This chapter is presented all the detail about the Nafion membrane which is used in the Experiment VIII.

D.1 Thickness and Basis Weight Properties

Membrane Type	Typical Thickness (microns)	Basis Weight (g/m^2)
N-115	127	250
N-117	183	360
N-1110	254	500

Figure D.1: Thickness and basis weight properties

D.2 Hydrolytic Properties

Property	Typical Value	Test Method
Hydrolytic Properties		
Water content, % water[6]	5	ASTM D 570
Water uptake, % water[7]	38	ASTM D 570
Thickness change, % increase		
from 50% RH, 23 °C to water soaked, 23 °C	10	ASTM D 756
from 50% RH, 23 °C to water soaked, 100 °C	14	ASTM D 756
Linear expansion, % increase[8]		
from 50% RH, 23 °C to water soaked, 23 °C	10	ASTM D 756
from 50% RH, 23 °C to water soaked, 100 °C	15	ASTM D 756

Figure D.2: Hydrolytic properties

D.3 Physical and Other Properties

Property	Typical Value	Test Method
Physical Properties		
Tensile Modulus, MPa (kpsi)		
50% RH, 23 °C	249 (36)	ASTM D 882
water soaked, 23 °C	114 (16)	ASTM D 882
water soaked, 100 °C	64 (9.4)	ASTM D 882
Tensile Strength, maximum, MPa (kpsi)		
50% RH, 23 °C	43 (6.2) in MD, 32 (4.6) in TD	ASTM D 882
water soaked, 23 °C	34 (4.9) in MD, 26 (3.8) in TD	ASTM D 882
water soaked, 100 °C	25 (3.6) in MD, 24 (3.5) in TD	ASTM D 882
Elongation at Break, %		
50% RH, 23 °C	225 in MD, 310 in TD	ASTM D 882
water soaked, 23 °C	200 in MD, 275 in TD	ASTM D 882
water soaked, 100 °C	180 in MD, 240 in TD	ASTM D 882
Tear Resistance - Initial, g/mm		
50% RH, 23 °C	6000 in MD, TD	ASTM D 1004
water soaked, 23 °C	3500 in MD, TD	ASTM D 1004
water soaked, 100 °C	3000 in MD, TD	ASTM D 1004
Tear Resistance[3] - Propagating, g/mm		
50% RH, 23 °C	>100 in MD, >150 in TD	ASTM D 1922
water soaked, 23 °C	92 in MD, 104 in TD	ASTM D 1922
water soaked, 100 °C	74 in MD, 85 in TD	ASTM D 1922
Specific Gravity	1.98	—
Other Properties		
Conductivity, S/cm	0.10 min	see footnote[4]
Available Acid Capacity, meq/g	0.90 min	see footnote[5]
Total Acid Capacity, meq/g	0.95 to 1.01	see footnote[5]

Figure D.3: Physical and other properties

Bibliography

[1] A. Ursa, I. S. Martn, and P. Sanchis, "Design of a programmable power supply to study the performance of an alkaline electrolyser under different operating conditions," 2nd IEEE Energy Conference & Exhibition, 2012.

[2] E. Troncoso and M. Newborough, "Implementation and control of electrolysers to achieve high penetrations of renewable power," International Journal of Hydrogen Energy, vol. 32, no. 13, pp. 2253-2268, Sep. 2007.

[3] P. C. Ghosh, B. Emonts, H. Janben, J. Mergel, and D. Stolten, "Ten years of operational experience with a hydrogen-based renewable energy supply system," Solar Energy, vol. 75, no. 6, pp. 469-478, Dec. 2003.

[4] X. Li, Y.J. Song, and S.B. Han, "Frequency control in micro-grid power system combined with electrolyser system and fuzzy PI controller," Journal of Power Sources, vol. 180, no. 1, pp. 468-475, May 2008.

[5] Md S. Opu, "Effect of operating parameters on performance of alkaline water electrolysis," Int. J. of Thermal & Environmental Engineering, vol. Volume 9, no. No. 2, pp. 53-60, 2015.

[6] D. Gardner, "Hydrogen production from renewables," Renewable Energy Focus, vol. 9, no. 7, pp. 34-37, Jan. 2009.

[7] V. M. Nikolic, G. S. Tasic, A. D. Maksic, D. P. Saponjic, S. M. Miulovic, and M. P. Marceta Kaninski, "Raising efficiency of hydrogen generation from alkaline water electrolysis - energy saving," International Journal of Hydrogen Energy, vol. 35, no. 22, pp. 12369-12373, Nov. 2010.

[8] Millet, P and Grigoriev, S 2013, "Water electrolysis technologies", in: Gandia, L, Arzamendi, G, and Diguez, P (eds.), Renewable hydrogen technologies, Elsevier, Amsterdam.

[9] U.F.Vogt, M. Schlupp, D. Burnat, A. Zttel. "Novel Developments In Alkaline Water Electrolysis". 8Th International Symposium Hydrogen and Energy. Switzerland: Empa, Laboratory of Hydrogen & Energy, Abt. 505 berlandstrasse 129 CH-8600 Dbendorf, 2014.

[10] Joonas Koponen,"Review Of Water Electrolysis Technologies And Design Of Renewable Hydrogen Production Systems". Master'S Thesis. Lappeenranta University of Technology LUT School of Energy Systems Degree Programme in Electrical Engineering, 2015.

[11] A. Ursua, L. M. Gandia, and P. Sanchis, "Hydrogen production from water electrolysis: Current status and future trends," Proceedings of the IEEE, vol. 100, no. 2, pp. 410-426, Feb. 2012.

[12] K. Mazloomi, N. b. Sulaiman, and H. Moayedi, "Electrical efficiency of electrolytic hydrogen production," Int. J. Electrochem. Sci., pp. 3314-3326, Apr. 2012.

[13] K. Zeng and D. Zhang, "Recent progress in alkaline water electrolysis for hydrogen production and applications," Progress in Energy and Combustion Science, vol. 36, no. 3, pp. 307-326, Jun. 2010.

[14] Johanna Ivy, "Summary of electrolytic hydrogen production," Milestone Completion Report, 2004.

[15] L. Bertuccioli, A. Chan, D. Hart, F. Lehner, B. Madden, and E. Standen, "Study on development of water electrolysis in the EU," Fuel Cells and Hydrogen Joint Undertaking, p. Final Report, Feb. 2014.

[16] A. Ursa, I. San Martn, E. L. Barrios, and P. Sanchis, "Stand-alone operation of an alkaline water electrolyser fed by wind and photovoltaic systems," International Journal of Hydrogen Energy, vol. 38, no. 35, pp. 14952-14967, Nov. 2013.

[17] M. Kiaee, P. Chladek, D. Infield, and A. Cruden, "Utilisation of alkaline electrolysers to improve power system frequency stability with a high penetration of wind power," IET Renewable Power Generation, vol. 8, no. 5, pp. 529-536, Jul. 2014.

[18] W. Jiang, et al. "Identification and Power Electronic Module Design of a Solar Powered Hydrogen Electrolyzer," IEEE Asia-Pacific Power and Energy Engineering Conference, pp. 1-4. 2012.

[19] M. Kiaee, A. Cruden, D. Infield, Y. Ma, T. G.Douglas, "The impact on the electrical grid of hydrogen production from alkaline electrolysers," IEEE Universities Power Engineering Conference (UPEC), 45th International, pp. 1-6. 2010.

[20] N. Gyawali and Y. Ohsawa, "Integrating fuel cell/Electrolyzer/Ultracapacitor system into a stand-alone Microhydro plant," IEEE Transactions on Energy Conversion, vol. 25, no. 4, pp. 1092-1101, Dec. 2010.

[21] M. ul-Karim1, M. T. Iqbal,"Dynamic modeling and simulation of alkaline type electrolyzers," Electrical and Computer Engineering, CCECE'09. IEEE Canadian Conference, pp. 711-715. 2009.

[22] K. Belmokhtar, M. L. Doumbia, K. Agbossou,"Dynamic model of an alkaline electrolyzer based an artificial neural networks," Ecological Vehicles and Renewable Energies (EVER), IEEE 8th International Conference and Exhibition, pp. 1-4. 2013.

[23] I. D. de Cerio Mendaza and B. Bak-Jensen,"Alkaline electrolyzer and V2G system DIgSILENT models for demand response analysis in future distribution networks," PowerTech (POWERTECH),IEEE Grenoble, pp. 1-8. 2013.

[24] M. Hammoudi, C. Henao, K. Agbossou, Y. Dub, and M. L. Doumbia, "New multi-physics approach for modelling and design of alkaline electrolyzers," International Journal of Hydrogen Energy, vol. 37, no. 19, pp. 13895-13913, Oct. 2012.

[25] C. Henao, K. Agbossou, M. Hammoudi, Y. Dub, and A. Cardenas, "Simulation tool based on a physics model and an electrical analogy for an alkaline electrolyser," Journal of Power Sources, vol. 250, pp. 58-67, Mar. 2014.

[26] A. Cruden, D. Infield, M. Kiaee, T. G. Douglas, and A. Roy, "Development of new materials for alkaline electrolysers and investigation of the potential electrolysis impact on the electrical grid," Renewable Energy, vol. 49, pp. 53-57, Jan. 2013.

[27] F. Rosalbino, D. Macci, E. Angelini, A. Saccone, and S. Delfino, "Electrocatalytic properties of Fe-R (R=rare earth metal) crystalline alloys as hydrogen electrodes in alkaline water electrolysis," Journal of Alloys and Compounds, vol. 403, no. 1-2, pp. 275-282, Nov. 2005.

[28] W. Hu, "Electrocatalytic properties of new electrocatalysts for hydrogen evolution in alkaline water electrolysis," International Journal of Hydrogen Energy, vol. 25, no. 2, pp. 111-118, Feb. 2000.

[29] Ph. Vermeiren, W. Adriansens, J. P. Moreels, R. Leysen, "Evaluation of the Zirfon^R separator for use in alkaline water electrolysis and Ni-H 2 batteries," International Journal of Hydrogen Energy, 23.5: 321-324.1998.

[30] Md Mamoon Rashid, Mohammed K. Al Mesfer, Hamid Naseem, Mohd Danish. "Hydrogen production by water electrolysis: a review of alkaline water electrolysis, pem water electrolysis and high temperature water electrolysis," International Journal of Engineering and Advanced Technology (IJEAT), vol. Volume-4, no. Issue-3, pp. 2249-8958, Feb. 2015.

[31] M. Wang, Z. Wang, X. Gong, and Z. Guo, "The intensification technologies to water electrolysis for hydrogen production - A review," Renewable and Sustainable Energy Reviews, vol. 29, pp. 573-588, Jan. 2014.

[32] Nunes SP, Peinemann K-V. Membrane technology. 2nd ed. Weinheim: WileyVCH Verlag GmbH & KGaA; 2007.

[33] K. Zeng, and D. Zhang. "Recent Progress In Alkaline Water Electrolysis For Hydrogen Production And Applications". Progress in Energy and Combustion Science 36, pp. 307-326.2010.

[34] Isao. Abe, "Alkaline Water Electrolysis". Energy Carriers And Conversation Systems - Vol. 1. Chiba, Japan: Encyclopedia of Life Support System (EOLSS)

[35] A. Ursa and P. Sanchis, "Static-dynamic modelling of the electrical behaviour of a commercial advanced alkaline water electrolyser," International Journal of Hydrogen Energy, vol. 37, no. 24, pp. 18598-18614, Dec. 2012.

[36] A. S. Tijani, N. A. B. Yusup, and A. H. A. Rahim, "Mathematical Modelling and simulation analysis of advanced alkaline Electrolyzer system for hydrogen production," Procedia Technology, vol. 15, pp. 798-806, 2014.

[37] O. Ulleberg, "Modeling of advanced alkaline electrolyzers: A system simulation approach," International Journal of Hydrogen Energy, vol. 28, no. 1, pp. 21-33, Jan. 2003.

[38] X. Changjun and Q. Shuhai, "Drawing impedance spectroscopy for Fuel Cell by EIS", Procedia Environmental Sciences, vol. 11, pp. 589-596, 2011.

[39] "Studying Impedance to Analyze the Li-Ion Battery with an App", COMSOL Multiphysics, 2017. [Online]. Available: https://www.comsol.com/blogs/studying-impedance-to-analyze-the-li-ion-battery-with-an-app/. [Accessed: 26- Apr- 2017].

[40] L. Ran, W. Junfeng, W. Haiying, & L. Gechen,"Prediction of state of charge of lithium-ion rechargeable battery with electrochemical impedance spectroscopy theory" In Industrial Electronics and Applications (ICIEA), 5th IEEE Conference on pp. 684 - 688, June, 2010.